TÉCNICO LISBOA

Optimization of sandwich plates with variable stiffness composite faces: free vibration and buckling behaviour

Daniel José Da Silva Fonseca

Thesis to obtain the Master of Science Degree in

Aerospace Engineering

Supervisors: Prof. Filipa Andreia De Matos Moleiro
Prof. Aurélio Lima Araújo

Examination Committee

Chairperson: Prof. Afzal Suleman
Supervisor: Prof. Filipa Andreia De Matos Moleiro
Member of the Committee: Prof. José Arnaldo Pereira Leite Miranda Guedes

December 2022

Dedicated to my mother,
sister, brother and to my love

Declaration

I declare that this document is an original work of my own authorship and that it fulfills all the requirements of the Code of Conduct and Good Practices of the Universidade de Lisboa.

Acknowledgments

I would like to start by thanking my supervisors, Prof. Filipa Moleiro and Prof. Aurélio Araújo, for the opportunity to explore in an interesting and new topic that allowed me to improve various number of skills. Thank you for the always present sympathy and support given to me in the meetings, allowing me to have a more clear and oriented path throughout the process, as well as all dissertations revisions that were crucial for optimizing the present document.

I want to thank my family, namely my mother. Thank you, mother, for all the commitment and effort you have put into my education and I really hope I made (and continue to make) you proud! I want to thank my sister and brother for all the support throughout these years, it is a pleasure being your sibling!

My love, Marta, thank you for all the support you have given to me in both bad and great phases. I love you!

My friends, I could not, of course, forget you. Diogo, Ricardo, António, Pedro, Rita, thank you for all the wonderful memories in Técnico and all the group support we had!

Resumo

Estruturas sanduíche com faces em compósito de rigidez variável combinam características de baixa densidade, proveniente sobretudo do núcleo, com um potencial extraordinário de melhoria da performance estrutural devido à extensão do campo de *design*, em comparação com sanduíches tradicionais. Na indústria aeroespacial o referido é especialmente relevante, tornando estas estruturas muito atrativas. Neste trabalho, as fibras das faces seguem uma lei de orientação linear. Um estudo da resposta estrutural, anterior à otimização, é realizado, principalmente em vibração e *buckling*. O objetivo é a identificação de tendências e possíveis correlações existentes entre a evolução da performance e os parâmetros das lâminas (T_0 e T_1), bem como o impacto da rigidez do núcleo nos resultados. O possível aparecimento de instabilidades locais provocadas pela combinação de fibras curvilíneas nas faces com fibras com um núcleo de baixa rigidez é, também, objetivo de estudo. Com o recurso a um algoritmo genético e ao *software Abaqus* para a realização das análises estruturais, processos de otimização são realizados. Quatro otimizações uniobjetivo são alvo de estudo: vibração, *buckling* na direção x e y e *buckling* com forças de corte. Uma estrutura com dimensões $1 \times 1\ m^2$, espessura do núcleo de $16\ mm$ e espessura de cada face de 2 mm, em que cada face é constituída por quatro lâminas, é submetida a estes processos de otimização. Concluiu-se que, na maioria dos casos de otimização, houve uma melhoria significativa fornecida por estas novas estruturas. Por exemplo, em *buckling* na direção y, para condições CCCC, houve uma melhoria de 67%.

Palavras-chave: Estruturas Sanduíche de Rigidez Variável, Instabilidades Locais, Algoritmo Genético, Frequências Naturais, Carga Crítica de Instabilidade

Abstract

Variable stiffness composite sandwich structures combine low density characteristics, provided by the core, with an immense potential of structural performance improvement due to the extended design space in comparison with traditional sandwich. These properties make variable stiffness sandwich structures very appealing for industries such as aerospace. In this work, the structures used possess face sheets that follow a linear fiber orientation law. Prior to the optimization phase, a study regarding the structural behaviour of these structures is made, primarly in terms of vibration and buckling. More concretely, the objective is to identify trends and possible correlations between the performance evolution and the laminas parameters (T_0 and T_1), as well as the impact of the core stiffness on the results. Possible onset of instabilities caused by face sheets with steered fibers is also investigated. Afterwards, an optimization process is made, resorting to *Matlab* genetic algorithm, combined with the structural analysis performed on *Abaqus*, using *Python* scripts. This process consists in four different uniobjective optimizations: free vibration, buckling in x and y directions and shear buckling. A plate with $1 \times 1\ m^2$, thickness of core of $16\ mm$ and thickness of face sheet of $2\ mm$, being each face sheet composed of four laminas, is subjected to the optimization processes. It was concluded that, in the vast majority of optimization cases tested, VSS have a better structural performance than CSS. For example, the performance improvement achieved by VSS over CSS, in buckling in y direction, for CCCC boundary conditions, ascended to 67%.

Keywords: Variable Stiffness Sandwich, Local Instabilities, Genetic Algorithm, Natural Frequencies, Critical Buckling Load

Contents

List of Tables

List of Figures

Nomenclature

Greek symbols

λ_{crit}	Critical buckling load factor.
$\nu_{12}, \nu_{13}, \nu_{23}$	Poisson ratios.
ω	Natural frequency value.
$\theta(x)$	Fiber orientation law.

Roman symbols

a	Length of the sandwich structure.
b	Width of the sandwich structure.
E_{11}	Longitudinal elastic modulus.
E_{22}, E_{33}	Transverse elastic moduli.
G_{12}, G_{13}, G_{23}	Shear moduli.
K	Maximum allowed curvature.
$(T_0)_i$	Fiber orientation of lamina i at $x = a/2$.
$(T_1)_i$	Fiber orientation of lamina i at $x = 0$ and $x = a$.
t	Total thickness of the sandwich structure.
t_c	Thickness of the core.
t_f	Thickness of each of the face sheets.

Glossary

CSS Constant Stiffness Sandwich is a type of sandwich structure whose face sheets are composed of traditional unsteered fibers (constant stiffness).

CTS Continuous Tow Shearing is a VSL manufacturing process (i.e. used for the face sheets) where in-plane shear deformation is used, that allows to avoid some particular manufacturing defects of other methods.

ESL Equivalent Single Layer theories, under some circumstances and assumptions, reduce 3D structures to an unique 2D shell structure, allowing for simpler and faster computations.

FEM The Finite Element Method is a numerical method often used in the resolution of various real life complex structural problems.

GA Genetic Algorithms are a type of metaheuristic optimization methods, with nature-inspired (natural selection theory) terminology.

VSL Variable Stiffness Laminates are a type of laminate structure with variable spatial stiffness, resorting to, for example, steered fibers.

VSS Variable Stiffness Sandwich is a type of sandwich structure whose face sheets are VSL.

Chapter 1

Introduction

1.1 Motivation

Aircraft material selection and structural design are two important aspects that need to be taken into account in an aircraft design process. The material usage trend in aviation has been in a constant change over the last century due to technological inventions and discoveries. In the early days of aviation, the most commonly used material was aluminium, especially after the Second World War, due to expensive military investments that allowed, for example, the development, by the Japanese Army, of the lighter Al-Zn alloy, which inaugurated the 7XXX family of aluminium alloys. The mass production of aluminium in the war, together with the favourable combination of its good mechanical properties, corrosion resistance, recyclability and its light weight when compared with others metals, motivated a aluminium-based material composition up to 80% of the aircrafts weight, until the 1980s.

The genesis of Airbus brought novelties to the aviation industry, namely with the design of the A320 and A340 aircrafts, in the 1980s, that used a percentage of composite materials in the order of 15-18% in relation to the total weight [1]. The use of composites was highly due to its great stiffness to weight ratio, that was much higher than aluminium, for example, thus turning into its primary competitor. Figure 1.1 illustrates the evolution of materials used in aviation. It can be seen that, nowadays, the percentage of composite materials used can reach up to nearly 60% of the aircraft's weight, with the perspective that this number can further increase in the future.

As mentioned, composite materials are highly used in modern aviation and there is a constant need to search for materials that combine better characteristics than the ones used currently. Thus, a lot of effort has been put recently in the investigation of ways to improve the performance of composite materials, namely composite sandwich structures. These structures are composed of composite face sheets with high stiffness, such as carbon fiber reinforced polymers, with a core typically of low density. The most common composite face sheets are composite laminates made of a stacking of straight fiber-reinforced laminas. Such face sheets are thus constant stiffness composites (CSC). Studies have been done in order to improve the capabilities of these structures and one of the main subtopics investigated in this field is the use of variable stiffness composites (VSC) as face sheets, originating the variable

stiffness sandwiches (VSS). VSC can be achieved by, for example, within each lamina, varying the fiber orientation, allowing for the expansion of the feasible design space.

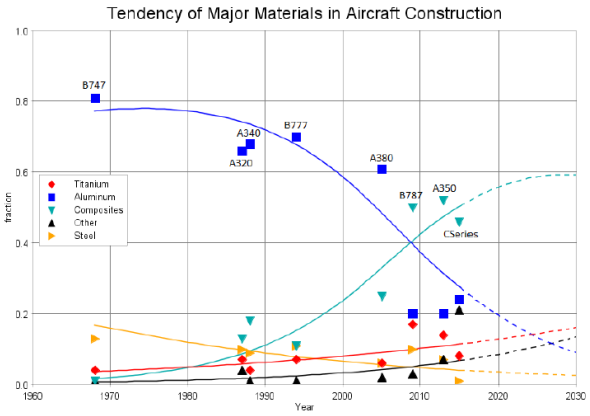

Figure 1.1: Historical evolution of aircraft's material composition [2].

In order to have a methodic and consistent *modus operandi* of improving VSS structures, that will be further explored later in this work, the use of optimization algorithms reveals to be an important tool. To make use of these algorithms, first, one must define, besides the objective function that is going to be minimized or maximized, the design variables of the problem to be solved. In the case of VSS, the thickness of the core and the laminates, the number of plies and fiber orientation within each lamina are examples of design variables that can be adopted. As stated before, the most popular way to vary the stiffness is through the spatial variation of fiber orientation and so, in this work, these will be the design variables. These algorithms can include constraints, such as manufacturing constraints, that will be used and are explained hereafter in this work.

Together with the optimization algorithm, it is also necessary to have an accurate mathematical model capable of predicting the mechanical behaviour of these structures that will be the base of the objective function in the optimization algorithm. To this extent, the finite element method (FEM) is used, being a reliable well-known tool of structural analysis which can handle complex geometries and boundary conditions.

1.2 Topic Overview

A brief description of general sandwich structures as well as the particular case of variable stiffness sandwiches is given in this section. Some notes on optimization algorithms are also addressed.

1.2.1 Laminated Composite Sandwich Structures

Sandwich structures are defined in one of the first articles dedicated specifically to this topic, as mentioned in Hoff and Mautner [3], as being a structure composed of one or more external layers (faces) of thin high-strength material and one (or more) thick internal layer of lightweight material (core). Even

though, nowadays, there is a lot of variety in what concerns sandwich structures, in both faces and core, this simple and straightforward definition still holds true and general in its essence.

The most commonly used sandwich structures in aeronautical applications are those denominated symmetric sandwich, which, as the name suggests, are composed of two face sheets (which, once again, can consist of multiple layers) where one face sheet is the symmetric, about the midplane of the core, compared to the other face sheet, as seen in figure 1.2 . These structures have face sheets that typically have a thickness of less than 2 mm for aeronautical applications [4]. The popularity of this type of sandwich structures is especially due to the fact that they have high bending stiffness as well as good buckling characteristics which makes these structures suitable for a wide variety of applications in aircrafts.

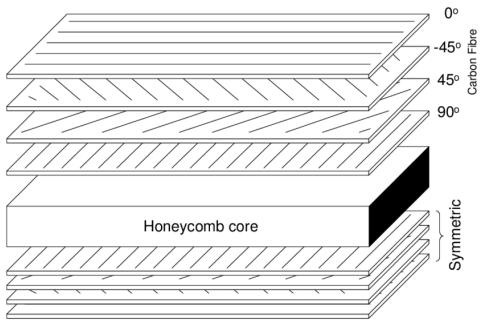

Figure 1.2: Example of a symmetric composite sandwich [5].

1.2.2 Variable Stiffness Sandwich

Currently, the vast majority of laminated composite structures, including the face sheets of composite sandwich structures, are made of a stacking of straight fibre-reinforced laminas. This is due to a variety of reasons, such as the ease of manufacturing. However, since there is a constant orientation in each ply, a limitation to the number of creative solutions emerges and, as consequence, a limitation in the improvement of mechanical properties.

Variable stiffness sandwich structures (that is, whose face sheets are variable stiffness composites) gained relevance in recent years precisely due to its capability of expanding the design space and the possibility of creating new structures with enhanced mechanical properties. Spatially varying material properties can be achieved through many ways such as spatially changing orientation of the fibers, changes in the fiber volume fraction, varying layer thickness or functionally graded materials [6].

1.2.3 Optimization Algorithms

Optimization algorithms provide to the designer a clear and objective path targetting the search for the best solution in a given problem. The range of options available in what concerns these types of algorithms is vast nowadays, which include meta-heuristic, stochastic methods, such as genetic algorithms and particle swarm optimization, as well as deterministic methods, such as gradient-based methods.

Meta-heuristic algorithms try to accomplish a compromise between computational cost and solution accuracy by finding optimum solutions with only information regarding the objective function and constraints of the previous iterations [7]. Genetic algorithms, particle swarm optimization, ant colony algorithms are examples of meta-heuristic methods. Gradient based methods, on the other hand, in addition to what the meta-heuristic algorithms use, also use the gradient information regarding the objective function values and constraints of previous iterations. These can be classified as first order methods, if they only use first derivative information, or second order methods, if additional derivative information from the Hessian matrix is required [8]. In particular, topology optimization has as objective finding the best solution in terms of material distribution in a predefined domain, given a set of loads and boundary conditions [7].

The selection of the optimization algorithm to be implemented depends heavily on a variety of factors, namely, the type of problem under analysis, number of design variables, mathematical model used in respect to the definition of the objective function.

1.3 Objectives

One of the objectives of this work is to explore and study the behaviour of sandwich panels as regards to vibration and buckling, namely the interference caused by the combination of the presence of high stiffness material (face sheets) with variable spatially orientation with a much lower stiffness and density material (core).

Another objective is to explore the design space provided by VSS and see what kind of optimum solutions can be achieved in different situations of mechanical problems, focusing on vibration and buckling, through the maximization of the objective function in both types of problem, that is, the maximization of the first frequency in vibration and the critical buckling load in buckling. The target is to reach solutions that are better in terms of mechanical response in buckling and vibration than the typical constrant sitffness sandwich (CSS) used. To this extent, optimization algorithms are thoroughly searched in this work to find the one most suitable to the problem in hands. So, exploring the capabilities of these algorithms and its proper use on sandwich structures is also an objective of this thesis.

To reach these objectives, this work relies on the support of Matlab [9], Python scripts and the use of the finite element method through the Abaqus commercial software [10].

1.4 Thesis Outline

The present work has 6 chapters. The current chapter, Chapter 1, gives a brief context and motivation around composites structures and their importance in the aerospace world. It also briefly mentions variable stiffness composites as well as optimization algorithms.

Chapter 2, named *Background*, dives deeply on the composite sandwich topic, namely, its failure modes, manufacturing methods, theories that are often used for laminated composites and a review of

literature concerning the main types of analysis that this work studies: vibration and buckling. Furthermore, it introduces variable stiffness sandwiches more concretely, in terms of mathematical formulation.

Chapter 3 is the first chapter of results derived from the analysis done in this work. In summary, this chapter focuses on the structural behaviour of variable stiffness sandwiches. Studies concerning core stiffness influence and the impact of steered fibers on the structural performance are done and corresponding results analysed.

Chapter 4 gives an holistic overview of optimization methods available and explains, in detail, the method chosen: genetic algorithm. It also explains how the different scripts interact to conceive a well-behaved optimization process.

Chapter 5 is the second chapter of results, this time concerning the optimization process. Discussion of the results is also made in this chapter.

Chapter 6 presents conclusions of the work made and future research that can be made following this work.

Chapter 2

Background

In this section, a contextualization of the world of variable stiffness composites is given. Firstly, a definition of variable stiffness composites is given in relation to its orientation, in mathematical terms. Then, manufacturing techniques of variable stiffness composite laminates used in VSS are introduced and discussed, as well as the inherent constraints of these types of processes. Sandwich failure modes are presented, along with its relation to variable stiffness composites. A brief theory description is made in relation to the most commonly used theories for modelling laminated composite plates, namely the Classical Laminated Plate Theory and the First-Order Shear Deformation Theory, as well as a discussion of vibration and buckling structural analysis. Moreover, when appropriate, literature review, namely in the field of VSS, is highlighted in the various subsections.

2.1 Variable Stiffness Sandwich

Traditional sandwich structures are composed of composite laminates as face sheets, as a stacking of straight fiber-reinforced laminas (i.e. constant stiffness composites). However, in recent years, there has been an evolvement in relation to more ambitious sandwiches such as VSS due to its capability of extending the number of possible and better solutions. Variable stiffness sandwiches can be achieved through a variety of methods, as stated previously. Among those methods, the most common is the variation of the fibers orientation within each lamina, used in the composite laminates face sheets, which is also the technique used in this work.

The fiber path definition is expressed in a mathematical equation where θ is the fiber orientation in a given location. In the literature, there are a lot of options regarding this definition. Huang et al. [11], for example, defines the fiber orientation in two different ways, depending on whether the path function is linear (equation 2.1) or quadratic (equation 2.2), where the path function is expressed as $z = f(x, y)$ and the a_n parameters are the coefficients of each term of the path function ($n = 1, 2$ for linear definition and $n = 1, 2, 3, 4, 5$ for quadratic definition).

$$\theta(x,y) = \begin{cases} \arctan\left(-\frac{a_1}{a_2}\right), & a_2 \neq 0 \\ \frac{\pi}{2}, & a_2 = 0 \end{cases} \tag{2.1}$$

$$\theta(x,y) = \begin{cases} \arctan\left(-\frac{a_1+a_3y+2a_4x}{a_2+a_3x+2a_5y}\right), & a_2 + a_3x + 2a_5y \neq 0 \\ \frac{\pi}{2}, & a_2 + a_3x + 2a_5y = 0 \end{cases} \tag{2.2}$$

A more complex definition is given by Wu et al. [12], where reference points are previously selected so that, by using Lagrangian polynomials, the interpolation of the fiber angles at these points establishes the fiber orientation as follows:

$$\theta(x,y) = \sum_{m=0}^{M-1}\sum_{n=0}^{N-1} T_{mn} \cdot \prod_{m\neq i}\left(\frac{x-x_i}{x_m-x_i}\right) \cdot \prod_{n\neq j}\left(\frac{y-y_j}{y_n-y_j}\right) \tag{2.3}$$

where T_{mn} is the reference points (x_m, y_n) fiber angles.

Falcó et al. [13] makes use of trigonometric functions, namely the sine function, to represent constant curvature path on the lamina, as shown:

$$\sin\theta = \sin T_0 + (\sin T_1 - \sin T_0)\frac{x}{d} \tag{2.4}$$

where T_0 and T_1 are the fibers angles at the center of the panel and at $x = d$, respectively, being d a characteristic length of the plate in the x direction.

Despite all the options available, such as the ones given previously, in this work the fiber orientation is defined by a linear function. The reason to adopt such definition herein is not only its ease of implementation given its simplicity, but also the fact that it is the most commonly used definition in the literature, compared to other alternatives. Another advantage of using this definition concerns the optimization task, which benefits from having a lower number of design variables than other definitions. The general linear formulation starts with a value of T_0 from a reference point A, which is the center of the plate, changes along an axis x', that is rotated of an angle ϕ from the coordinate x axis, and finally reaches the final fiber angle value T_1 at $x' = d$, being d the distance from the reference point A [14]:

$$\theta(x') = \phi + (T_1 - T_0)\frac{|x'|}{d} + T_0 \tag{2.5}$$

The value of ϕ is taken as being 0 in this work. A visual representation of the linear orientation definition is given in figure 2.1.

In this work, the linear variation definition along the x' direction, that is, where the orientation θ depends only on the x' coordinate (note: $x' = x - a/2$, with $\phi = 0$), is used. This definition is mathematically expressed in equation 2.6.

$$\theta(x') = (T_1 - T_0)\frac{|x'|}{a/2} + T_0 \tag{2.6}$$

where $d \equiv a/2$ (valid for $\phi = 0$, which is the case adopted in this work), being a the length of the plate

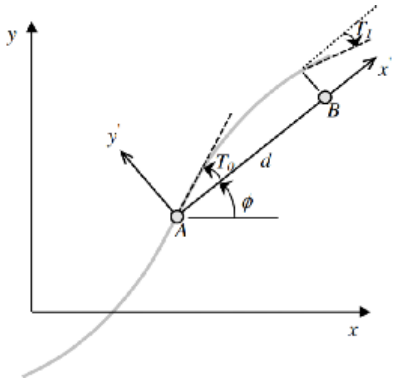

Figure 2.1: Linear fiber orientation definition [15].

$(-a/2 \leq x' \leq a/2 \Leftrightarrow 0 \leq x \leq a)$.

In terms of notation, a variable stiffness lamina is represented by $<T_0, T_1>$, where T_0 is the fiber angle at the center of the lamina ($x' = 0$) and T_1 the fiber angle at $x' = a/2$, where a is the length of the plate in the x direction.

2.2 Manufacturing Methods and Constraints

In the composites industry, as in other industries, the manufacturing processes are of great importance due to its financial impact. Thus, any manufacturing method must be feasible in a mass production context and must be able to conceive products with the least possible defects. Bearing this in mind, caution must be taken to integrate, at least to some degree, realistic constraints concerning the manufacturing process, which is discussed later in this work.

Since the fabrication of sandwich structures are greatly standardized nowadays and come as no relevant novelty, this section will focus more on the production of the composite laminates face sheets, which due to its variable stiffness characteristic, poses new challenges to the manufacture of this type of composites. Nonetheless, some sandwich manufacturing processes are presented and briefly described.

2.2.1 Variable Stiffness Composites

There are currently two main techniques to implement a given path orientation definition: the shifted method and the parallel method. In the shifted method, the reference path is simply copied along a direction, in a translation movement. This allows for greater feasible designs, a greater stiffness variation when compared to the parallel method and makes the implementation of curvature constraints simpler. The main disadvantages of this method are the possible formation of gaps and overlaps, which in turn cause a variation in the thickness of the laminate. The parallel method consists in the placement of a given course that is in exact contact with adjacent courses. A course is a group of fibers that are placed at the same time by the manufacturing machine. This allows, unlike the shifted methods, for the fabrication of plies with no gaps or overlaps. However, a great disadvantage of the parallel method

is that it may occur that some courses have a significant high curvature, especially in plies with high stiffness variation, which in turn makes some designs with this method unfeasible due to manufacturing constraints. Figures 2.2 and 2.3 illustrate both these methods.

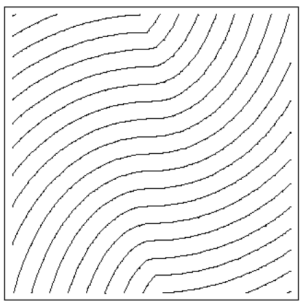

Figure 2.2: Parallel fiber method [16].

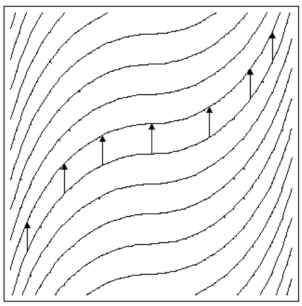

Figure 2.3: Shifted fiber method [16].

The main manufacturing processes of variable stiffness composites (face sheets) are: automated fiber placement (AFP), continuous tow shearing (CTS) and tailored fiber placement (TFP). A brief description of each one is done in this subsection to illustrate the effort involved in the manufacturing area to conceive VSC as accurately as possible.

Automated fiber placement

Automated fiber placement (AFP) originated in the 1980s from the combination and improvement of two previously existing processes: the automated tape laying (ATL) and the filament-winding. It emerged to overcome precisely the weaknesses of these two processes.

In this process, the laying of prepreg tow is done by using a computer, which has as result a high-speed and efficient production of laminates with curvilinear fibers. Each unit of fiber in a course is called a tow. The multiaxis AFP machine follows the exact contour of the mandrel and keeps the delivery head in contact with the tool. The delivery head can lay down up to 32 parallel tows at the same time. A loaded roller is used to compact the tow as they are placed [17]. An example of a fiber placement machine head is presented in figure 2.4.

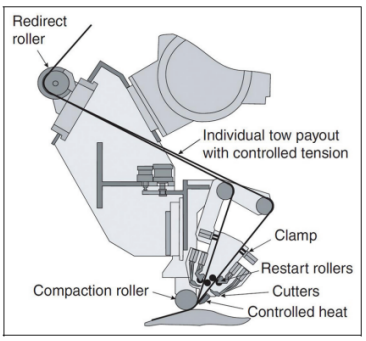

Figure 2.4: Head of an AFP machine [18].

Although the AFP process is widely used in different applications, it has some concerning drawbacks, namely in what relates to the manufacturing of VSC. The most notable disadvantage is the fact that it

cannot reproduce faithfully the fiber orientation given by the shifted method or the parallel method. This is due to the process-induced defects inherent to the AFP method, such as the formation of gaps and overlaps. In the shifting method using the AFP process this is more noticeable: since the reference path is shifted in a given direction, the same course has different curvatures on the inner and outer edges, causing a mismatch between two adjacent courses and, thus, the formation of overlaps or gaps [19]. In general, the AFP, when following the curved tow path, causes the inner side of fibers to buckle and the outside to stretch, originating defects.

Continuous tow shearing

Continuous tow shearing (CTS) emerges as an alternative to the AFP with a new way of handling the fiber orientation deposition, where in-plane shear deformation is used. The continuous shearing of a tow avoids the development of fiber buckling and straightening present in the AFP case [20]. This is especially important in the shifted method, because the gaps or overlaps that would be visible if the AFP method was used are completely avoided and therefore the fibers can follow accurately the fiber orientation definition. However, it must be clear that to achieve this, the tow deposition is slower than the AFP case. In figure 2.5, the differences between the lamina formed with the AFP and CTS processes are illustrated.

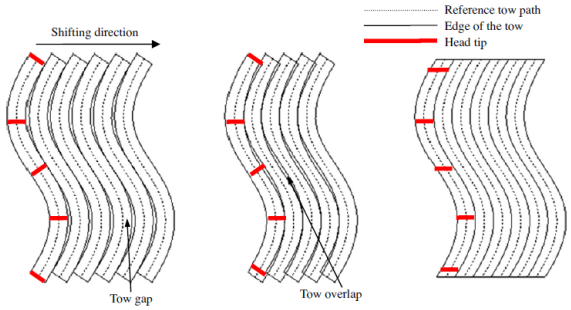

Figure 2.5: Differences between AFP and CTS methods. The figure on the left represents AFP process where gaps are formed; the middle figure illustrates AFP process where overlaps are formed; the right figure represents the CTS method where no gaps or overlaps are formed [20].

Assuming that a shifted method is used, and since the CTS process avoids or at least it decreases the probability of gaps and overlaps, the model created and explained later in this report does not take into account these particular defects.

Tailored fiber placement

Tailored fiber placement (TFP) is a variant manufacturing method of the AFP process. It emerges, as the CTS technique, as an alternative to the most used AFP process. Its embroidery preform manufacturing nature allows for the use of any fiber roving, that is, carbon, glass and aramid for example, unlike the 3D printing, that has a limited number of materials that can be used. Curves that can be previously programmed in a 2D space receive the continuous roving, which is fixated by a stiching yarn onto a flat textile base material. The combination of the rotation of the roving pipe with the movement, in

two perpendicular directions, of the base material allows for the roving to be placed according to a fiber orientation definition given by the designer [21].

The TFP process, known as well as dry tow placement in some articles, has the advantage at preserving the finished preform for an unlimited amount of time, as long as it is preserved at room temperature. Even though overlaps and gaps can still occur in TFP, as it occurs in AFP, these defects can be mitigated through the rearrangement of fibers within the dry tow. On the other hand, new defects may appear due to, for example, some irregularities that can be present in the fabric, such as wrinkles, because of the tension provoked by the stiching yarn. This causes the poorly fixation of the laid tows on the substrate. Moreover, the tension force caused by the machine head, that does not have a tow feeding mechanism to pull the tows, increases the buckling phenomenon inside the tow path and a gap area appears in the outside of the tow path [22]. Figures 2.6 and 2.7 illustrate these particular defects of the TFP process.

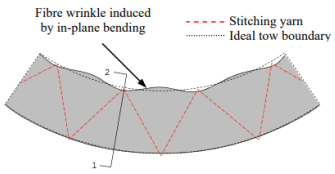

Figure 2.6: Ideal tow deformation in TFP process. [22].

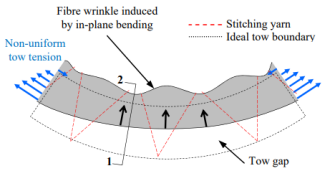

Figure 2.7: Real tow deformation in TFP process. [22].

2.2.2 Sandwich

Since there are a lot of different types of core structures, as seen in figure 2.8, the manufacturing method of sandwich panels differs from case to case. The range of options available to manufacture such structures is vast but commonly used techniques include the prepreg lay-up, wet lay-up and adhesive bonding.

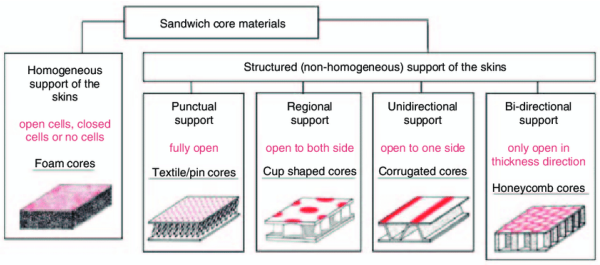

Figure 2.8: Sandwich core materials classification [23].

The prepreg lay-up and the wet lay-up are one-step methods to manufacture sandwich structures. The prepreg lay-up makes use of prepregs that ensure the good impregnation of the reinforcement, being the resins of better quality in terms of properties than those used in wet lay-up. The face sheets prepregs, after being made, are then directly laid on the core's surface, in which a primer (usually, resin) can be applied to promote a good adhesion to the faces without any need for an adhesive film. Then, the whole structure is subjected to cure. The main difference between these two methods is that the prepreg

lay-up uses fabrics of composite with pre-impregnated resin, commonly referred as prepregs, and, thus, there is no need to impregnate manually and separately the resin in the fabric as in the wet-layup case.

Adhesive bonding is another method where layers of adhesive are placed between the face sheets and the core, being the whole structure subjected to a determined temperature and pressure required by the adhesive resin. For better structural performance, a vacuum bag and autoclave are also typically used. An advantage of adhesive bonding is that it can be used with practically any type of materials of core and face sheets, especially in cases where there is no alternative to this method, which can, for example, happen when faces are not from polymeric materials [24].

2.2.3 Curvature Constraint

There are many types of manufacturing defects that inevitably originate constraints on those processes. As described before, these defects vary from process to process. Although this work assumes that no overlaps or gaps are formed, assuming a CTS technique, there is still one type of constraint that is practically universal in all manufacturing processes of VSC, which is, in fact, implemented in the optimization process model: curvature constraint.

Not only this curvature constraint is implemented to give a realistic approach to the results, but also to prevent fibers from kinking (local shear deformation failure mode of the matrix). This is done by limiting the curvature of the fibers to a pre-defined maximum value. The general formula for the curvature of a single variable function, $f(x)$ is given by equation 2.7:

$$K = \frac{\frac{d^2 f}{dx^2}}{\left(1 + \left(\frac{df}{dx}\right)^2\right)^{3/2}} \tag{2.7}$$

The first derivative of the function that defines the fiber path is $df/dx = tan(\theta(x))$. Moreover, considering that this definition is antisymmetric about the y-axis (which is vertical since $\phi = 0$), only the curvature of half the plate needs to be computed, which is very convenient in terms of computation time, namely in the optimization process. Substituting equation 2.6 in $f(x)$ in equation 2.7 gives rise to the curvature equation 2.8 used in this work:

$$K = \frac{2(T_1 - T_0)}{a} \cos\left((T_1 - T_0)\frac{|x'|}{a/2} + T_0\right) \tag{2.8}$$

In the literature, there are a multitude of values assigned to the curvature constraint. Some authors, such as Akhavan and Ribeiro [25] and Waldhart [26], use 3.28 m^{-1} for the maximum allowable curvature. Blom [27] uses the value of 1.57 m^{-1} to replicate the limitations of a typical fiber placement machine. Furthermore, Kim et al. [28] reports that the curved paths used in the CTS process show a curvature 10 times bigger than the typical curvature exhibited by paths produced with the AFP process. Nonetheless, most values of curvature constraint available in literature are associated with the AFP process. Due to the lack of information concerning curvature values for CTS process, even though it allows the production of high curvature paths, in this work the value of $3.28m^{-1}$ is used in optimization process, as in [25, 26].

2.3 Sandwich Failure Modes

When analysing and designing a composite sandwich structure, it is of utmost importance to guarantee that the conceived structure is capable of resisting certain load scenarios to avoid failure. In this respect, careful thought must be taken in the assessment of sandwich failure modes, since these structures can fail in a multitude of different ways.

Structure failure in a sandwich structure can be caused by geometry factors as well as material properties of the face sheets and core. In the case of VSS, extra caution must be taken, since the presence of a variable fiber orientation introduces some novelties in the structure mechanical behaviour. The presence of a low density and stiffness core in comparison with the face sheets, adding to the fact that typically the thickness of the core is much higher than the thickness of face sheets in a sandwich structure contribute to the occurrence of failure modes more often than straight fiber configurations, thus the need for a careful design, namely of the fiber orientation law. Nonetheless, VSS suffer from failure modes derived from the same mechanical principals as conventional constant stiffness composite sandwich [29]. The main sandwich failure modes include face wrinkling, face dimpling, general buckling and shear crimping.

Face wrinkling, for instance, is a short wavelength instability that occurs more often in sandwich structures composed of a low density and stiffness core with a considerable thickness with thin facesheets. Face dimpling is another type of local instability which can occur in sandwich structures with a honeycomb core, for example. The onset and wavelength of face dimpling depends of the core cell size [30]. Shear crimping is a failure mode characterized by sudden shear failure of the core, due to its low shear stiffness, being a short wavelength buckling, where transverse shearing dominates rotation in what concerns displacement. Illustrative examples of these failure cases are represented in figure 2.9.

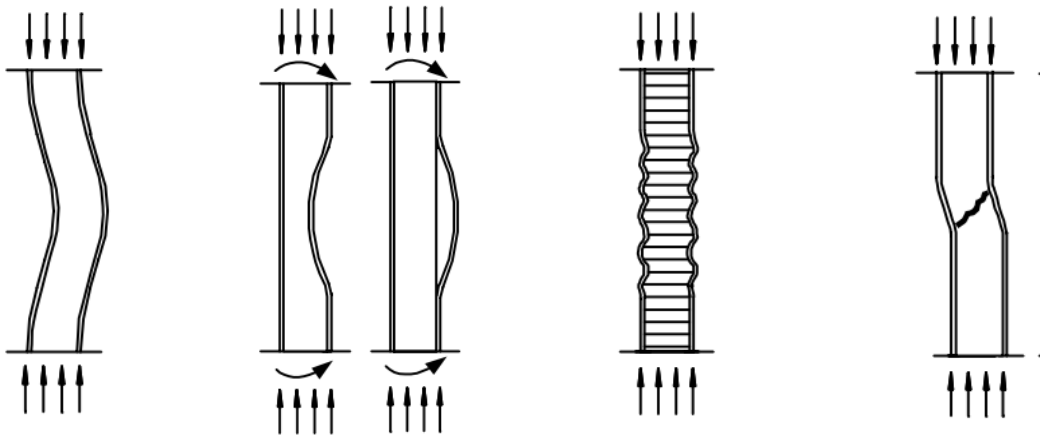

(a) General buckling. (b) Face wrinkling. (c) Face dimpling. (d) Shear crimping.

Figure 2.9: Examples of typical failure modes of sandwich structures [31].

Vescovini and Dozio [32] report that these type of failures, when in the presence of thick variable stiffness panels, are predominantly related to core crushing and it occurs more often than in straight fiber configurations, due to the fact that in VSS the fiber steering causes load redistribution. Thus, in this work [32], specific combinations of parameters in the orientation law are carefully selected so that these

chosen VSS achieve their purpose of being an improvement over traditional configurations, rather than being worse, which would happen in the presence of a failure mode.

Phenomenons such as shear crimping, where transverse shear effects are significant, become more common when composite sandwich structures are used, due to the significant difference between its transverse shear stiffness and in-plane stiffness, as demonstrated by Coburn and Weaver [33]. Moreover, in this work it is also also concluded that the stress redistribution that occurs in VSS causes a increase in the load applied in some areas which in turn can be superior to the local critical load, contributing to an even faster onset of shear crimping than in the case of straight fiber configurations.

2.4 Laminated Plate Theories

Since sandwich panels studied in this work are a type of structure that includes laminates as face sheets, it is of interest to briefly describe the most common theories behind the characterization of such laminates, which are also present in commercial finite element software. From the vast list of theories developed over the years, two of the more simple theories are still very relevant today: the classical laminated plate theory and the first-order shear deformation theory, both being equivalent single-layer theories (ESL).

2.4.1 Classical Laminated Plate Theory

The most simple theory in ESL is the classical laminated plate theory, which is an extension of the classical plate theory applied to composite structures. In this theory, some assumptions are made, which are known as Kirchhoff hypothesis [34]:

1. Directions orthogonal to the midplane of the laminate remain straight and rotate in order to remain orthogonal to the deformed mid-plane (thus, $\varepsilon_{xz} = 0$ and $\varepsilon_{yz} = 0$).

2. These orthogonal directions (transverse normals) are inextensible (i.e, $\varepsilon_{zz} = 0$, where z is in the thickness direction).

Besides the Kirchhoff hypothesis, further assumptions are made, namely: 1) all laminas are perfeclty bounded together; 2) the lamina's material are linearly elastic and may be, in the general case, orthotropic, where one of the material principal directions of orthotropy is orthogonal to the mid-plane; 3) the thickness of each lamina is uniform; 4) it is assumed infinitesimal strains are considered, i.e., $|\varepsilon_{ij}|<<1$; 5) no applied transverse shear stress on top and bottom surfaces.

With this theory formulation, the displacements field takes the following form:

$$\begin{aligned} u(x,y,z,t) &= u_0(x,y,t) - z\frac{\partial w_0}{\partial x} \\ v(x,y,z,t) &= v_0(x,y,t) - z\frac{\partial w_0}{\partial y} \\ w(x,y,z,t) &= w_0(x,y,t) \end{aligned} \tag{2.9}$$

where u_0, v_0 and w_0 are membrane displacements on the plane $z = 0$.

The CLPT is particularly suitable for plates with a side to thickness ratios of 100 or higher, i.e., very thin laminates.

2.4.2 First-Order Shear Deformation Theory

The first-order shear deformation laminated plate theory (FSDT) is derived from the same assumptions as the classical laminated plate theory but with one of the Kirchhoff hypothesis relaxed: transverse normals, once rotated, no longer need to remain perpendicular to the deformed midplane. With this hypothesis relaxed, the FSDT accounts for transverse shear strains, unlike the classical plate theory. The vertical displacement w is still independent of the thickness coordinate z since the assumption of inextensibility of transverse normals still holds.

With the former in mind, the displacements field for FSDT is the following [34]:

$$\begin{aligned} u(x, y, z, t) &= u_0(x, y, t) + z\phi_x(x, y, t) \\ v(x, y, z, t) &= v_0(x, y, t) + z\phi_y(x, y, t) \\ w(x, y, z, t) &= w_0(x, y, t) \end{aligned} \tag{2.10}$$

where u_0, v_0 and w_0 are still the membrane displacements on the plane $z = 0$, in addition to ϕ_x and ϕ_y, unknown functions that are to be determined, which represent the rotations of a transverse normal about the y and x axes, respectively.

The accuracy of FSDT can hold for plates with a side to thickness ratio of 50 or higher, in which case the rotation functions ϕ_x and ϕ_y approach the respective slopes of the transverse deflection, that is, $\phi_x = \partial w_0/\partial x$ and $\phi_y = \partial w_0/\partial y$, thus converging to CLPT.

It is important to note that these two theories, although being accurate in the specific case of thin laminates, are, in the general case, not adequate, especially in the case of soft core sandwiches. This topic is further explored in section 3 of this work.

2.5 Structural Analysis

2.5.1 Vibration

The study of a system's dynamic response is one of the most important aspects of structural analysis since it allows to determine the natural frequencies of the structure as well as its modes, that is, the way the system deforms at those frequencies. The knowledge of the natural frequencies of a system is crucial considering that an exterior perturbation on the system at one of these frequencies causes the structure to excite and enter a phenomenon called resonance, where the amplitude of the system's response increases continuously at that frequency, leading to an inevitable structural failure. In addition to the possible onset of structural failure, there are other negative aspects related to vibration, such as the associated noise levels and the reduction of the structural life and performance. Due to such

reasons, vibration is often considered an undesirable phenomenon and usually a designer takes this into account when conceiving a structure, i.e., the structure is designed such that its natural frequencies are safely and reasonably distant from the expected frequencies to be encountered from an exterior perturbation in the desired application of the structure.

Typically, when studying dynamic phenomena, the first frequency, commonly known as fundamental frequency, is the most important frequency to be determined, although the remaining higher frequencies can be of interest as well, depending on the context. The objective is to maximize or minimize the fundamental frequency when designing a structure.

Regarding the aerospace topic, vibration is a crucial factor since, for example, an airplane, namely its wings, are constantly subjected to dynamic stresses induced by the air's turbulent flow. If the frequencies of the turbulent flow are close to the natural frequencies of the wings, catastrophic structural failure such as flutter may occur. Thus the need for a careful design and, especially, a reliable optimization process of the vibration characteristics of the airplane's structural components. As reported by Pastel et al. [35], typically it is expected that high frequency external perturbations cause less structural problems to the wing since these higher modes have, normally, low response amplitude. The vortices formed by turbulent airflow around the wing can cause low frequency vibration phenomena. Thus, since more extreme dynamic stresses are induced at lower frequencies and since the objective is that the structure to be conceived can be used in aerospace applications, the optimization process in this work aims to maximize the fundamental frequency of the structure.

The general equations of motion to model the vibration phenomenon in a multiple degree-of-freedom (N-DoFs) system are the following, in matrix form:

$$[M]\{\ddot{x}\} + [C]\{\dot{x}\} + [K]\{x\} = \{f(t)\} \tag{2.11}$$

where $[M]$ is the mass matrix, $[C]$ is the damping matrix, $[K]$ is the stiffness matrix and $\{f(t)\}$ is the force applied to the system.

In the case of an undamped free vibration both the damping matrix and the force term are null ($[C] = 0$, $f(t) = 0$). As a standard approach, the free vibration response, $\{x(t)\}$, is considered in the following form:

$$\{x(t)\} = \{X\}\sin(\omega t) \tag{2.12}$$

where $\{X\}$ is the amplitude vector.

Substituting equation 2.12 in line with the special case of undamped free vibration in equation 2.11, the following equation is obtained:

$$([K] - w^2[M])\{X\} = 0 \tag{2.13}$$

which is a eigenvalue and eigenvector type of problem, where ω are the undamped natural frequencies of the system (eigenvalues) and $\{X\}$ are the undamped normal modes (eigenvectors).

In upcoming paragraphs, a literature review concerning vibration analysis of VSS and variable stiffness laminates (VSL) is done with the aim of providing an updated state of the art. To the author's knowledge, after the examination of papers available, a conclusion was reached that the investigation information regarding VSS is scarce in comparison with the research done on VSL. Nevertheless, although the main topic of the present work focuses on VSS, research on VSL is also presented due to its relevance to the formulation of robust VSS models.

Tornabene et al. [36] conducts a vibration analysis over foam core variable stiffness composite sandwiches by employing a combined structural theory that consists of an equivalent single layer approach based on the Carrera Unified Formulation. Moreover, in this work, to enhance and enrich the model, it is also added the Murakami's function to capture some particular effects related to soft core sandwich structures, with the vibration problem being solved numerically through the Generalized Differential Quadrature method. For more details on the theories and methods cited, see Tornabene et al. [36]. In what concerns the definition of the curvilinear fiber orientation definition, in this work, different functions are used including the sine-wave, exponential and power-law distributions. It was concluded that the use of variable stiffness laminates as face sheets of sandwich structures can indeed vary quite significantly the vibration response and that there is room for further exploration of the capabilities of this type of structure.

Loja et al. [37] studied and optimized the structural behaviour of laminated plates in vibration (also in statics and buckling). To this end, it is used a first order shear deformation theory coupled with an adaptive hybrid optimization approach. The fiber paths are defined through a linear fiber orientation law in the study of three-ply laminates. In what relates to the vibration response, in this work it is concluded that, for simply supported boundary conditions, the optimal fundamental frequency can be designed to be 5.61% higher than traditional constant stiffness laminates.

A variable kinematic model is adopted by Vescovini and Dozio [32] to study the structural performance of variable stiffness laminate plates and variable stiffness sandwich structures. Two types of path fiber orientation laws are used: orientation angle varying along x and orientation angle varying along y. In either case, the linear fiber orientation law is used. In terms of sandwich materials, this work makes use of a sandwich structure with a low density and a high density core subjected to multiple boundary conditions. The results obtained using the proposed model are compared with other literature data and it is concluded that the model presented a good accuracy.

Another VSL vibration study was conducted, by Akhavan and Ribeiro [25], through the development of a p-version finite element based on the third-order shear deformation theory. A linear fiber orientation law is also used and manufacturing constraints are included, namely in terms of curvature, that create more realistic laminates. The study concludes that the introduction of a varying fiber orientation induces changes in the mode shapes that are typically seen in constant stiffness laminates, as well as an increase or decrease (depending on the parameters used that define the VSS configuration) of the natural frequencies value.

Honda and Narita [38] use spline functions to define the fiber orientation, where the fibers assume a quasi-quadratic, quasi-cubic or an arbitrary shape based on those spline functions. It is employed

a Ritz solutions to formulate frequency equations. In the end, this work notes that the vibration mode shapes given by curvilinear fibers are very particular to these types of structures and very different from traditional laminates. In fact, it is also stated that the mode shapes are similar to the fiber shape analysed and that this effect vanishes when symmetric layers are introduced. Moreover, it is mentioned that, depending on which boundary conditions are applied, VSL can perform better or worse, in vibration behaviour, in comparison with traditional laminates.

When papers present studies regarding vibration, it is usually related to a linear vibration analysis. However, for example, Houmat [39] presents a geometrically nonlinear vibration analysis on variable stiffness composite plates, based on the assumptions of Von Kármán's nonlinear thin plate theory, and compares its results to the usual linear vibration analysis. The inclusion of non-linearities in the model causes the laminate to exhibit a hardening behaviour, whose effect can be seen, as the laminate is subjected to dynamic stresses in the nonlinear regime, in the increase in frequency required to cause an increase in amplitude. In fact, in this work it is reported that the difference between the nonlinear and linear results can be as high as 20%, mostly due to the hardening phenomenon, which is more intense in the antisymmetric laminate case. This work also comes to the conclusion that antisymmetric laminates have a lower performance, that is, lead to a slightly lower fundamental frequency values than symmetric laminates, both in a linear and nonlinear vibration analysis. The main conclusion is that the optimal fundamental frequency, within a linear or a non-linear analysis, is a result of the same optimized laminates, even if the value of the fundamental frequency itself is different for each type of analysis. In the end, the VSL thus designed demonstrate the improvement capability over CSL.

2.5.2 Buckling

In addition to the study of a structure's dynamic response, the knowledge of the instability behaviour of a system when subjected to certain load scenarios emerges as an equally important factor to be accounted for in the design phase. The instability phenomenon, very frequently referred to as buckling, is characterized by a sudden change in the deformation shape of the structure. When subjected to a compressive loading, the system enters an equilibrium compression state; however, for certain values of applied force this equilibrium can be disrupted and a static instability (buckling) occurs, where sudden transverse displacements dominate, leading to an abrupt bending of the structure and, as consequence, an extreme decrease in structural performance. The value of force that causes the onset of the buckling phenomenon is called the critical buckling load and, as the fundamental frequency in the vibration case, is one key factor to be determined in any structural system under analysis.

In the aerospace environment, buckling can affect the wings if these are not designed to account for this instability occurrence. Due to its great flexibility, bending is induced in the wings because of the difference of pressure between the lower and upper wing's surfaces, originating lift, which in turn bends the wing in the upper direction. This bending action gives rise to a compression state in the upper surface and a tensile state in the lower surface. In a scenario where the bending of the wing is significant, the compression loads present in the upper surface could surpass the critical buckling load

of the structure. In addition to this, wing skins are usually thin and slender, that is, the thickness is much smaller than the other dimensions, which contributes to the buckling manifestation. One solution that is employed in the aeronautic industry is the use of closely space ribs in wings. This allows to reduce the characteristic length associated to the skin panels, effectively increasing the critical buckling load of such structures. The skin panels are, in this way, more robust to the onset of buckling. However, there is still the need for the maximum effort in the material selection for the wing as well as its geometry to avoid this phenomenon, since these are the two main factors for the instability occurrence. More precisely, it is of the designer's interest to increase as much as possible the critical buckling load so that the load needed for buckling to happen is higher (and, in this way, much harder to reach), therefore delaying the beginning of this phenomenon to the greatest extent. Hence, the optimization process regarding the buckling case aims to maximize the critical buckling load.

Euler's critical load formula is one of the most famous and used formulas in the calculation of buckling loads. This equation (2.14), although not directly applicable in most real cases, it gives an insight to a fast, simple first calculation of the critical buckling load of a structure.

$$P_{cr} = \frac{\pi^2 EI}{L^2} \tag{2.14}$$

where P_{cr} is the critical buckling load, E is the elastic modulus, I is the section moment of inertia and L is the characteristic length.

As in the vibration case, the more commonly used equation for buckling is one that reflects a eigenvalue and eigenvector problem. Unlike Euler's formula, the linear buckling formulation is widely applied to a variety of problems and is given, in matrix form, in the following way:

$$([K_0] - \lambda_i[K_\Delta])\{v_i\} = 0 \tag{2.15}$$

where $[K_0]$ is the stiffness matrix corresponding to the base state, $[K_\Delta]$ is the differential initial stress and load stiffness matrix due to the incremental loading pattern (also referred to as geometric stiffness matrix), λ_i are load multipliers (eigenvalues), v_i are the buckling mode shapes (eigenvectors) and the subscript i refers to the ith buckling mode [10].

As previously stated in the vibration subsection, research regarding VSS is rarer than VSL and that is also true when it comes to buckling analysis. Thus, literature related to VSS is presented as well as literature concerning VSL.

Some of the previous mentioned works, besides vibration analysis, also present buckling results. Vescovini and Dozio [32] is one of those cases, both in terms of VSL and VSS. In this topic, before a parametric study is done, a preliminary analysis is made to comprehend how the failure modes, namely local core crushing mechanisms, emerge on thick variable stiffness sandwich depending on the fiber's curvature. Furthermore, this type of behaviour is magnified by the fiber steering component of VSS which worsens the buckling performance. Regarding the theories studied in this work, it is concluded that the layerwise theory, derived from the variable-kinematic approach, using Carrera's Unified Formulation and the Ritz method, is indeed necessary when analysing a sandwich with low density cores, which have

low transverse shear stiffness, and that equivalent layer theories become inaccurate in these cases.

Similarly, Loja et al. [37] also obtains buckling results regarding only VSL, with the goal of optimizing the buckling performance, namely the maximization of the critical buckling load. For the optimization of a single layer VSL, it was possible to conclude that the optimized VSL solution improves the critical buckling load by almost 16%, in an uniaxial compression state, and by 43.448%, in a biaxial compression state, in comparison with CSL, when simple supported boundary conditions are used. In what concerns the optimization of a three layer VSL, similar results are obtained, that is, VSL improve the buckling performance over traditional laminates.

Coburn and Weaver [33] use a piecewise linear method for the fiber orientation law, with the sandwich panel being modelled as a Mindlin-Reissner two-dimensional plate, which accounts for transverse shear flexibility. In this work, the Ritz method is used to formulate the eigenvalue and eigenvector problems that model the buckling behaviour. In addition, a parametric study is performed by varying the parameters that govern the fiber orientation law. It was concluded that local instabilities occur more often in VSS when the sandwich core is of low density, which can make the buckling performance of VSS worse than classical sandwich.

Chen et al. [40] implemented a new method based on a modified extended high-order sandwich plate theory coupled with a Rayleigh-Ritz procedure to formulate the equations than govern the buckling problem in VSS. The theory converged to the same values of case studies available in literature and it is also concluded that VSS can improve buckling performance. However, for some cases such as certain fiber orientation laws or core density, there is an onset of different instabilities that cause this performance to greatly decrease.

Vescovini et al. [41] presents a new unified tool based on the combination of a sublaminate generalized unified formulation and the Ritz method with the objective of, not only analysing the instability behaviour of VSS, but also, in the more general case, providing a method of improved efficiency to study structural response. The parametric study done aimed at gaining knowledge about the way a sandwich with VSL as face sheets reacted to different boundary conditions and loads in a buckling scenario and how instabilities emerge and its consequence on the performance, revealing that the proposed method is in line with the results obtained in other research, while being time efficient.

Chapter 3

Structural Behaviour of Variable Stiffness Sandwich

This section is dedicated to the deep analysis of the structural behaviour of VSS. First, a study is done on how the stiffness of the core affects the structural performance of both variable stiffness and constant stiffness composite sandwich configurations. Then, additional analyses are made: one where the impact of the fiber variation is studied where the sandwich core is of high stiffness and another where the sandwich core is of low stiffness. The main focus is to do a parametric study, primarily with the low stiffness sandwich core since it is the most common case when using sandwich structures, in what concerns the orientation angle of VSS. To this extent, an indepth study of the structural characteristics of VSS with a soft core comprising statics, free vibration and various cases of buckling analysis is done. Furthermore, the model created and used to obtain the results is introduced in this section, as well as its validation, namely in vibration and buckling.

3.1 Model Implementation and Validation

The finite element commercial software *Abaqus* is used to create the model. In this case, three possible ways of modelling VSS structures are considered: a complete 3D element based model for both core and face sheets; an equivalent 2D single layer shell model comprising both core and face sheets; and, finally, a mixed model, where the core is modelled with 3D elements and the face sheets with 2D shell elements. After some experiments, the 3D model was discarded due to its high computational cost that would make the optimization process impractical. The equivalent 2D single layer shell model was also not chosen due to its inability to accurately represent the behaviour of the core. Indeed, the equivalent 2D single layer shell model uses assumptions that are more appropriate when using structures whose transverse flexibility is not high and its thickness is relatively small. In cases such as this one, where the core is both thick and possesses low transverse stiffness, the 2D model is not the most adequate. The former is also stated in Tornabene et al. [36]. Thus, to achieve a compromise between the computational cost and the accuracy of both the structure modelling and the results, a

mixed model is used, where the core is modelled with 3D elements to account for its high thickness and transverse flexibility and the face sheets are modelled with 2D shell elements, due to its low thickness and flexibility.

It is also worth noting that in this work the structure is completely modelled, that is, a symmetric structure with half the elements is not used because the use of a complete structure model is considered good practice, namely in the buckling and vibration analysis, to accurately capture both the symmetric and non symmetric modes. Regarding the type of analysis made, linear free vibration and linear buckling analysis, available in the *Abaqus* commercial software, are the ones chosen.

Figure 3.1 presents the general sandwich structure used, the general coordinate system and dimensions. In annex, visual representation of the loads applied in the different structural analysis made throughout this work are presented.

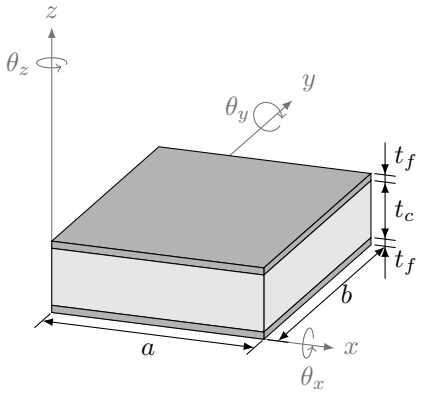

Figure 3.1: Illustrative representation of general sandwich structure used with a core (in light grey) and face sheets (in darker grey). General coordinate system and dimensions are also represented.

The model creation is done using *Python* scripts. The fiber orientation law is implemented through angle variation of the local coordinate system of each set of elements in the x direction (since, in this work, θ only varies according to x). So, at each element, the x coordinate of the centroid is calculated and the angle θ of the element in question is computed based on its centroid, being the angle constant in that element. Moreover, the compatibility between the 2D shell elements of the face sheets and the 3D elements of the core is assured with the use of *Abaqus* feature *Tie constraint*, which ties two surfaces together so that there is no relative motion between them, that is, the translation degrees of freedom of the nodes of the shell surfaces (face sheet) are equal to those of the 3D surface (core). Note that the shell mid-plane is used as the reference plane, being the shell translated half its thickness from the core top and bottom surfaces. Although the nodes visualized are those of the mid-plane, which are present in the tie constraint, the *Abaqus* software accounts for the shell thickness.

In what concerns the type of elements used, S8R (eight node shell element) elements are used for the face sheets while C3D20R (twenty node solid element) elements are used for the core. These types of elements use reduced integration, which minimizes the shear locking effect in the transverse shear deformation components of the element's stiffness matrix and, in addition, also reduce the computational time required when comparing to full integration elements. The choice of quadratic elements instead of linear elements is explained by the fact that the second order nature formulation of quadratic elements,

besides being less prone to shear locking, allow for a better representation of the geometry, namely curved surfaces (that can be present as a post deformation consequence).

The boundary conditions definition that is used in this work for buckling analysis follows the definition given by Hassan and Kurgan [42]: clamped boundary (C), which is free to have only in-plane displacements; simply supported boundary (S), which can have a free in-plane translation and also free rotation about its axis; free boundary (F), which is not restrained in any form. To this extent, the clamped boundary is achieved by forcing the vertical displacement of the nodes to be zero (i.e. $U_z = 0$) and also by forcing those same nodes to be coupled in terms of normal displacement, in order to maintain the boundary completely straight and vertical. For example, if the $x = 0$ boundary is clamped, then all nodes at this boundary have $U_z = 0$ as well as coupled y displacement (normal displacement). When applicable, that is to say in the face sheets, the nodes are also forced to have null rotation about the vertical axis ($\theta_z = 0$) as well as null rotation about the boundary direction (e.g., if $y = 0$ is clamped, then $\theta_x = 0$). In relation to simply supported conditions, the vertical displacement is set to zero ($U_z = 0$) and, when applicable in the case of the face sheets due to its shell nature, a null rotation about the normal axis of the boundary is also forced (e.g., for simply supported $x = 0$, $\theta_x = 0$ for all shell nodes in that boundary).

Is worth noting that the first two letters of a given boundary condition refer to the conditions applied to $x = 0$ and $x = a$ boundaries while the latter two letters refer to $y = 0$ and $y = b$. For example, CCSS represents clamped boundary condition on x boundaries and simply supported boundary condition on y boundaries.

In order to guarantee accurate results it is important, in any kind of analysis that involves finite elements, to do a mesh convergence study. To this extent, a sandwich structure whose face sheets are composed of four variable stiffness composite lamina is used as test case. In this regard, the fiber orientation values associated to each lamina (T_0 and T_1) are assigned in a way that allows the mesh convergence results obtained to be generalized to other values of T_0 and T_1. Bearing in mind that this mesh study is also valid for the optimization processes present later in this work, the VSS test case used does not follow the curvature constraint of the optimization processes, that is, the curvature present in some laminas in this example is higher than the allowed in the optimization. Nonetheless, this does not constitute a problem since VSS with higher values leads to a higher fiber orientation variation in the lamina. Thus, a more refined mesh is needed to achieve accurate results and a more regular and realistic representation of the fibers' orientation. The properties of the VSS used as test example are present in table 3.1.

Table 3.1: Properties of the variable stiffness sandwich structure test case used in the convergence study ($a/b = 1$, $a/t = 50$ and $t_c/t_f = 8$)

Face sheets		Core
Material	Configuration	Material
CFRP (table 3.7)	[<-20,60>,<-70,-10>, <30,50>, <40,-80>]	Core D (table 3.8)

The mesh convergence study here presented explores the influence of in-plane, in this case of both face sheets and core, and out of plane, in this case of only the core due to its 3-D element nature,

discretization (xy and z, respectively). Moreover, the test case is analysed in both vibration and buckling. Table 3.2 shows that both vibration and buckling results are not particularly sensible to changes in thickness discretization, especially in the comparison of results with 2 thickness elements with models with more than 2 thickness elements. Regarding the in-plane study, in order to achieve accurate results with a reasonable computation analysis duration as well as a continuous, regular and realistic representation of the fiber orientation path in each lamina, a mesh of 40×40 xy elements with 2 elements in the thickness of the core is chosen due to its compromise of the premisses previously presented.

Table 3.2: Mesh convergence study. Deviation values (in percentage) are in relation to the $150 \times 150 \times 2$ mesh results.

No. of in-plane elements	Fundamental frequency, f (Hz)				Critical buckling load factor (λ_{crit})			
	No. of elements in thickness				No. of elements in thickness			
	1	2	3	4	1	2	3	4
5×5	266.780 (1.099%)	266.780 (1.099%)	-	-	17.843 (2.380%)	17.843 (2.380%)	-	-
10×10	264.160 (0.106%)	264.150 (0.102%)	264.140 (0.099%)	264.140 (0.099%)	17.450 (0.126%)	17.449 (0.120%)	17.448 (0.115%)	17.448 (0.115%)
20×20	263.740 (0.053%)	263.730 (0.057%)	263.720 (0.061%)	263.720 (0.061%)	17.399 (0.166%)	17.398 (0.172%)	17.398 (0.172%)	17.398 (0.172%)
40×40	263.760 (0.045%)	263.750 (0.049%)	263.750 (0.049%)	263.750 (0.049%)	17.410 (0.103%)	17.409 (0.109%)	17.409 (0.109%)	17.409 (0.109%)
50×50	263.800 (0.030%)	263.790 (0.034%)	263.790 (0.034%)	-	17.416 (0.069%)	17.415 (0.075%)	17.415 (0.075%)	-
80×80	263.860 (0.008%)	263.850 (0.011%)	-	-	17.425 (0.017%)	17.424 (0.023%)	-	-
100×100	-	263.870 (0.004%)	-	-	-	17.426 (0.011%)	-	-
150×150	-	263.880	-	-	-	17.428	-	-

After guaranteeing that the results are mesh independent and realistically represent continuous and regular fiber paths, a model validation analysis is made involving both CSS and VSS to assure that the structural behaviour of the model in both vibration and buckling reproduces valid results and in accordance with the available literature information.

In terms of CSS, the vibration test case used is a sandwich structure with face sheets composed of only one constant stiffness lamina. The material used in the face sheets has properties $E_1 = 131.1\ GPa$, $E_2 = 6.9\ GPa$, $E_3 = 6.9\ GPa$, $\nu_{12} = 0.32$ $\nu_{13} = 0.32GPa$, $\nu_{23} = 0.49$, $G_{12} = 3.588\ GPa$, $G_{13} = 3.088\ GPa$, $G_{23} = 2.3322\ GPa$ and $\rho = 1000\ kg/m^3$ while the core's material has the following properties: $E_1 = 0.2208\ MPa$, $E_2 = 0.2001\ MPa$, $E_3 = 2760\ MPa$, $\nu_{12} = 0.99$ $\nu_{13} = 0.00003$, $\nu_{23} = 0.00003$, $G_{12} = 16.56\ MPa$, $G_{13} = 545.4\ MPa$, $G_{23} = 455.4\ MPa$ and $\rho = 70\ kg/m^3$. The sandwich structure has $a/b = 1$ and $t = 0.4$. Table 3.3 shows that for different constant stiffness composite face sheet configurations as well as for different core to face sheet thickness ratios (t_c/t_f) the model results are in line with the literature results, with very acceptable deviation values (around 1% or less).

Table 3.3: Model validation with constant stiffness sandwich structures in vibration. Results shown are a dimensionless frequency $\Omega = \omega a^2 \sqrt{\frac{\rho^{face}}{E_y^{face} t^2}}$

Face sheet configuration	h_c/h_f	Ref [43]	Present model	Deviation, %
[<45,45>]	2	3.950	3.908	1.060
	8	4.414	4.398	0.375
[<60,60>]	2	4.262	4.206	1.328
	8	4.536	4.519	0.371

.

As for the buckling validation, the square ($a/b = 1$) sandwich structure considered consists of an orthotropic soft core and face sheets composed of 10 cross-ply layers. The face sheet layers are made of a material with properties $E_1 = 19E$, $E_2 = E_3 = E$, $\nu_{12} = \nu_{13} = 0.32$, $\nu_{23} = 0.49$, $G_{12} = G_{13} = 0.52E$, $G_{23} = 0.338E$. The core's material has properties $E_1 = 3.2 \times 10^{-5}E$, $E_2 = 2.9 \times 10^{-5}E$, $E_3 = 0.4E$,

$\nu_{12} = 0.99\ \nu_{13} = \nu_{23} = 3.2 \times 10^{-5}$, $G_{12} = 2.4 \times 10^{-3} E$, $G_{13} = 7.9 \times 10^{-2}$, $G_{23} = 6.6 \times 10^{-2}$. The value that is used for E is $10\ \ GPa$. Once again, as in the vibration case, table 3.4 demonstrates that the model results are in accordance with the literature results for different thickness ratios with deviations of 0.5% or lower.

Table 3.4: Model validation with constant stiffness sandwich structures in buckling. The results shown are a dimensionless critical buckling load $\overline{N} = a^2 N_0 / (E_2^{face} h^3)$. N_0 is the compressive load along x.

a/h	Face sheet configuration	h_f/h	Ref [44]	Present model	Deviation, %
20	$[(<0,0>,<90,90>)_5]$	0.025	2.554	2.540	0.557
		0.050	4.659	4.640	0.411
		0.075	6.422	6.391	0.483
		0.100	7.897	7.860	0.461

In addition to CSS validation, it is necessary to validate the model in terms of VSS. Similarly to CSS, the model is validated in both vibration and buckling for VSS. The small deviations obtained (below 0.4%) for the vibration analysis of VSS, presented in table 3.5, demonstrate that the model is reliable for square ($a/b = 1$) sandwich structures with steered fibers in its face sheets as well as for different width to total thickness ratios (b/t).

Table 3.5: Model validation with variable stiffness sandwich structures in vibration, in terms of non-dimensional fundamental frequency $\overline{\omega} = 2\pi f a^2 t^{-1} \sqrt{\frac{\rho^{face}}{E_y^{face}}}$.

Core material	Face sheet configuration	b/h	ED2 [36]	ED4 [36]	LD1 [36]	LD2 [36]	Present model	Deviation, % (LD2)
Aluminium honeycomb [36]	[<0,45>, <-45,-60>, <0,45>]	10	3.682	3.361	3.311	3.309	3.296	0.390
		50	4.100	4.042	4.030	4.030	4.025	0.130
		100	4.143	4.114	4.108	4.108	4.098	0.250

The buckling validation analysis, whose results are shown in table 3.6, consisted in the testing of different variable stiffness composite face sheet configurations (composed of two layers) and also different core materials. The deviations obtained are all considerably low and acceptable (around 1%), demonstrating, once again, the robustness of the model used in this work, in this case in what concerns buckling.

Table 3.6: Model validation with variable stiffness sandwich structures in buckling ($b/t = 50$), in terms of nondimensional uniaxial x critical buckling force, $\overline{N}_x = \frac{N_x a^2}{E_x^{face} t^3}$.

Core material	Face sheet configuration	ED2 [32]	ED4 [32]	LD1 [32]	LD2 [32]	Present model	Deviation, % (LD2)
H Core (table 4.1)	[<0,30>, <0,-30>]	1.643	1.462	1.425	1.425	1.411	0.971
	[<0,60>, <0,-60>]	1.698	1.648	1.638	1.637	1.621	1.011
L Core (table 4.1)	[<0,30>, <0,-30>]	1.516	1.365	1.332	1.332	1.315	1.281
	[<0,60>, <0,-60>]	1.597	1.548	1.539	1.538	1.518	1.254

3.2 Core Stiffness Influence Study

The analysis of the relationship between the stiffness of the core and the results obtained, namely the possibility of the onset of particular failure modes, is one of the studies performed herein. To this extent, isotropic and orthotropic cores are used. In order to conclude about the effect of the variation of core's stiffness on the results, this study begins with a particular core material and, afterwards, alters its

properties to successively create new materials with progressively lower stiffness, both in the isotropic and orthotropic cases. The reference material (the first core of the isotropic table and the last core on the orthotropic table) for the isotropic case is a standard aluminium alloy [45] while for the orthotropic case the reference is an aluminium honeycomb [36]. The materials used are presented in tables 3.7, 3.8 and 3.9.

Table 3.7: Properties of the face sheet material used in the optimization processes [32].

	E_{11} (MPa)	E_{22} (MPa)	E_{33} (MPa)	ν_{12}	ν_{13}	ν_{23}	G_{12} (MPa)	G_{13} (MPa)	G_{23} (MPa)	ρ (kg/mˆ3)
CFRP	173000	7200	7200	0.29	0.29	0.29	3760	3760	3760	1540

Table 3.8: Orthotropic core materials used (ρ = 72 kg/m^3).

Core material	E_{11} (MPa)	E_{22} (MPa)	E_{33} (MPa)	ν_{12}	ν_{13}	ν_{23}	G_{12} (MPa)	G_{13} (MPa)	G_{23} (MPa)
Core A	4400	4400	1536	0.99	0.0000864	0.0000864	27000	36900	22200
Core B	4400	4400	1536	0.99	0.0000864	0.0000864	2700	3690	2220
Core C	0.44	0.44	1536	0.99	0.0000864	0.0000864	2700	3690	2220
Core D [36]	0.44	0.44	1536	0.99	0.0000864	0.0000864	0.27	369	222

Table 3.9: Isotropic core materials used (ρ = 2700 kg/m^3).

Core material	E (MPa)	ν
Core E [45]	70000	0.33
Core F	700	0.33
Core G	7	0.33
Core H	0.7	0.33

In every case of the results obtained presented on the following tables, all clamped boundary conditions (CCCC) are used and, in the buckling case, a normal compression force of 100 kN is applied. Each face sheet has one lamina.

Table 3.10 presents the results from the buckling analysis (x and y direction) of isotropic cores with different stiffness with variable stiffness composite face sheets in multiple configurations. The first observation that can be made is that, for the same $<T_0, T_1>$, the tendency, as expected, is that, with the progressively smaller values of the core's stiffness, the sandwich performance decreases in terms of critical buckling load, in both directions. Furthermore, in this analysis it is possible to conclude as well that pairs of configurations of the type $<T_0, 0>$, $<-T_0, 0>$ and $<0, T_1>$, $<0, -T_1>$ have exactly the same performance. That is, for example, configuration $<80, 0>$ has the same performance as $<-80, 0>$ and configurations $<45, -45>$ and $<-45, 45>$ also have the same performance. This conclusion must be taken with special care since the face sheets are composed of only one lamina. So, this observation is true for the context of one lamina face sheets tested, being possible that the laminate structural behaviour with face sheets composed of multiple lamina could be different. This more complete study is done in subsequent sections.

A more in-depth observation of these tables reveals that, for the cases tested, CSS have better performance in buckling in x direction in every isotropic core variation and have better performance in cores E and F, in buckling in y direction. Although VSS have a worse performance, for the cases tested, in x buckling, it exhibits better structural behaviour in y buckling for cores G and H, benefiting, therefore,

from the fact that these cores have lower stiffness than those where VSS perform worse in y buckling (cores E and F).

Another interesting inference that can be made from these results is that, for x buckling, the difference in performance between the best CSS and best VSS is of 5.78% in core E, increases drastically to 72.77% in core F and then decreases in both core G and H (2.3% and 17.17%, respectively). Moreover, while the best CSS configuration is $<0, 0>$ for all cores, the best VSS configuration varies, being $<80, 0>$ the best VSS in core E and $<45, -45>$ the best VSS in cores F, G and H. Similar analysis can be performed in y buckling but, in this case, the conclusions are different. As mentioned previously, CSS have the better performance for the more stiff cores E and F, where the difference in the performance between the best CSS and VSS configurations is of 3.36% and 20%, respectively. This scenario changes with the more flexible cores G and H, where VSS becomes the better type of sandwich. The difference in performance, in theses cases, is of 7.79% in core G and increases to 55.81% in the most flexible core H. Therefore, besides benefiting from the more flexible cores, VSS structural advantage over CSS increases proportionally to the decrease of the stiffness of the core. As it occurred in the x buckling case, the best CSS did not change with the variation of core, being the configuration $<90, 90>$ the best in this type, while its VSS counterpart has as best configuration $<90, 0>$ for core E and $<0, 90>$ for cores F, G and H.

Table 3.10: Critical buckling load factor (in x and y directions) for multiple $<T_0, T_1>$ configurations and multiple isotropic cores.

$<T_0,T_1>$	Critical buckling factor λ_{crit}							
	Core E		Core F		Core G		Core H	
	Buckling x	Buckling y	Buckling x	Buckling y	Buckling x	Buckling y	Buckling x	Buckling y
<0,0>	50.689	39.009	17.293	5.601	0.800	0.534	0.193	0.085
<45,45>	44.152	44.152	7.818	7.818	0.502	0.502	0.115	0.115
<90,90>	39.009	50.689	5.601	17.293	0.534	0.800	0.085	0.193
<0,70>	45.982	41.521	9.990	8.979	0.596	0.718	0.126	0.142
<0,80>	44.929	43.189	8.997	12.91	0.570	0.810	0.112	0.203
<0,90>	43.953	44.846	7.737	14.406	0.543	0.862	0.101	0.300
<70,0>	46.309	47.855	8.465	7.839	0.570	0.396	0.122	0.096
<80,0>	47.916	48.441	8.267	7.597	0.571	0.331	0.107	0.089
<90,0>	47.438	49.043	7.310	7.525	0.557	0.314	0.098	0.089
<0,-70>	45.982	41.521	9.990	8.979	0.596	0.718	0.126	0.142
<0,-80>	44.929	43.189	8.997	12.910	0.570	0.810	0.112	0.203
<0,-90>	43.953	44.846	7.737	14.406	0.543	0.862	0.101	0.300
<-70,0>	46.309	47.855	8.465	7.839	0.570	0.396	0.122	0.096
<-80,0>	47.916	48.441	8.267	7.597	0.571	0.331	0.107	0.089
<-90,0>	47.438	49.043	7.310	7.525	0.557	0.314	0.098	0.089
<45,-45>	43.123	39.965	10.009	5.788	0.782	0.560	0.164	0.093
<-45,45>	43.123	39.965	10.009	5.788	0.782	0.560	0.164	0.093

Regarding the vibration results, presented in table 3.11, with isotropic cores, with these VSS configurations case studies, it has demonstrated with the current study that in all types of isotropic cores here tested, VSS can indeed surpass CSS in terms of vibration performance. Vibration differences between the best CSS and the best VSS are more constant throughout the different cores, unlike the buckling case where the differences changed significantly between cores. In vibration, the mean difference of all cores is around 7%, being VSS the best sandwich configuration. Configuration $<90, 90>$ is the best

CSS while $<90, 0>$ is the best VSS across all isotropic cores. Unlike some buckling cases, the modes obtained for vibration did not exhibit particular local failure modes.

Table 3.11: Fundamental frequency f (Hz) for multiple $<T_0, T_1>$ configurations and multiple isotropic cores.

$<T_0,T_1>$	Fundamental frequency f (Hz)				$<T_0,T_1>$	Fundamental frequency f (Hz)			
	Core E	Core F	Core G	Core H		Core E	Core F	Core G	Core H
<0,0>	182.170	102.737	23.916	11.214	<0,-70>	165.263	79.136	22.710	9.588
<45,45>	174.642	87.137	23.331	10.499	<0,-80>	164.802	78.498	22.693	9.525
<90,90>	182.170	102.737	23.916	11.214	<0,-90>	164.624	78.262	22.711	9.512
<0,70>	165.263	165.263	22.710	9.588	<-70,0>	189.330	100.200	25.202	11.576
<0,80>	164.802	164.802	22.693	9.525	<-80,0>	192.828	104.730	25.454	11.849
<0,90>	164.624	164.624	22.711	9.512	<-90,0>	195.722	108.960	25.654	12.079
<70,0>	189.330	100.200	25.202	11.576	<45,-45>	168.200	83.792	23.363	10.045
<80,0>	192.828	104.730	25.454	11.849	<-45,45>	168.200	83.792	23.363	10.045
<90,0>	195.722	108.960	25.654	12.079					

As explained previously, this study comprehends also orthotropic cores, besides the already analysed isotropic cores. This way VSS are tested in the presence of the more complex defined orthotropic cores.

Table 3.12 displays the results concerning x and y buckling for multiple orthotropic cores and the same $<T_0, T_1>$ configurations as in the isotropic case. As it occured previously in the isotropic cores study, as the stiffness of the orthotropic core decreases, the buckling performance also decreases across all configurations.

Unlike the isotropic case, here the VSS configurations tested perform better, in x buckling, in more stiff cores (A and B) whereas in the less stiff cores C and D the CSS tested had a higher critical buckling load factor. In fact there is a change in performance when the core changes from A to B, being the difference of performance between the best VSS and CSS configurations of 8.43% and 4.58%, in cores A and B respectively, with $<0, 70>$ as the best configuration overall and $<0, 0>$ the best CSS configuration. From core A to B one can infer that, since the best lamina configuration of $<T_0, T_1>$ for both CSS and VSS did not change, this change of performance is due to the stiffness of the core. Namely, in this case, the critical buckling load is altered due to the change in the shear stiffness (G_{xy}, G_{xz} and G_{yz}). However, in the x buckling case, the change from core B to core C impacts drastically the results. Besides being a CSS now the best configuration, the difference between the best configurations of CSS and VSS increases to 81.75%. Nevertheless, the best configurations still remain the same as before, but now they change positions in terms of which has better performance, allowing, once again, to infere that the core stiffness plays an important role, being, in this case, the change in the normal stiffness the responsible of this alteration.

In terms of vibration results, present in table 3.13, just like the isotropic cores case, the modes obtained are all of global nature, not exhibiting visible local failure modes, which, once again, allows to infer that the buckling case is more sensible to the onset of local instabilities with the core's stiffness variation. It can be seen that VSS have the better performance in all orthotropic cores tested, for the set of configurations used, although the difference between the best CSS and VSS stabilizes at around

Table 3.12: Critical buckling load factor (in x and y directions) for multiple $<T_0, T_1>$ configurations and multiple orthotropic cores.

$<T_0,T_1>$	Critical buckling factor λ_{crit}							
	Core A		Core B		Core C		Core D	
	Buckling x	Buckling y	Buckling x	Buckling y	Buckling x	Buckling y	Buckling x	Buckling y
<0,0>	101.770	96.876	86.708	77.468	23.553	6.866	18.557	5.412
<45,45>	97.201	97.199	80.551	80.299	11.057	10.966	7.440	7.375
<90,90>	96.918	101.590	79.958	85.036	6.789	23.135	5.151	16.270
<0,70>	110.350	64.814	90.679	49.810	12.959	15.195	9.610	9.054
<0,80>	105.560	75.026	87.768	56.276	11.265	22.400	8.684	11.910
<0,90>	101.640	88.673	83.552	69.543	9.367	29.723	7.359	12.836
<70,0>	82.487	140.710	68.946	103.340	11.000	9.761	8.211	7.235
<80,0>	99.587	107.340	81.958	85.067	10.550	9.513	8.057	6.946
<90,0>	100.310	91.346	82.483	70.938	9.104	10.146	6.991	6.767
<0,-70>	110.350	64.814	90.679	49.810	12.959	15.195	9.610	9.054
<0,-80>	105.560	75.026	87.768	56.277	11.265	22.400	8.684	11.910
<0,-90>	101.640	88.673	83.552	69.543	9.367	29.723	7.359	12.836
<-70,0>	82.487	140.710	68.946	103.340	11.000	9.761	8.211	7.235
<-80,0>	99.587	107.340	81.958	85.065	10.550	9.513	8.057	6.946
<-90,0>	100.310	91.346	82.483	70.937	9.104	10.146	6.991	6.767
<45,-45>	87.386	93.340	76.718	71.693	12.691	7.210	9.885	5.499
<-45,45>	87.386	93.340	76.718	71.693	12.691	7.210	9.885	5.499

4% for cores A, B and C and decreases drastically to only 0.67% in the softer core D, opposed to the constant average 7% verified in the isotropic case. For this set tested, $<0, 0>$ and $<90, 0>$ are the best CSS and VSS configurations in all cores, respectively.

Table 3.13: Fundamental frequency f (Hz) for multiple $<T_0, T_1>$ configurations and multiple orthotropic cores.

$<T_0,T_1>$	Fundamental frequency f (Hz)				$<T_0,T_1>$	Fundamental frequency f (Hz)			
	Core A	Core B	Core C	Core D		Core A	Core B	Core C	Core D
<0,0>	732.947	674.390	349.449	278.406	<0,-70>	702.538	644.130	249.500	204.401
<45,45>	722.102	659.470	283.041	224.692	<0,-80>	701.754	643.420	246.050	202.115
<90,90>	732.007	667.371	345.549	258.078	<0,-90>	701.472	643.299	244.715	200.917
<0,70>	702.538	644.130	249.496	204.401	<-70,0>	753.366	687.411	330.743	260.938
<0,80>	701.754	643.420	246.050	202.115	<-80,0>	760.057	692.709	348.761	271.000
<0,90>	701.472	643.299	244.715	200.917	<-90,0>	765.328	696.930	365.646	280.283
<70,0>	753.366	687.411	330.743	260.938	<45,-45>	708.205	649.495	271.145	218.040
<80,0>	760.057	692.709	348.761	271.000	<-45,45>	708.205	649.495	271.145	218.040
<90,0>	765.328	696.930	365.646	280.283					

A particular aspect regarding the mode shape results is the onset, in some scenarios, of local failure modes or a coexistence of local and global instabilities. In both vibration and x buckling analysis, the local instability phenomenon is not present with this specific orientation law, for the set of configurations tested. However, for y buckling there are some configurations in which local instabilities occur. This phenomenon tends to occur in sandwich structures with specifically softer isotropic or orthotropic cores. In the latter, these instabilities are exacerbated and take a more irregular shape than in soft isotropic cores. Examples of the onset of local instabilities are configurations $<0, 70>$, $<0, 80>$ and $<0, 90>$ for isotropic core G and orthotropic core D.

Figure 3.2 presents the mode shapes, in y buckling, regarding the isotropic core G with configurations

$<0, 70>$, $<0, 80>$ and $<0, 90>$. It is possible to see that, in configuration $<0, 70>$, there is a coexistence of the traditional global mode with the presence of local instabilities, which progressively become the dominating mode as T_1 increases towards $90°$ (for $T_0 = 0°$, in this case). These failure modes are not transversal to all VSS, however. Configurations with high curvature exacerbate this phenomenon, as demonstrated by the degree of dominance of such modes over global modes as T_1 increases (e.g. curvature increases) for $T_0 = 0°$.

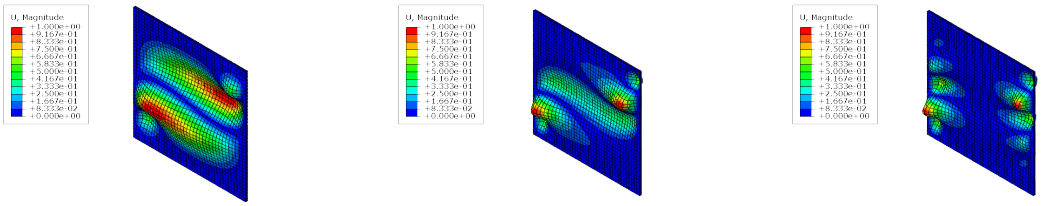

Figure 3.2: Fundamental mode shapes for configurations $<0, 70>$ (left), $<0, 80>$ (center) and $<0, 90>$ (right) with core G.

The mode shape regarding $<0, 90>$ configuration for orthotropic core D, in y buckling, is shown in figure 3.3. As previously mentioned, the instabilities occurred in this case are more intense and irregular than in the isotropic test core. Furthermore, it leads to an abrupt decrease of performance in buckling, since this local mode emerges much sooner than the global buckling mode of the structure. So, in this regard, $<0, 90>$ configuration, which is the best performing configuration in the soft core C, looses its performance advantage to CSS configurations, namely $<90, 90>$, due to, precisely, these instabilities. These local instabilities favour even more the onset of global instabilities modes, due to the decrease of flexural rigidity of the structure.

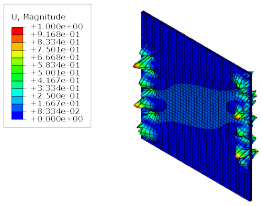

Figure 3.3: Fundamental mode shape for configuration $<0, 90>$ with core D.

Therefore, it is possible to conclude that, although VSS can indeed bring benefits in terms of structural performance, careful thought must be taken in its design in order to conceive a structure that does not contribute to the earlier onset of such local failure modes with its drastic performance consequences. These type of failures are more often seen in y buckling, for the orientation law used and in the presence of softer cores.

3.3 High Stiffness Core Variable Stiffness Sandwich Study

A more in-depth analysis concerning the impact of fiber steering in VSS on the structural performance is evaluated, in the current and subsequent sections. The present case covers the topic of high stiffness core. Although the main interest related to sandwich structures is in the presence of a low stiffness

core, this study is done to investigate possible correlations between the use of steered fibers and the corresponding structural performance in more stiff cores, which are rarer, as mentioned, but nonetheless can still be produced. To this extent, the structures are subjected to uniaxial buckling in both directions (x and y) and also to free vibration. A set of four different boundary conditions are applied comprising CCCC, SSSS, CCSS and SSCC. In terms of VSS configurations used, three values of T_0 are fixed ($0°$, $45°$ and $90°$) while T_1 varies for each of the T_0 values, taking the values of $0°$, $30°$, $45°$, $60°$ and $90°$. Moreover, face sheets are composed of two lamina and studies have been done with symmetric and antisymmetric face sheet configurations. For clarity, the antisymmetric plots presented have as data the T_0 and T_1 of the first lamina, being implicit that the second lamina is of the form $<-T_0, -T_1>$. The materials used are an aluminium alloy for the core (Core E in table 3.9) and CFRP for the face sheets (table 3.7).

Regarding uniaxial x buckling, figure 3.4 presents the results for both symmetric and antisymmetric laminates. Both plots are similar to each other, with some few differences in some cases. The general trend for fully simply-supported conditions (SSSS) is equal in both cases, with $<0, 60>$ being the best symmetric configuration and $<45, 45>$ the best antisymmetric (and overall) configuration. Indeed, buckling performance increases in all three cases of T_0 when T_1 varies from $0°$ to around $45°/60°$, then decreasing until T_1 reaches $90°$. In what concerns CCCC and CCSS boundary conditions, the general trend remains and the following is verified: $<0, 0>$ is the best configuration in all of these cases and, afterwards, the performance decreases continuously in all T_0 until T_1 reaches $90°$, with only minor differences in the case of $T_0 = 45°$ for both symmetric and antisymmetric configurations where the maximum value of critical buckling load is reached at $T_1 = 30°$. The SSCC curves for symmetric and antisymmetric have similar behaviour, being the best configuration a VSS: $<45, 30>$ antisymmetric configuration.

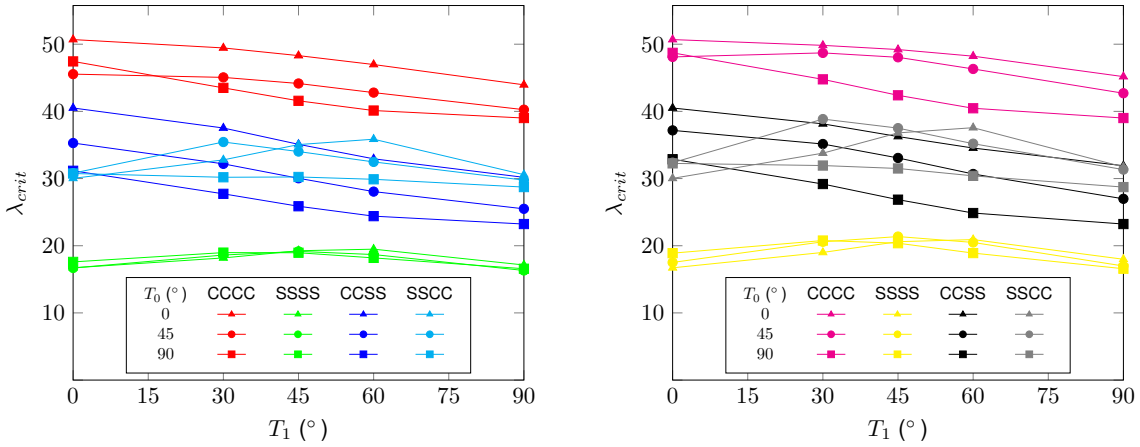

Figure 3.4: Uniaxial x buckling critical load λ_{crit} evolution with T_0 and T_1 in multiple boundary conditions for symmetric (left plot) and antisymmetric (right plot) face sheet configurations.

Uniaxial y buckling results are presented in figure 3.5. For CCSS conditions, for each T_0, the critical buckling increases with the increase of T_1, with the exception of $T_0 = 90°$, for which it reaches maximum buckling load at $T_1 = 0°$ and then decreases continuously. While in the CCCC case, the symmetric configuration $<90, 90>$ and the antisymmetric configurations $<90, 0>$, $<90, 90>$ and $<45, 90>$ have very similar buckling performance between each other, the same is not verified in CCSS conditions, where

the antisymmetric $<90, 0>$ configurations stands out as the best performing in uniaxial y buckling. When applying SSCC conditions, for both symmetric and antisymmetric laminates, the buckling performance evolution is similar to the one observed in CCCC conditions. Regarding SSSS conditions, the evolution detected in uniaxial y buckling has similarities with the uniaxial x case, although, in addition to the fact that the antisymmetric $<45, 45>$ configuration still remains as the best performing one, the antisymmetric $<45, 60>$ also has a comparable result.

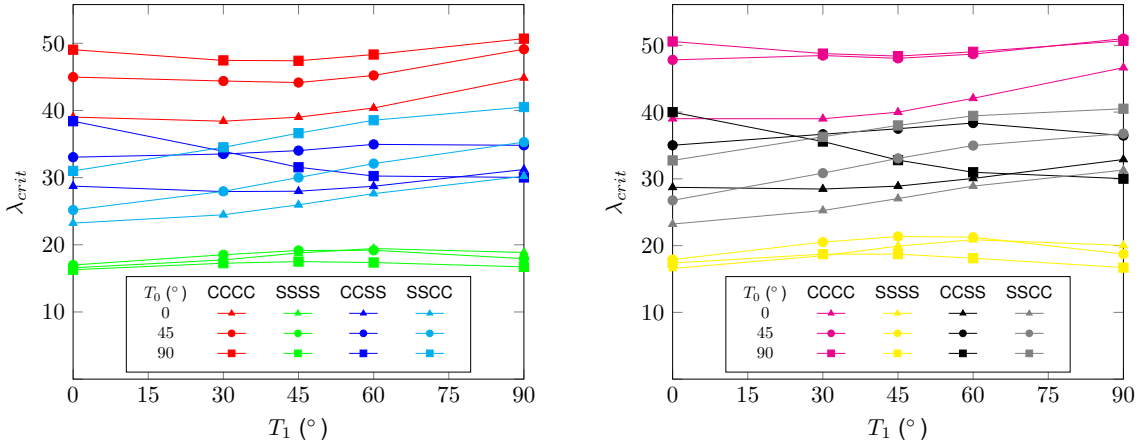

Figure 3.5: Uniaxial y buckling critical load λ_{crit} evolution with T_0 and T_1 in multiple boundary conditions for symmetric (left plot) and antisymmetric (right plot) face sheet configurations.

In terms of vibration results, figure 3.6 shows a performance advantage of CSS over VSS, namely in SSCC and CCSS conditions, albeit, in the latter, the antisymmetric $<45, 0>$ has a comparable vibration performance with the best performing configuration $<0, 0>$. The SSSS condition diverges from the general tendency of the other curves. In this case, namely when using symmetric laminates, there is not much difference between all configurations tested. The antisymmetric configuration $<45, 45>$ has the better performance, even though, once again, the minor differences between configurations. All clamped conditions (CCCC) is where VSS demonstrate their performance advantage, with $<90, 0>$ antisymmetric configuration being the best performing one.

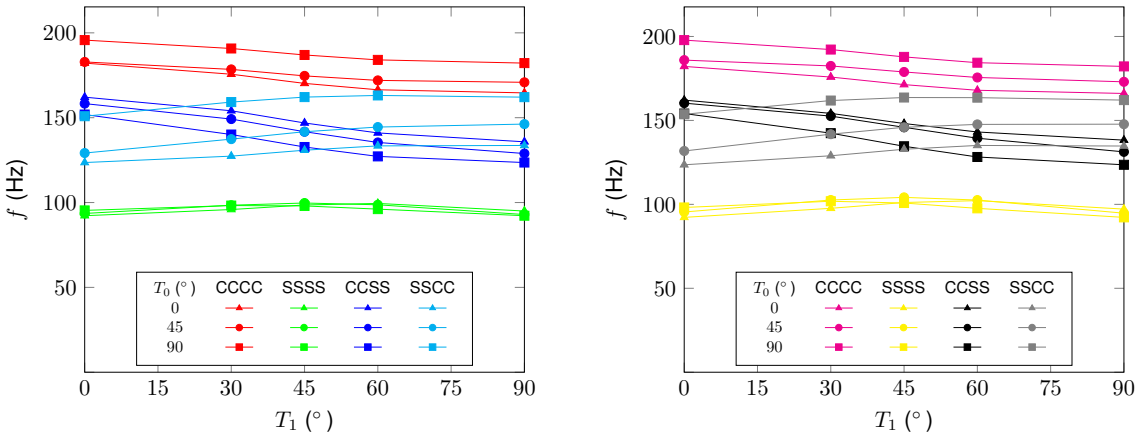

Figure 3.6: Fundamental frequency f (Hz) evolution with T_0 and T_1 in multiple boundary conditions for symmetric (left plot) and antisymmetric (right plot) face sheet configurations

It is worth noting that every mode is of global nature, being local modes of instability not present

or not noticeably visible, both in buckling analysis and vibration, with steered or unsteered fibers. This was expected since the last study allowed to conclude that sandwiches with high stiffness cores have lower probability of occurrence of local instabilities since there is not a noticeable difference between the stiffness (namely transversal stiffness) between face sheets and core, being the core capable of supporting considerable stress induced in the structure. However, as previously mentioned, these higher stiffness cores have as a great disadvantage their usually high density which, specifically for aeronautical applications, is not desirable.

3.4 Low Stiffness Core Variable Stiffness Sandwich Study

The third and final analysis of this set of studies conducted consists on an in-depth investigation of the structural behaviour of low stiffness core VSS. As mentioned, the more detailed analysis that is made in this study is justified by the fact that these kind of structures with low stiffness cores are the most predominant in practical applications (namely, aerospace). Thus, several structural analysis are made ranging from structural statics to free vibration to a multitude of different kinds of buckling scenarios, being symmetric and antisymmetric composite face sheets (each with two laminas) configurations tested as well as different boundary conditions. For antisymmetric face sheets configurations, the plots present the pair $<T_0, T_1>$ for the first lamina. The material used for the face sheets is the same as in the previous study (CFRP), while the core's material is an aluminium honeycomb (core D, table 3.8).

3.4.1 Statics

Although the main focus of this work is the study of vibration and buckling characteristics of VSS, in this particular analysis the static mechanical behaviour of VSS is investigated in order to have an holistic overview of the capabilities of such structures. One important variable concerning static structural response is the maximum static deflection, which is desirable to be as low as possible. To this extent, a uniform load in the z direction (vertical direction) of 100 kPa is applied on the upper surface of the structure (i.e. $100kN$ of total force on a plate of $1 \times 1\ m^2$).

Figure 3.7 presents the results for symmetric face sheet configurations. As expected, changing boundary conditions from clamped to simply supported to completely free results in a higher value of maximum deflection. From the upper left and upper right plots, it is possible to observe that, for cases where both x edges are clamped, symmetric configurations with $T_0 = 0^\circ$ tend to have a better performance (lower maximum deflection), while in cases where both y edges are clamped such as FCCC or FFCC, configurations with $T_0 = 90^\circ$ have the advantage. In any of these cases, there is a tendency for CSS to be better than VSS (e.g. $<0, 0>$ for CFFF and $<90, 90>$ for FFCC). Besides the best performing configuration being different in these plots, the maximum deflection evolution with T_1 is also different: in the upper left plot the maximum deflection generally increases with increasing T_1, for a given value of T_0, while for the upper right plot it generally decreases with increasing T_1. The main exception to this is the CCCC case, where there are a lot of similarities in what concerns the performance for different

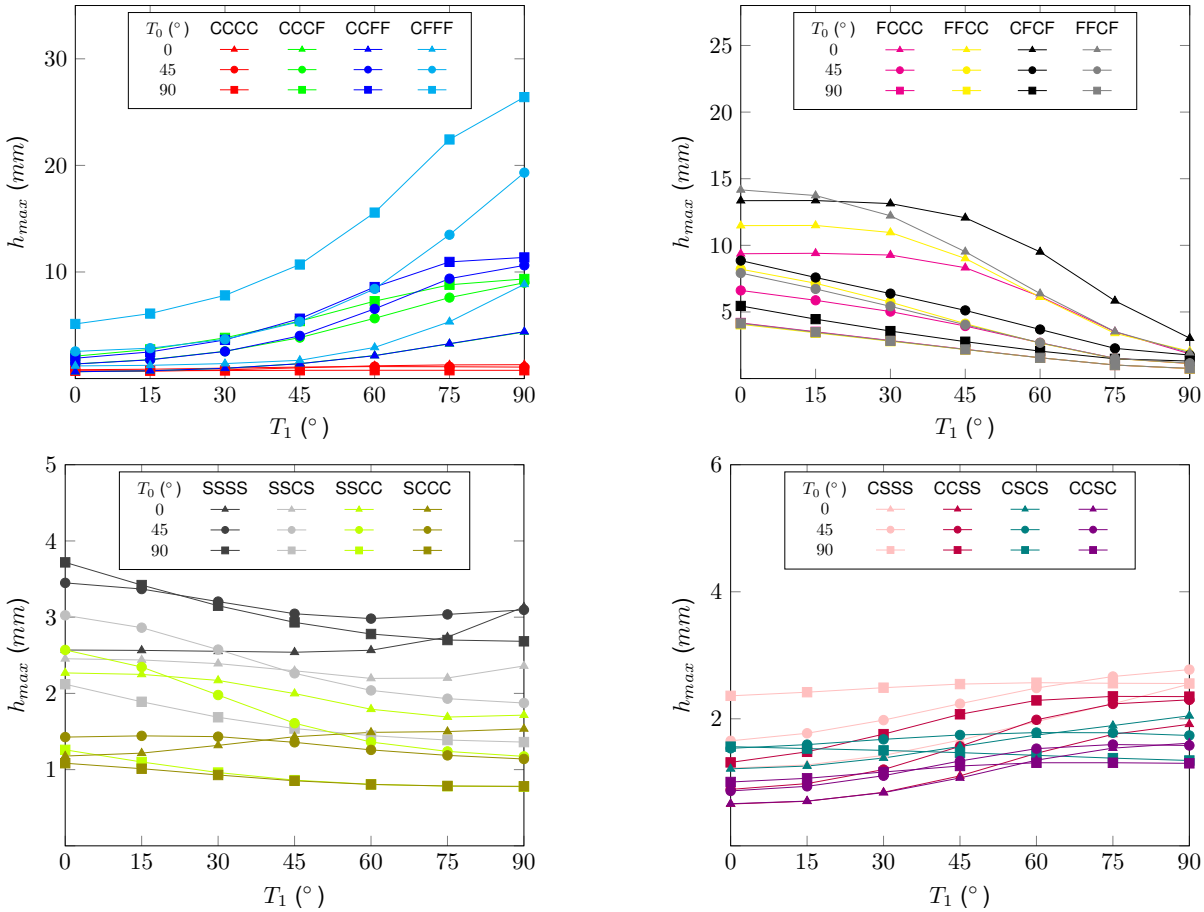

Figure 3.7: Maximum static deflection h_{max} (mm) evolution with T_0 and T_1 in multiple boundary conditions.

values of T_0 and T_1.

Similar trends are found in the lower left plot of figure 3.7. Although the performance evolution is not so pronounced as in the previous two plots, CSS $<90, 90>$ and $<0, 0>$ remain the best configurations for conditions where both y edges are clamped (SSCC, SCCC). For fully simply supported conditions (SSSS), albeit the considerable increase from $T_1 = 60°$ onwards, the configuration combination of $T_0 = 0°$ and $T_1 = 0°$ has the lowest value of maximum deflection.

Overall, the results show that, for symmetric configurations and for the sets of T_0 and T_1 tested, CSS tend to have better structural static characteristics than VSS.

Results for antisymmetric face sheet configurations are shown in figure 3.8. The use of these configurations does not culminate in any major differences in performance comparatively to symmetric cases. In fact, CSS configurations still remain as the better options to choose when it comes to static structural behaviour in the majority of the boundary conditions tested. However, there are some scenarios such as SCCC where VSS configurations, namely $<90, 45>$, $<90, 60>$ and $<90, 75>$, have very competitive and similar results to the best CSS configuration ($<90, 90>$) in those conditions.

In addition to the previously mentioned, the lower right plot of figure 3.8 presents some encouraging results for VSS configurations owing to the fact that some particular cases of these configurations, such as $<45, 30>$ in CSCS conditions, have a slightly better performance than CSS configurations.

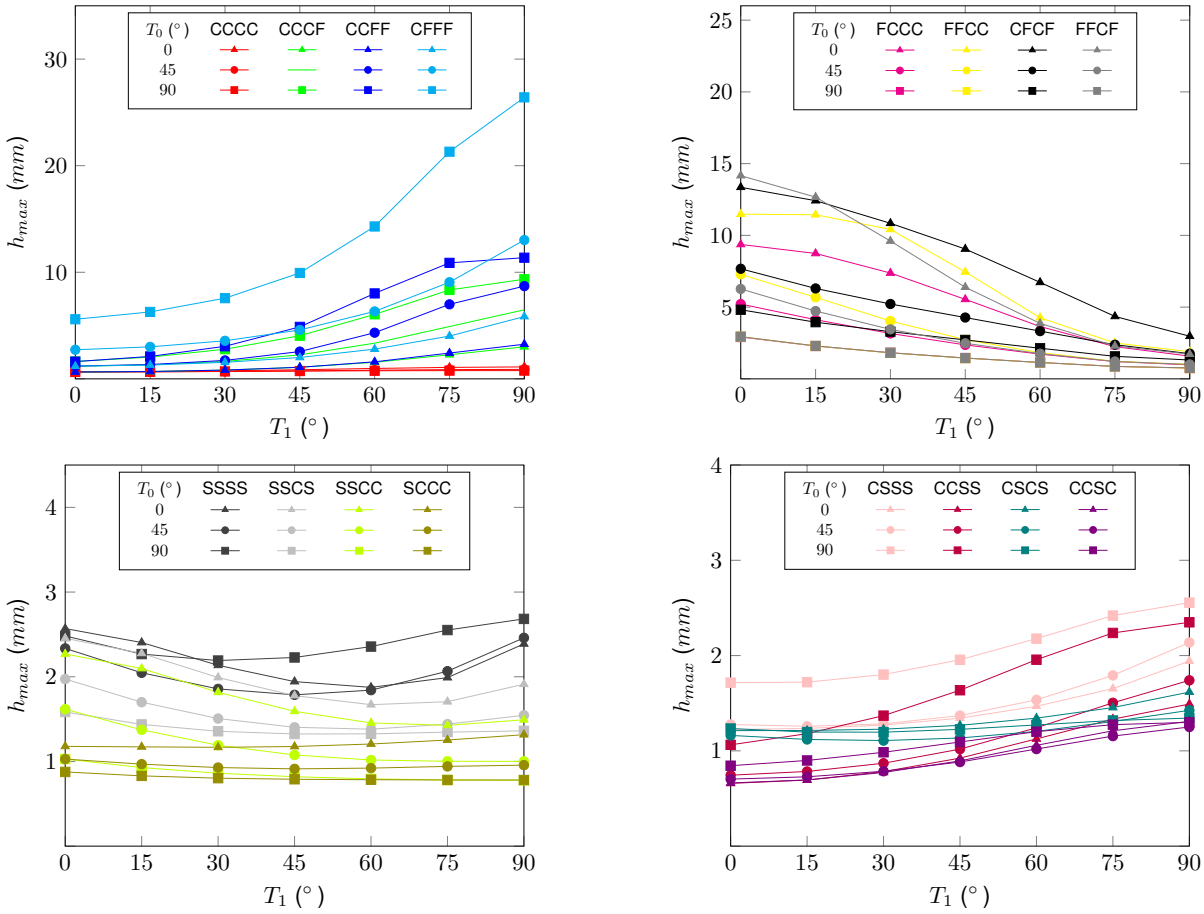

Figure 3.8: Maximum static deflection h_{max} (mm) evolution (antisymmetric facesheet configuration) with T_0 and T_1 in multiple boundary conditions.

3.4.2 Free Vibration

Regarding the free vibration analysis, in what concerns the symmetric face sheet configurations results (figure 3.9), it is possible to observe that for boundary conditions such as CCCC, CCCF, CCFF, CFFF, CCSC, CCSS or CSSF, the general trend is that, with the increase of T_1 for a given value of T_0, the fundamental frequency decreases. Furthermore, it is possible to note that the inclusion of more free boundary conditions in the structure leads to a decrease in the frequency. However, there are some cases, such as FFCC, where the inclusion of one more free boundary condition (in comparison with FCCC) leads to only a negligible decrease in performance when $T_0 = 90°$. For the remaining two values of T_0, it is possible to see that the frequency values of the two boundary conditions converge as T_1 approaches $90°$.

Another interesting conclusion is that, for some boundary conditions such as CSCS, CSSS or SSSS, the frequency curves, for a given T_0, are practically constant, not varying significantly with T_1. This pattern is most seen in scenarios where simply supported boundary conditions are introduced. For these boundary conditions, changing the value of T_0 will affect the vibration results, but only in a small magnitude for most cases, demonstrating that it is not completely insensible to the presence of steered fibers but, at the same time, the effect of variable stiffness face sheets is more pronounced in other applied conditions.

The overview of the symmetric face sheets results (figure 3.9) allows to conclude that CSS tend to have a better performance than VSS, for the sets of configurations tested, in the majority of the boundary conditions although, in some cases such as CCSC or CCCC, VSS have a competitive or even a better performance than CSS.

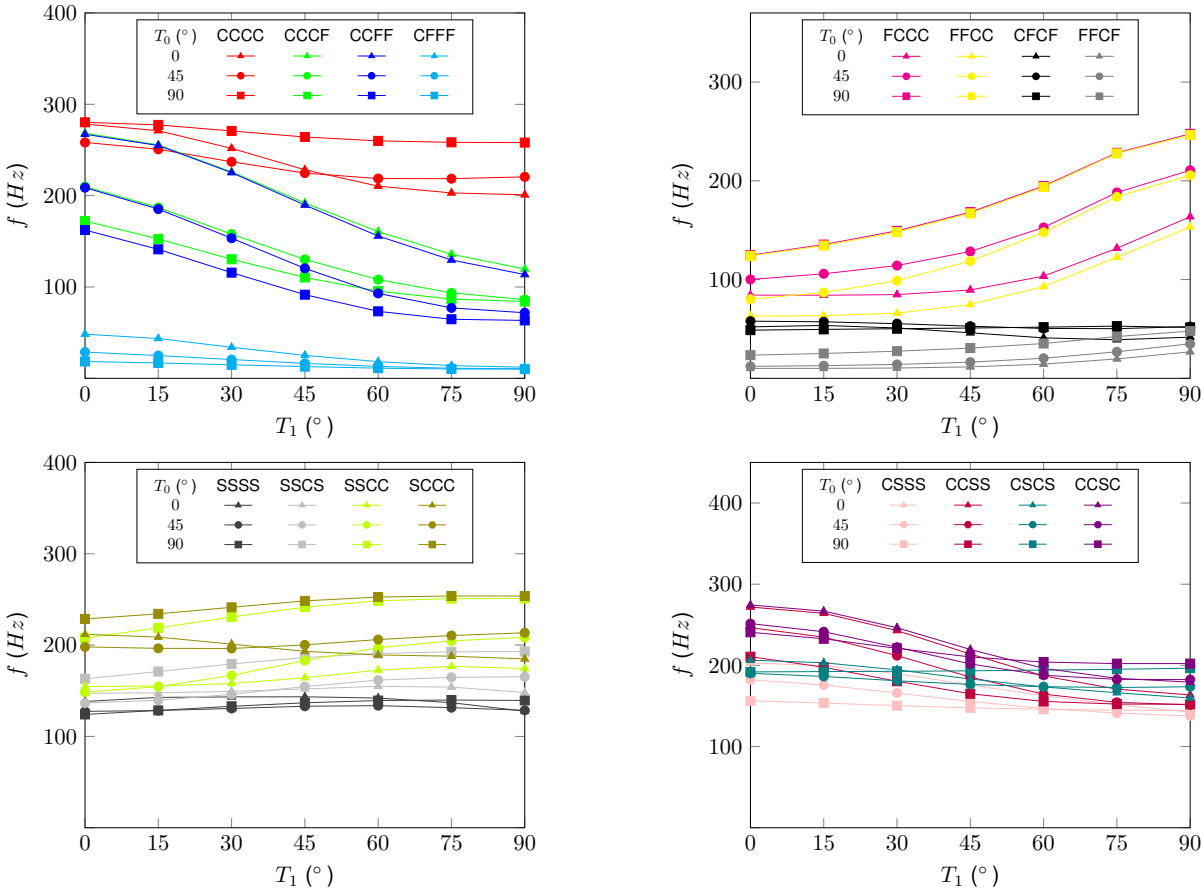

Figure 3.9: Fundamental frequency f (Hz) evolution with T_0 and T_1 in multiple boundary conditions.

Regarding the antisymmetric face sheets results (figure 3.10), the general trend conclusions made for the symmetric cases are also applicable in the antisymmetric cases in what concerns the fundamental frequency evolution with T_1, for a given T_0, in the different boundary conditions. In scenarios where at least one of the y boundaries ($y = 0$ and $y = b$) has a free condition applied and remaining boundaries are clamped, sandwiches with antisymmetric face sheets with $T_0 = 0°$ tend to have a better performance than the cases with $T_0 = 45°$. On the other hand, when at least one of the x edges is free and the remaining boundaries are clamped, the inverse tends to occur: sandwiches with $T_0 = 90$ have the better performance. Generally, antisymmetric and symmetric face sheets configurations do not present significant differences in terms of fundamental frequency. There are, nonetheless, some exceptions: for example, in CCSC scenario, the VSS $<45, 0>$ is the best antisymmetric configuration while in symmetric case the CSS $<0, 0>$ is the best option, although the value of the frequency obtained itself does not change much, as it occurs in other cases.

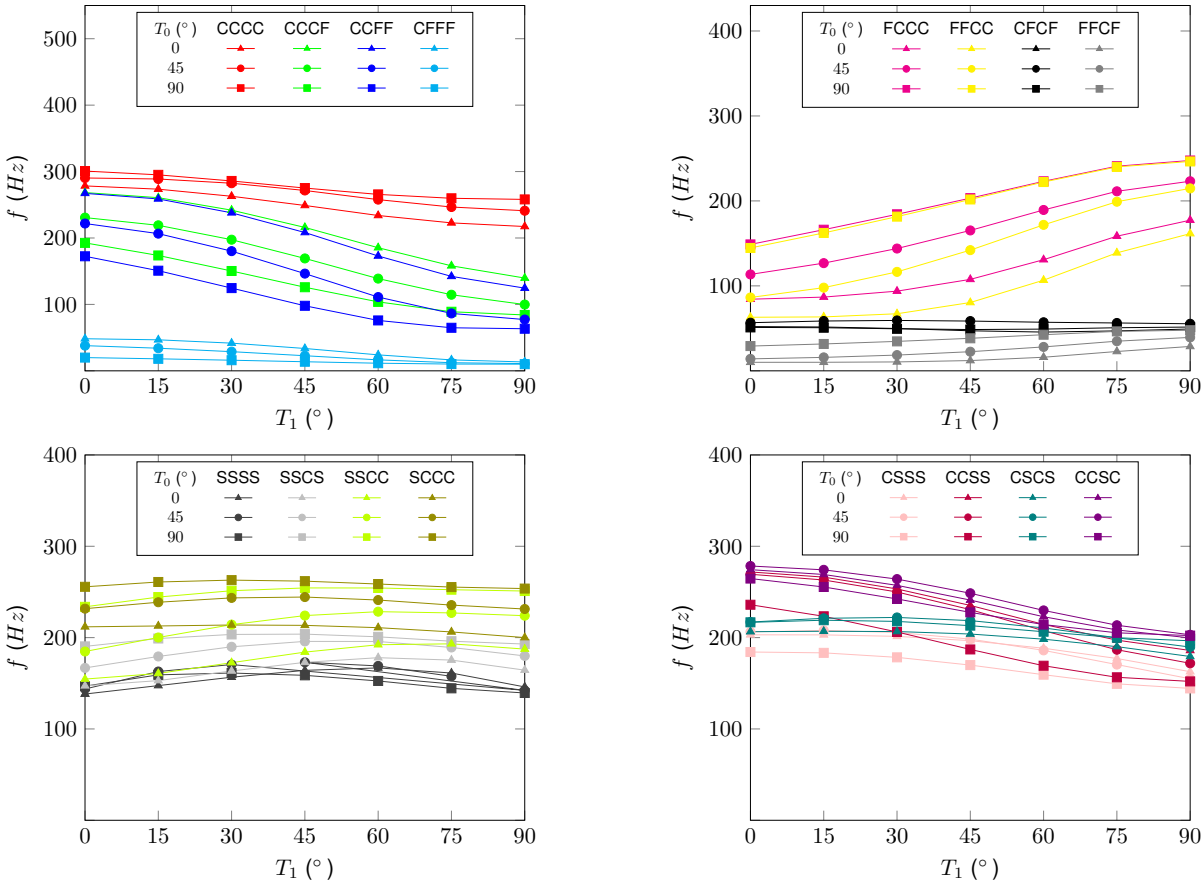

Figure 3.10: Fundamental frequency f (Hz) evolution (antisymmetric facesheet configuration) with T_0 and T_1 in multiple boundary conditions.

3.4.3 Buckling

Uniaxial buckling

The results obtained related to uniaxial x buckling of both CSS and VSS with symmetrical face sheet configuration (figure 3.11) show that, for scenarios where at least one of the x edges ($x = 0$ or $x = a$) is clamped and the remaining boundaries are either free or clamped, the CSS symmetrical configuration $<0, 0>$ has the best x buckling performance, as shown by the upper left plot of figure 3.11. In these same cases, besides this trend, there is also another visible pattern: for a given T_0, the increase of T_1, generally, decreases the buckling performance of the structure.

However, if at least one of the y edges (instead of x edges in the previous case) is clamped and the remaining boundaries are either clamped or free (upper right plot of figure 3.11), the evolution of the critical buckling load is not so straightforward. While for cases such as CFCF and FCCC with $T_0 = 45°$ or $T_0 = 90°$, the previous trend of decreasing performance with the increase of T_1 still holds, the same does not apply for $T_0 = 0°$ with the same boundary conditions. In the latter, there is an increase in performance, being the VSS symmetrical configuration $<0, 15>$ the best performing structure for both boundary conditions. Then, with the further increase of T_1, the decrease of performance is once again visible as it occurred in the other examples. For the FFCF tests, it can be stated that the performance increases with T_1, although there is no significant differences of critical buckling load between different

T_0 cases, with the $<0, 90>$ configuration having the highest buckling performance. It is worth also noting that, in FFCC conditions, for $T_0 = 0°$, the performance increases until $T_1 = 75°$, where it reaches its peak, and then decreases until $T_1 = 90°$.

In the lower left plot of figure 3.11 it is possible to verify that VSS have a performance advantage over CSS in buckling in x direction. In all of the boundary conditions cases present in this plot (SSSS, SSCS, SSCC and SCCC), only in the SCCC scenario a CSS configuration ($<0, 0>$) is able to compete with the best configuration $<0, 15>$. In the remaining boundary conditions, the symmetrical VSS configuration $<0, 45>$ has the highest buckling load for SSCS and SSCC while for SSSS $<0, 30>$ has an advantage over the remaining ones. It is also worth stating that in these cases as well as in many other boundary conditions cases, the increase in T_0 (i.e., varying from $0°$ to $45°$ to $90°$) leads to a general decrease in performance, typically.

Regarding the results with CSSS, CCSS, CSCS and CCSC boundary conditions, visible in the lower right plot of figure 3.11, the decrease in performance with T_1 is once again verified, being $<0, 0>$ the configuration with the highest critical buckling load factor. The observation of the right plot of figure A.5 allows for the conclusion that in some boundary conditions the buckling performance does not change much, being almost insensible to the presence of steered fibers, such as in the FSCF scenario, while in other cases such as SFCC and CFCS, there are differences if T_0 is changed but the variation of T_1 produces only minor alterations to performance.

The results for antisymmetric face sheet configurations dictate that the behaviour of these structures, unlike the vibration case, have a quite significantly different response in comparison with the symmetric counterparts. An example of the previously stated is visible in the CCCC test: while, in the symmetric configurations, for all T_0 there is rapid decrease of performance with the increase of T_1, in the anti-symmetric configurations the decrease of performance is very slow and, in the case of $T_0 = 45°$, it actually increases until it reaches the peak of critical buckling load at $<45, 30>$, after which decreases, as seen in the upper left plot of figure 3.12. It can be seen that for the set of boundary conditions of the plot, the overall best configuration does not change ($<0, 0>$) from the symmetric to the antisymmetric study. However, the introduction of an antisymmetric configurations improves the performance for most of the remaining configurations, such as $<45, 0>$, which had a critical buckling factor of around 12 in the symmetric configuration, and in the antisymmetric this value increases to around 15.

The differences to the symmetric configurations results are even more noticeable, for example, in the upper right plot of figure 3.12. For the FFCC case, the best critical buckling load factor ascends to almost 6, with a $<45, 30>$ configuration, while for the symmetric case the best performance was around 3, with a $<0, 75>$ configuration. Better critical buckling load factors are also achieved with antisymmetric configurations for the remaining boundary conditions of the plot, with $<0, 60>$, $<0, 45>$ and $<0, 90>$ having the best performance in FCCC, CFCF and FFCF, respectively.

For the remaining plots of figure 3.12 there is a general conclusion that antisymmetric VSS cases, besides being an upgrade in performance in comparison with the symmetric configurations, bring also a significant upgrade in the overall x buckling performance.

The uniaxial y buckling analysis of symmetrical face sheet configurations reveals different conclu-

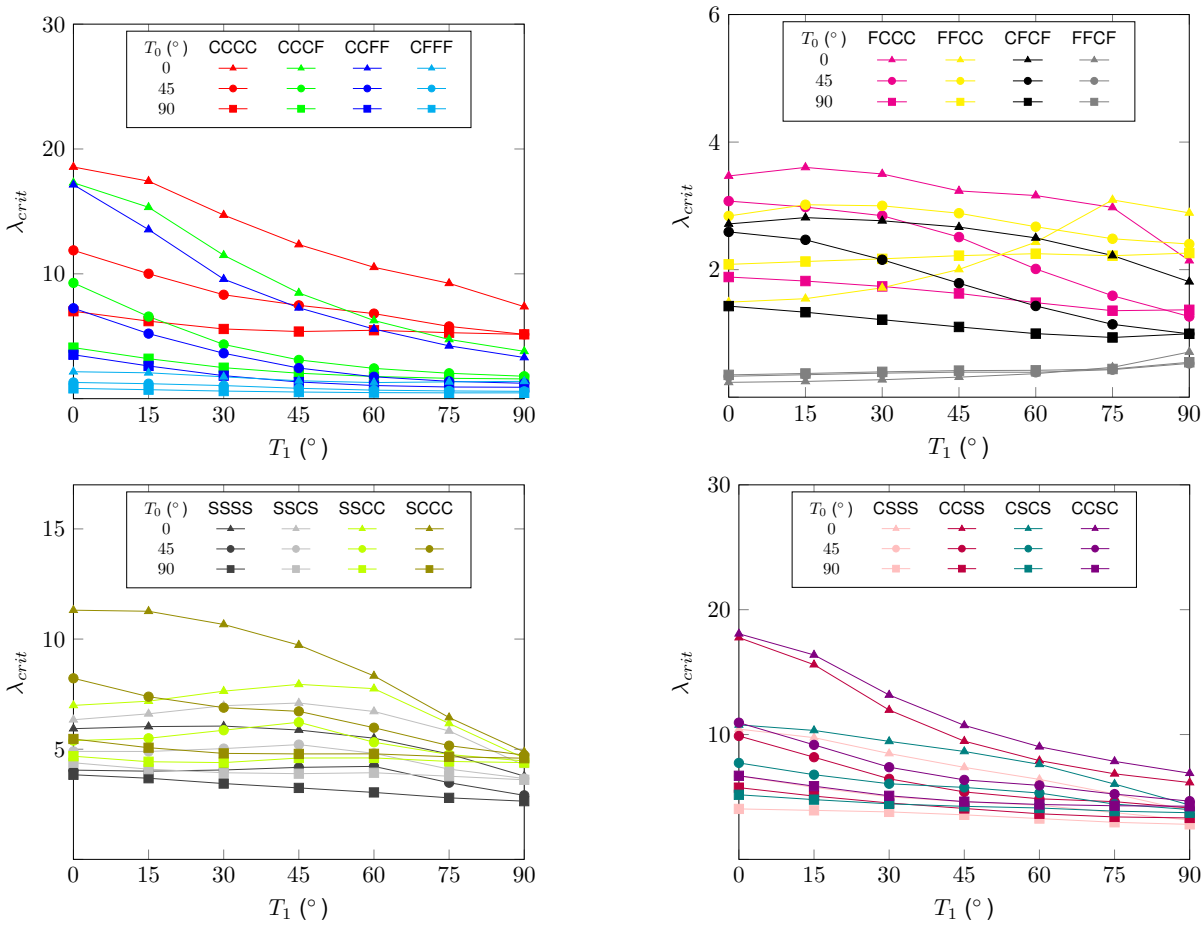

Figure 3.11: Uniaxial x buckling critical load factor (λ_{crit}) evolution with T_0 and T_1 in multiple boundary conditions.

sions regarding the evolution of buckling performance in comparison with x buckling. For instance, in the upper left plot of figure 3.13, when CCCC conditions are applied, it is possible to observe that the VSS $<45, 90>$ configuration has better performance than other configurations, including CSS. For the same boundary conditions, the uniaxial x buckling has a CSS configuration as its best configuration, which allows to conclude that, not only the performance depends on the boundary conditions applied and whether CSS or VSS are used, but also in which direction the buckling analysis is made. Furthermore, for this boundary condition, the performance increases, for a given T_0, with the increase of T_1, whereas for the remaining conditions of the same plot (CCCF, CCFF and CFFF) the performance stagnates at a certain value or decreases slowly. The increasing performance trend with increasing T_1 is also visible for FFCC and FCCC conditions, in the upper right plot, with the $<90, 90>$ CSS configuration having the best performance. For CFCF and FFCF scenarios, the buckling performance is less sensible to T_1 variation.

From the lower left and lower right plots of figure 3.13, it is possible to conclude that the combination of simply supported and clamped boundary conditions leads to a general trend of increasing performance with increasing T_1. For SCCC, SSSS, CCSC, CCSS and CSSS, the symmetrical VSS $<45, 90>$ configuration has the highest critical buckling load factor while for CSCS, SSCC and SSCS, the best y buckling performance configuration is the CSS $<90, 90>$. The right plot of figure A.6 shows that, for

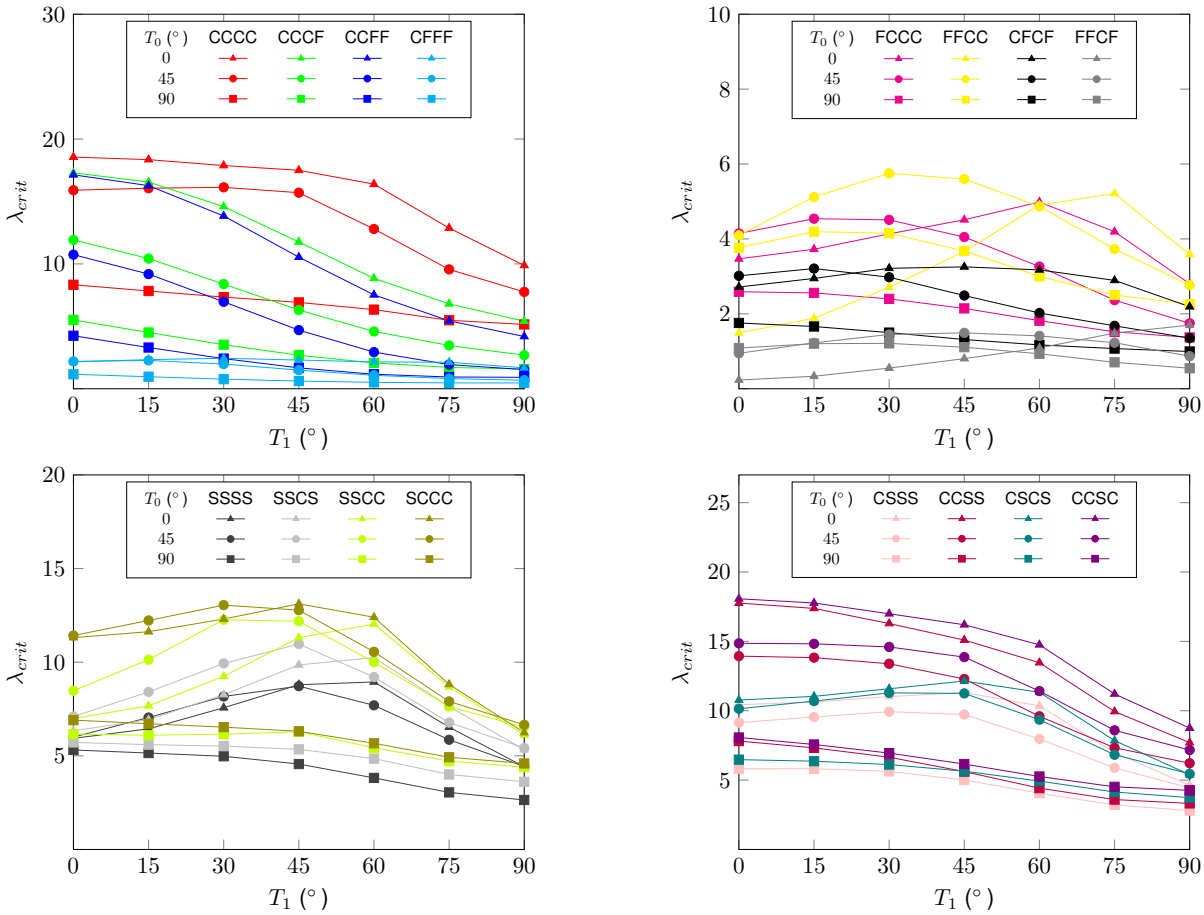

Figure 3.12: Uniaxial x buckling critical load factor (λ_{crit}) evolution (antisymmetric facesheet configuration) with T_0 and T_1 in multiple boundary conditions.

more diversified boundary conditions (i.e, clamped, simply supported and free conditions are applied at least once in the structure), there is a tendency, in the context of the set of configurations tested, for CSS configurations to have a performance advantage over VSS, namely being $<90, 90>$ CSS the configuration with the highest buckling critical factor. However, there is a exception present in the CSSF case, where the VSS configuration $<90, 45>$ has the best performance, in that boundary condition, out of all symmetrical configurations.

In contrast to the results obtained in uniaxial x buckling, antisymmetric face sheet configurations do not always perform better than the symmetrical cases, having, in some scenarios, worse performance. In figure 3.14, there are a multitude of curves in the different plots that have a similar behaviour: the buckling performance increases until $T_1 = 45°$, then decreases until $T_1 = 75°$ and once again increases until $T_1 = 90°$. The former is verified, for example, in CCCC, SCCC and CCSC conditions for configurations with $T_0 = 45°$. So, although there are plenty of curves with the same increasing performance behaviour with increasing T_1 as it was detected in the symmetrical cases, the introduction of the antisymmetric lamina produced a less straightforward curve evolution for the critical buckling load factor for some boundary conditions.

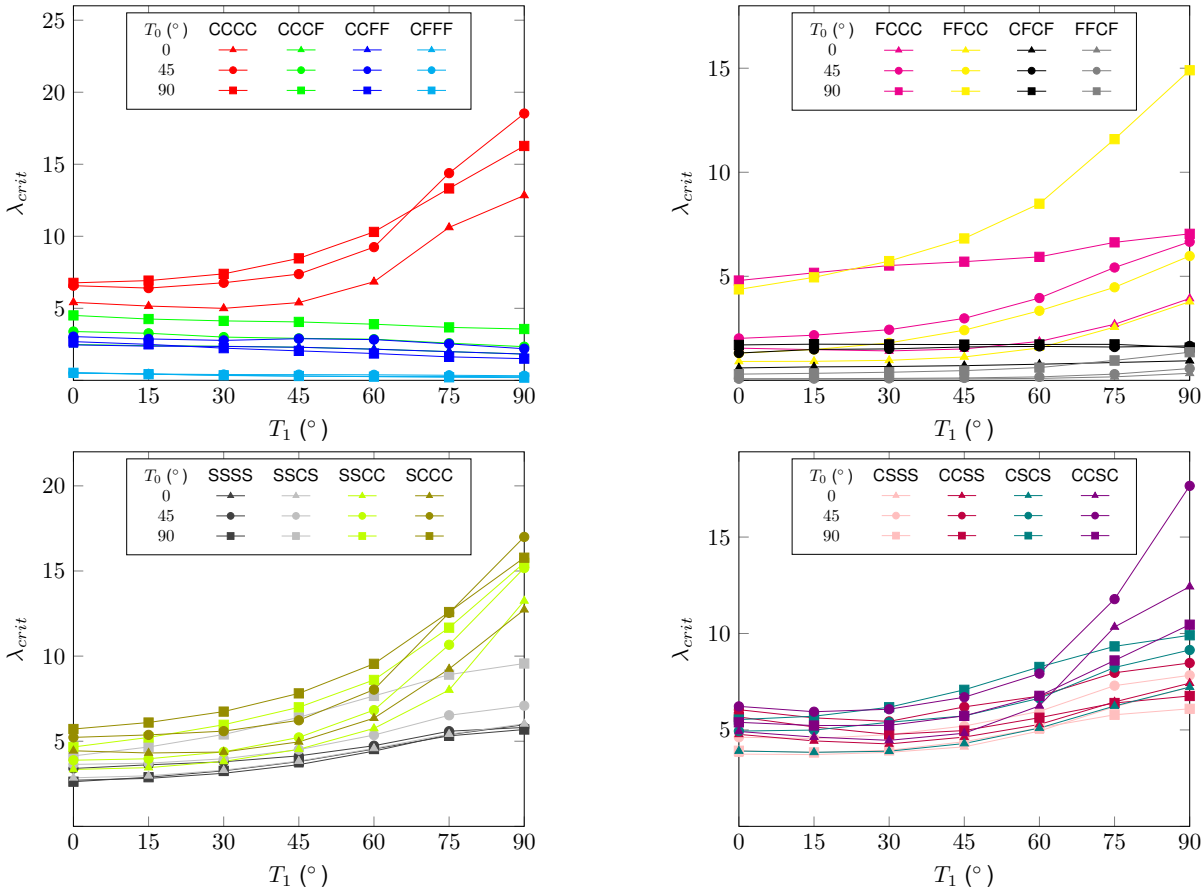

Figure 3.13: Uniaxial y buckling critical load factor (λ_{crit}) evolution with T_0 and T_1 in multiple boundary conditions.

Biaxial buckling

The effects of the simultaneous application of compression forces in both directions (x and y) is studied in this biaxial buckling analysis. To this extent, compression forces of 100 kN are applied in each direction.

The first conclusion taken from the results of the symmetrical configurations, visible in figure 3.15, is that, as expected, since the structure is subjected to a combination of different direction forces, the overall critical buckling load factor is smaller than in the previous uniaxial cases. In the upper left plot of figure 3.15, the CCCF and CCFF curves have a decreasing performance behaviour with increasing T_1. In either scenario, the best performing configuration is a VSS: $<90, 0>$ in the first and $<0, 30>$ in the second. The CCCC curves have an irregular behaviour, namely with $T_0 = 45°$ and $T_0 = 90°$, with buckling performance increasing and decreasing in turns with increasing T_1.

The lower left and lower right plots of figure 3.15 show that scenarios involving a combination of clamped and simply supported boundary conditions, for symmetrical configurations, lead to an almost constant performance curves, with only a small increase with T_1. One of few exceptions that stands out is the $T_0 = 0°$ curve for CCSC, where there is an initial decreases until $T_1 = 30°$ followed by an increases until it reaches the peak performance at $T_1 = 90°$, being the latter the best performing symmetrical configuration with this boundary condition. Results for more diversified scenarios are presented

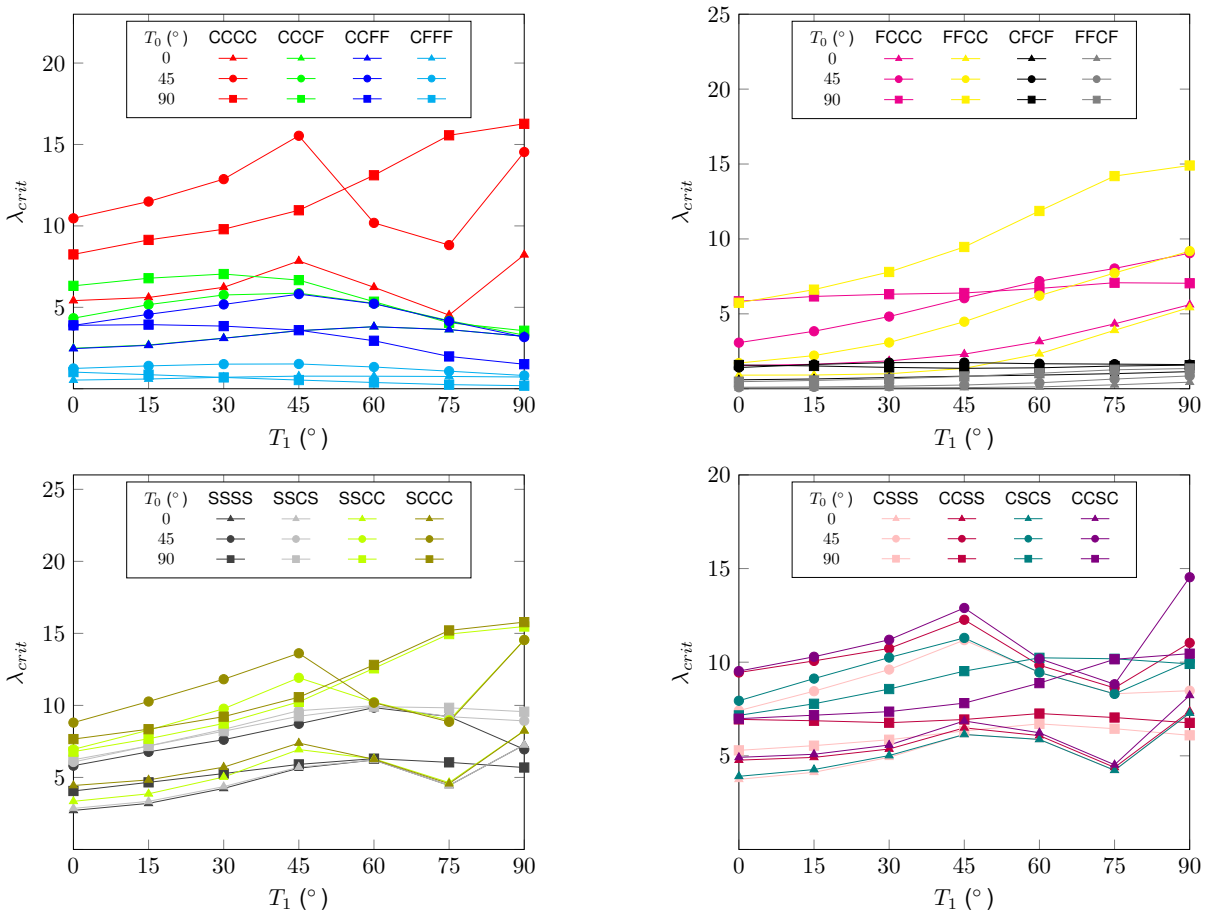

Figure 3.14: Uniaxial y buckling critical load factor (λ_{crit}) evolution (antisymmetric facesheet configuration) with T_0 and T_1 in multiple boundary conditions.

in annex, in figure A.7.

The inclusion of antisymmetric face sheets to the sandwich structures leads to a considerable rise in buckling performance (figures 3.16), reaching values of critical buckling load factor, in some cases, twice as high as the ones obtained with symmetrical configurations. In the upper right plot of figure 3.16 this is especially noticeable for FFCC conditions, with the VSS antisymmetric configuration $<90, 15>$ having a critical buckling factor of around 4 which is more or less double the value for the best symmetric configuration $<90, 60>$ (around 2).

Observing the different plots presented, in the majority of the boundary conditions scenarios, the best configuration tends to be a VSS. Furthermore, although in some cases the curve evolution is steady (it either increases or decreases in a smooth manner), there are some curve examples for which the behaviour is more irregular, such as CCCC with $T_0 = 0°$ or SCCC with $T_0 = 0°$, where multiple increases and decreases in the same curve are present.

The overview of these antisymmetric results leads to a conclusion that the introduction of steered fibers in the face sheets is a major advantage and upgrade in relation to CSS, namely for the biaxial analysis considered in this particular study, allowing for the great improvement of structural performance in this type of instability.

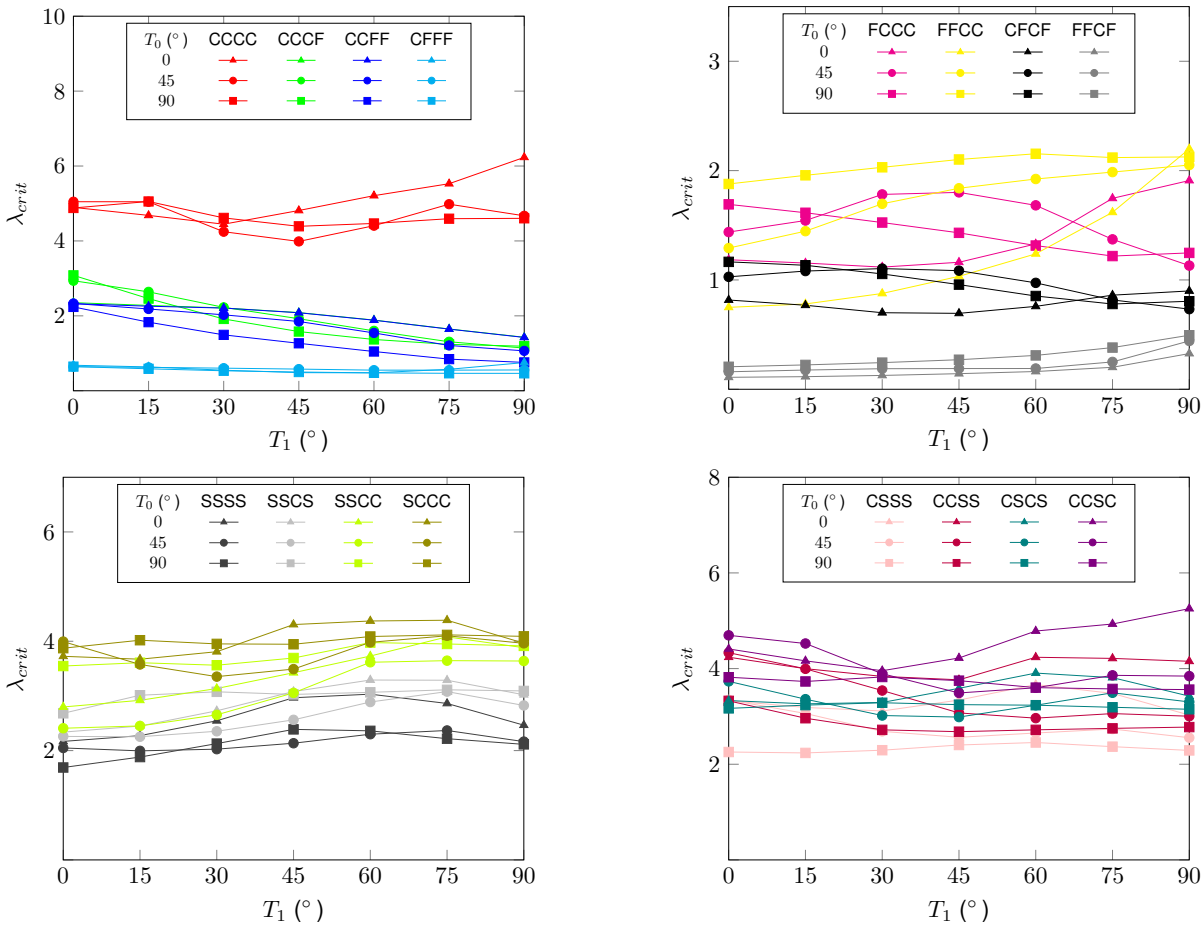

Figure 3.15: Biaxial buckling critical load factor (λ_{crit}) evolution with T_0 and T_1 in multiple boundary conditions.

Shear buckling

Uniaxial buckling in both directions as well as biaxial buckling are, usually, the most analysed types of buckling when studying a structure. However, there are other types of buckling scenarios, such as shear buckling, that are examined in this section with the objective of having a more complete understanding of low stiffness composite sandwich structures mechanical behaviour, namely VSS. For the results obtained in terms of shear buckling, shear forces are applied in the x and y edges of the structure, having in mind that these forces have to cancel the action of each other in both magnitude and direction as well as the torque produced. The value used for shear forces was 100 kN.

Figure 3.17 presents the symmetric configurations results for shear buckling. The upper left plot of figure 3.17 demonstrates that although there are, for CCCC conditions, similar critical buckling load factors for the three values of T_0 when T_1 is less than $30°$, above this value, symmetric $T_0 = 90°$ configurations dominate other configurations for this boundary condition. A different evolution of performance is seen in CCCF and CCFF, where for all T_0, the performance decreases with T_1, with a minor increase in some cases near $T_1 = 90°$, and the configurations with $T_0 = 0°$ tend to have the best performance.

The lower left and lower right plots of figure 3.17 present similar trends in boundary conditions comprising of only clamped and simply supported edges. In these cases, the performance, in general,

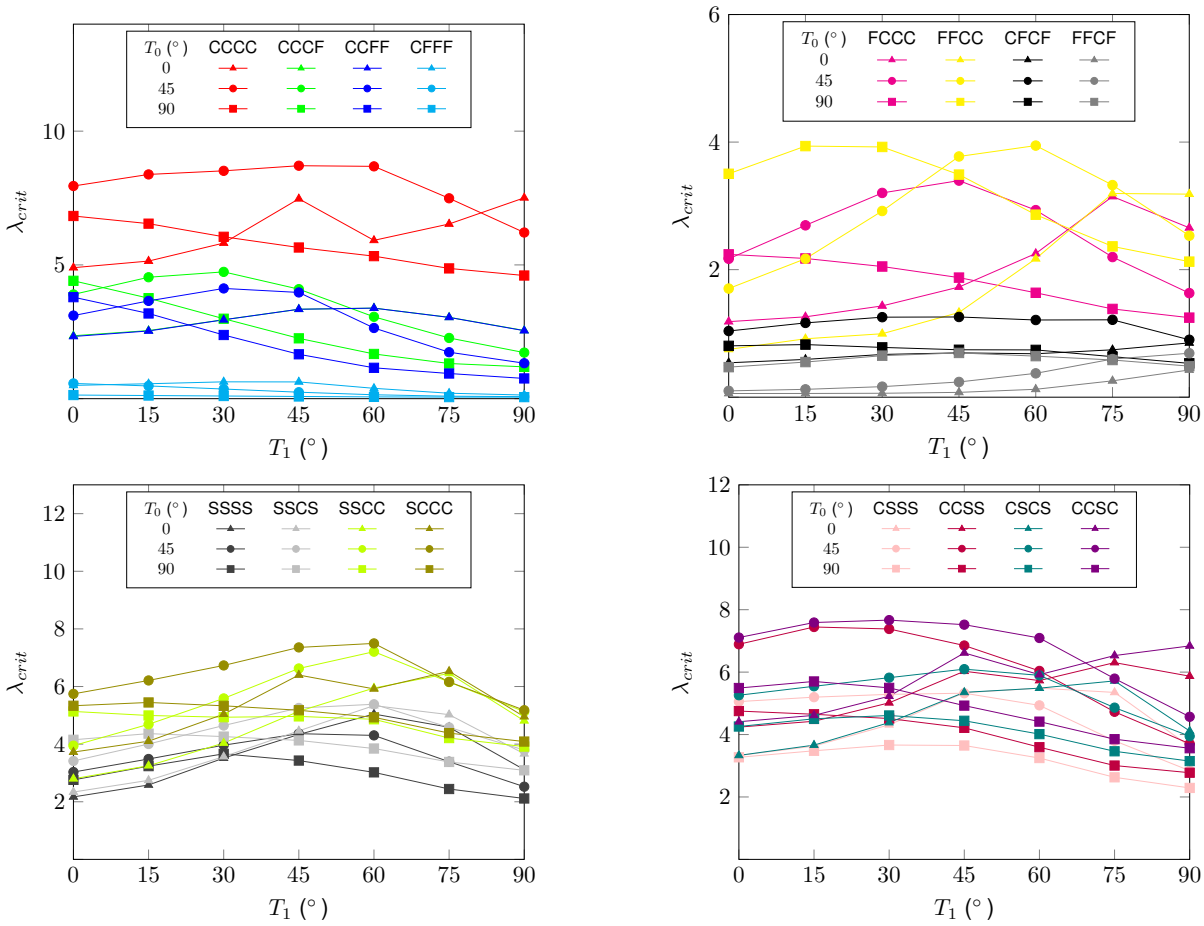

Figure 3.16: Biaxial buckling critical load factor (λ_{crit}) evolution (antisymmetric facesheet configuration) with T_0 and T_1 in multiple boundary conditions.

decreases initially until T_1 reaches around $45°$, and then increases until $T_1 = 90°$. There are some exceptions such as the $T_0 = 0°$ configurations in CCSC, whose increasing performance phase is delayed until $T_1 = 75°$, and the $T_0 = 90°$ configurations in CSSS, in which an decrease, instead of an increase, is verified after $T_1 = 60°$.

The antisymmetric face sheet configurations results shown in figure 3.18 reveal a significant rise in the critical buckling factor in multiple boundary conditions when comparing to symmetric results. In CCCC conditions, the antisymmetric CSS $<45, 45>$ configuration has a slight performance advantage over the VSS $<45, 30>$ configuration, being well above the best performing symmetric structure (a 64% increase in critical buckling factor). In other conditions such as CCFF, FFCC, SCCC or SFCC, in addition to the better performance obtained by antisymmetric configurations, the introduction of steered fibers improved the performance over non-steered ones, with the VSS $<45, 60>$ configuration being the one with the highest buckling factor in FFCC, for example.

Moreover, there is a particular aspect visible in antisymmetric results which is the dominance of configurations with $T_0 = 45°$, in terms of performance, in comparison with other configurations. This is seen in multiple boundary conditions where configurations with this value of T_0 have the upper edge. It is known that, in a pure shear state, $45°$ constant stiffness fibers have the best structural performance among non steered fibers. The better structural capability of $45°$ fibers in a shear state scenario is

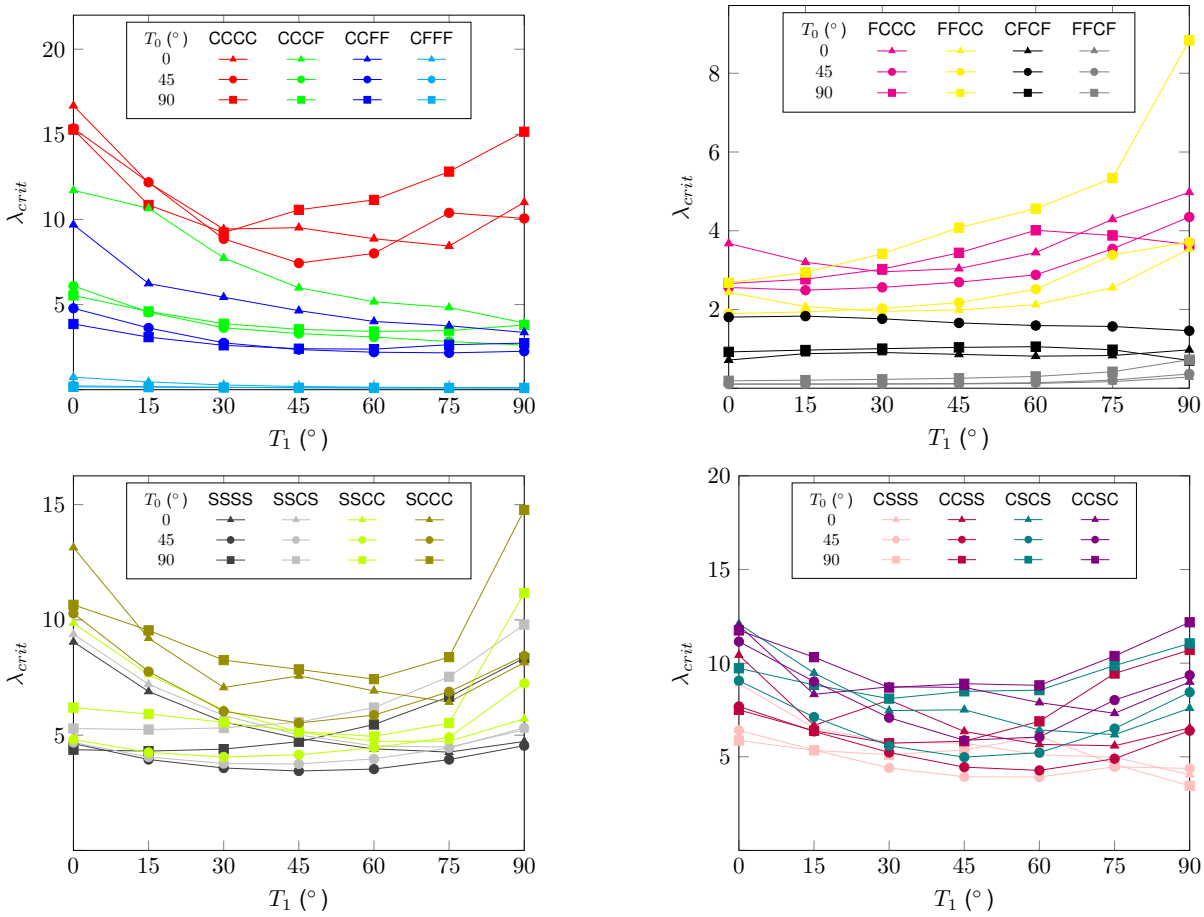

Figure 3.17: Shear buckling critical load factor (λ_{crit}) evolution with T_0 and T_1 in multiple boundary conditions.

still visible in VSS results since the best antisymmetric (and overall) configurations in shear buckling take advantage of this and all of them have a $45°$ fiber orientation in the half-length mark (at $x = a/2$, $T_0 = 45°$).

Multiload buckling

The final buckling study regarding low stiffness core sandwiches consists on the combination of the previous scenarios, that is, a biaxial compression state coupled with shear forces, in an effort to see the impact of the simultaneous application of the various forces.

Figure A.9 shows that the best symmetrical configurations are CSS, namely $<0, 0>$ for boundary conditions such as CCCC, CCCF, CCFF and CFFF. For other conditions, such as FFCC, CFCF , SCCC or SSCC a CSS configuration is still the better option, although in these cases the CSS $<90, 90>$ configuration is the option to choose instead of $<0, 0>$.

In general, an initial decrease followed by an increase in performance, more visible in the CSSS, CCSS, CSCS and CCSC cases while, in the presence of more complex boundary conditions, presents a continuous increase or decrease in performance, depending on the scenario. Regardless of the boundary condition, the main conclusion is that, for symmetric configurations, CSS tend to have a performance advantage over VSS.

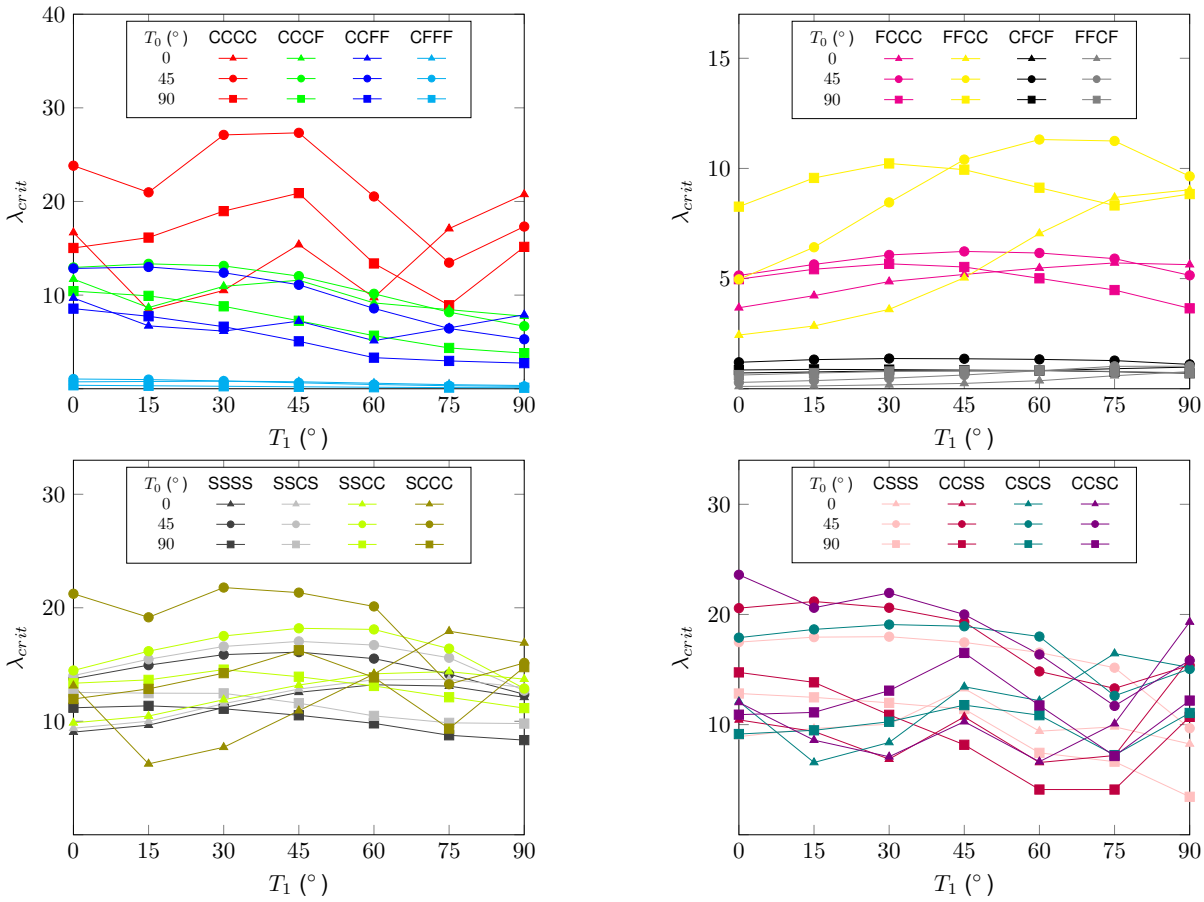

Figure 3.18: Shear buckling critical load factor (λ_{crit}) evolution (antisymmetric facesheet configuration) with T_0 and T_1 in multiple boundary conditions.

As it occurred in previous studies, the use of antisymmetric configurations leads to a significant rise in critical buckling loads, as shown in figure A.10. VSS antisymmetric configurations with $T_0 = 45°$ have, generally, the better multiload buckling performance across the set of boundary conditions tested. Some exceptions to the prior statement include the CFCF and the SSSS scenarios where $<0, 90>$ and $<0, 75>$ are the best configurations, respectively.

In the light of the results presented in the multitude of different types of structural analysis, it is possible to conclude that VSS can indeed have structural performance advantages over CSS. Therefore, an optimization process involving VSS is justified, allowing for a quantitative overview of the improvement brought by the best VSS configuration over the best CSS configuration.

Chapter 4

Optimization Methods and Framework Execution

When designing a particular structure, most often an engineer not only wants to know how does a specific design behave, but also, more importantly, wants to design the best possible structure in a given scenario. Therefore, optimization methods emerge as a vital tool to search for that best design. Nowadays, due to the importance gained by composite structures, namely in the aerospace sector, a lot of research has been made to determine which type of optimization algorithm fits best to the most typical structural problems applied to composite structures.

According to El-Omari [46], the multitude of different optimization algorithms available can be classified taking into account different overlapping categories. However, it must be clear that the following categories enumerated are not the only ones that can be used to classify optimization algorithms. The categories considered are the following:

- **Problem functionality**: the algorithms can be problem-independent or problem-specific. As the names suggest, problem-independent algorithms can be used for different kinds of problems, being its intrinsic code generic in that sense. On the other hand, problem-specific algorithms are created with the objective of being able to solve a specific type of problem.

- **Output optimality**: optimization algorithms, in this category, are classified into deterministic and nondeterministic algorithms. The former, given a particular input data set, produces the same, unique and probably optimal output, independently of the number of repeated runs the algorithm has been subjected. Typically, this type of algorithms are used for small-scale problems since the solutions can be obtained in a reasonably amount of time. For large-scale problems, this type of algorithms, in some cases, is not practical due to the unfeasible amount of time needed to reach a solution. Nondeterministic algorithms exhibit an opposed behaviour to deterministic ones since different algorithm runs may produce slightly different solutions, for the same input data. Usually, some degree of randomness, that normally follows specific rules, exists in such algorithms which causes the discrepancy in behaviour. Nonetheless, the different runs are considered valid.

Nondeterministic algorithms are extensively used in the search of estimated solutions due to their different performance degree dictated, in part, by the level of intrinsic uncertainty. This is especially useful when exact algorithms can not compute an optimal solution or when such exact algorithms can not find a solution in an acceptable amount of time.

- **Searching scope**: algorithms can also be grouped into global search and local search methods. Local search algorithms can become stuck in local-optimal solutions while global search algorithms try to find the global optimal solution considering the entire search space as a whole. However, the latter can be more time-consuming.
- **Number of objectives**: in this category, the optimization problems and algorithms are essentially classified into two labels, whether there is only one single objective function or more than one objective function to optimize at the same time. In the multi objective function case, more than one objective function is evaluated and often occurs that these objectives are contradictory, that is, the optimal results for each objective function follow different directions.
- **Number of starting solutions**: optimization algorithms can also be classified based on the number of starting solutions in population-based algorithms and single-solution (trajectory) algorithms. The former generates multiple random solutions, being afterwards improved towards the global optimal solutions through multiple iterations. The latter starts with one random solution and then improves it throughout the whole process. Each iteration only contains one solution. Population-based algorithms give more emphasis to exploration (extensive search of solutions in the whole solution space), which allows for a better search of the overall optimal global solutions, thus making these algorithms more robust to local-optimal solutions. On the other hand, single-solutions algorithms focus on exploitation of the search space (targets a specific region of the solution space to find a more refined output).

Classic exact methods can be unsuitable for complex optimization problems due to their inability of finding a solution or their unfeasible time cost. To overcome this, approximation and heuristics algorithms have been developed, which allow the computation of optimal or close to optimal solutions. However, heuristic methods are usually problem-specific techniques and are often too greedy, which leads to a local optimal solution instead of a global one. Thus, a new variant of heuristic methods, meta-heuristics, was developed to solve the disadvantages of heuristic algorithms.

An important and also commonly used class of methods is gradient-based methods. These usually are classified as deterministic, local-search optimization algorithms that solve optimization problems based fundamentally on the calculation of the first derivative or the entire Hessian matrix. These can essentially be divided according to the information needed in the process: first-order gradient methods only require the first derivative information while second-order and higher-order gradient methods make use of more derivative information from the Hessian matrix [8].

Meta-heuristic algorithms are usually problem-independent methods and are considered high-level heuristics. Although problem-independent, which allows for an easier implementation in different scenarios, optimization parameter tuning, inside the algorithms, is necessary, nonetheless, since different

problems can lead to different values of these parameters. A major proportion of the meta-heuristic algorithms are nature-inspired. Although the use of such algorithms can not guarantee, *a priori*, the real overall optimal solutions, these methods allow for the computation, in a realistic and acceptable computational time, of approximate solutions that, if optimization parameters are tuned in an adequate manner, are close to the optimal solution [46]. Moreover, meta-heuristic algorithms do not require the additional information regarding the derivatives of both the objectives functions and constraints, which is an advantage taken into account that it can be cumbersome to obtain such information. Meta-heuristic methods are usually the preferred ones when it comes to composite structures and have been proven to be effective tools regarding the design of these structures. This type of algorithms include, for example, the particle swarm optimization, ant colony optimization and genetic algorithm.

Particle swarm optimization algorithm is based on the following key ideas: position and velocity of a particle. A given particle belongs to a multi-dimensional space, where other particles also exist and fly through this space to find the best position they have seen. An important aspect about this algorithm is that each particle has a memory sense, that is, is capable of remembering the best position that it travelled to in its journey. Moreover, the swarm has a collective memory, where the particles, besides knowing the personal best position, also know the others best position and, with this knowledge, adjust their next move. This way, each particle updates its velocity and position based on previous information of the swarm, through the mathematical equations that can be more detailed in Xu and You [47].

Ant colony optimization is also inspired in a physical phenomenon, in this case, nature related. This method is one of the most recent ones and replicates ant's behaviour in search of food [48]. In the journey of finding food, real ants are able to find the shortest path from the food it encounter to its nest home, without using visual clues. Ants do this by leaving a pheromone trail on their way, with each ant choosing a path that probabilistically depends on the intensity of pheromone trails laid by previous ants, being paths of rich pheromone the probabilistically preferred ones for ants. These trails of pheromone decay continuously by evaporation.

Although the before mentioned algorithms are a choice to consider in what respects the optimization of VSS, the optimizer that it is used in this work is a genetic algorithm. This is primarily due to the fact that genetic algorithm is the most widely preferred method used in the optimization of composite structures, as reported by Xu et al. [7], and, thus, with more information about its performance, especially when it includes variable stiffness components. Even though gradient-based methods can be, in some cases, more time-efficient if analytic or semi-analytic calculation methods are used for the computation of derivatives, this class of methods was not chosen due to its much higher susceptibility, in comparison to meta-heuristic algorithms such as the genetic algorithm, of reaching local-optimal solutions. Furthermore, *Matlab* contains a toolbox that allows for the easier and more user friendly implementation of this powerful algorithm, with the option of thorough parameter tuning of the algorithm, as explained later in this work. For these reasons, a more detailed description of the genetic algorithm is given in the following section.

4.1 Genetic Algorithm

Genetic algorithms (GA), as the name suggests, are a family of search algorithms inspired by the mechanics of natural selection and genetics. The key idea of natural selection, which is the idea of survival of the fittest, is used in the so called individuals (which form a population), being these individuals composed of structured information with a degree of randomness. Basically, every individual holds a pre-determined type of information usually in the form of bits (0 and 1) since this is the most efficient way for computers to handle information. In every generation, a new set of individuals is generated based on information of its parents (individuals of previous generation) and newly created information to increase the level of exploration of the algorithm. The level of randomness introduced in such individuals does not make the genetic algorithm a purely random search optimizer, since it is adjusted to a point where it allows for the search of new individuals (which otherwise would not be generated) without leading to divergence of results, if the parameters are adequately adjusted. Thus, the search range as well as the performance of the algorithm are improved [49].

In terms of terminology, there are a lot of analogies between biological systems and artificial genetic systems. For instance, each individual in a genetic algorithm is represented by a vector which is called chromosome. Each chromosome has multiples genes, which in turn are components of the vector. Each gene is basically representing a specific value regarding a specific design variable. Depending on the codification of information, a gene can have partial information from a design variable or the totallity of that information.

To implement the genetic algorithm, this work resorts to the *Matlab* function *ga* which allows for a more intuitive and user friendly way of applying this sort of algorithm.

The algorithm starts by randomly generating the first population. Besides the size of the population, a creation function is also specified, which allows the user to define how the initial population is generated. From the options available, *gacreationnonlinearfeasible* is the creation function chosen since the optimization problem includes non linear constraints, allowing for feasible individual generation regarding those constraints.

Afterwards, new populations are sequentially generated, being the individuals of the current population used to create the following population, at each step. In order to do so, the algorithm computes the fitness value of each individual of the current population, commonly known as raw fitness scores. The fitness function is also called objective function and it is the function to minimize or maximize. After computing the raw fitness scores, the algorithm converts these scores into values within a range more suitable for the selection function, in a process called fitness scaling. The scaled fitness values are also named expectation values.

The range in which the raw scores are converted to expectation values is of high importance due to its impact on the performance of the genetic algorithm, primarily due to the selection operator. Since the selection function makes use of the scaled fitness values in order to determine the parents of the next generation (by assigning a higher probability to those individuals which have higher expectation), a narrow range of these values has as consequence a low diversity in the individuals. In this case,

the individuals will have approximately the same chance of reproduction, therefore making the search slower. However, the opposite, that is, a wider range of scaled values, is also not appropriate because, in this scenario, the highest scale valued individuals dominate in terms of the gene pool of the population due to its extremely fast reproduction (caused by the high values of scaled values in comparison with other individuals). Thus, this wider range causes the algorithm to narrow the search space and prevents it from finding other individuals out of that dominating high expectation individuals for the parent selection [50].

In the *Matlab* genetic algorithm the user can select the fitness scaling function, *FitnessScalingFcn*, from a range available in the software. Out of those options, *fitscalingrank* is the function selected in this work. This particular option scales the raw scores proportionally to the rank of each individual instead of its raw fitness value. More precisely, the scaling is proportional to $1/\sqrt{r}$ where r is the rank of the individual, which is defined as its position in the sorted scores. The most important aspect of rank fitness scaling is that it removes the spread of raw scores. To better illustrate this effect, figures 4.1a and 4.1b are presented.

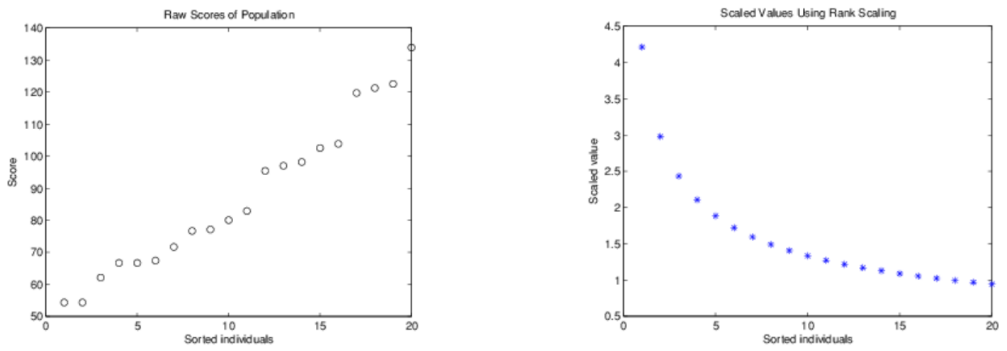

(a) Raw scores.

(b) Rank scaling.

Figure 4.1: The effect of rank scaling [50].

As it can be seen in the figure above, the rank scaling option allows for a smoother and more well behaved distribution of the individuals in terms of its strength. It also allows for less fit individuals to be closer to each other, while better fit individuals stand out with their expectation value. By default, the genetic algorithm of *Matlab* minimizes the fitness function and, thus, lower raw scores correspond to higher scaled values, therefore higher probability of being selected as parents.

The previously mentioned selection function is one of three main operators of the genetic algorithm: selection, crossover and mutation. As stated before, the selection function chooses the parents for the next generation depending on each individual's scaled values. Regarding the selection operator, there are many options than can be used in the *Matlab* genetic algorithm which include, for example, tournament selection, wheel roulette and uniform selection. The tournament technique consists in the selection of individuals according to their fitness values, through a process of stochastic roulette wheel done in groups of individuals with a specified size (tournament size), after which those with the better (high in the case of maximization) fitness values in each group evaluated are added to the pool of parents of the next generation. This technique is the chosen one for this work since, according to Chahar et al.

[51], as long as the tournament size is not large (in which case it would decrease diversity) the tournament selection has multiple advantages in comparison with other techniques such as the possibility of parallel implementation and the preservation of diversity (when tournament size is adequate). Thus, a tournament size of two is chosen to appropriately make use of the advantages of this technique.

After the parents selection, the reproduction phase of the algorithm follows, where the creation of the next generation is defined, through the use of crossover and mutation operators, as well as the elite individuals parameter. The *EliteCount* parameter allows for the algorithm to guarantee that the best individuals from a certain generation survive to the following generation. The default size of 5% of the population size is used for this parameter.

Regarding the crossover operator, it specifies how the selected parents combine to generate new individuals (children) for the next generation. Popular choices for this operator include the single point crossover and the two point crossover. In the single point crossover a random number is selected, corresponding to a specified position in the parent's chromosome, being the information of the parents after that point swapped, originating the offspring. The two point crossover is similar but in this case two positions are randomly chosen, being the information of the parents between these two points swapped. For a visual representation of these types of crossover, figures 4.2a and 4.2b are presented.

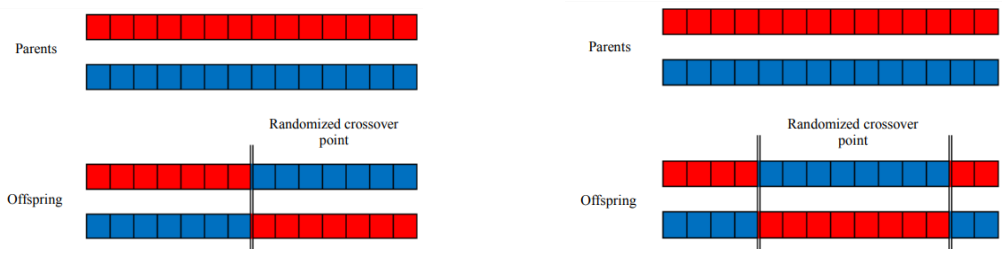

(a) Single point crossover. (b) Two point crossover.

Figure 4.2: Two popular functions of the crossover operator [52].

Besides these two crossover functions and many others not mentioned in this work, there is another function that is relevant to state. The Laplace crossover is a type of crossover that is often used in optimization problems that include integer design variables, which is addressed in the following sections of this work. The first step in this crossover function is to generate uniform random numbers $u_i, r_i \in [0, 1]$. Furthermore, another random number defined as β_i, in this case that satisfies the Laplace distribution, is generated in the following form:

$$\beta_i = \begin{cases} a - b\log(u_i), & r_i \leq 1/2 \\ a + b\log(u_i), & r_i > 1/2 \end{cases} \tag{4.1}$$

where a is a location parameter and $b \in \mathbb{Z}^+$. With this β_i parameter, the two offsprings, $y^1 = (y_1^1, y_2^1, ..., y_n^1)$ and $y^2 = (y_1^2, y_2^2, ..., y_n^2)$, are obtained from two parents, $x^1 = (x_1^1, x_2^1, ..., x_n^1)$ and $x^2 = (x_1^2, x_2^2, ..., x_n^2)$, through the following equations [53]:

$$y_i^1 = x_i^1 + \beta_i |x_i^1 - x_i^2|$$
$$y_i^2 = x_i^2 + \beta_i |x_i^1 - x_i^2| \tag{4.2}$$

The last main operator of the algorithm is mutation. It specifies how frequently the algorithm does small changes in the individuals of a generation in order to create children that, otherwise, would not be possible if only the crossover operator existed. This way, the mutation operator allows for a greater diversity in the search space for solutions outside of the crossover spectrum. However, carefull thought must be taken in what concerns the quantity of mutations per generation the algorithm has. A higher percentage of mutations can cause the algorithm to drift from good results and, thus, slow considerably the convergence rate. On the other hand a low percentage of mutations narrows quite significantly the search space of solutions and increases the probability of a local minimum result.

As it occurred in the crossover operator, there are plenty of options regarding the mutation function such as gaussian or uniform mutation. This work adopts the power mutation function, which is the most adequate mutation function for integer problems. As the name indicates, a random number s is generated, which satisfies the power distribution $s = (s_1)^p$, where s_1 is a uniform random number between 0 and 1 and $p \in \mathbb{Z}$ is the index of mutation that governs the intensity of the mutation perturbation. The offspring, x, are derived in the proximity of a parent solution, $\overline{x}$, through the following law [53]:

$$x = \begin{cases} \overline{x} - s(\overline{x} - x^l), & t<r \\ \overline{x} + s(x^u - \overline{x}), & t \geq r \end{cases} \tag{4.3}$$

where t is given by $t = \frac{\overline{x} - x^l}{x^u - \overline{x}}$, x^u and x^l are, respectively, the upper and lower bounds of the design variable and r is a uniformly distributed random number between 0 and 1.

4.2 Problem formulation

The objective of the optimization processes of the present work is to maximize the fundamental frequency, in the vibration case, and to maximize the critical buckling load, in the buckling case. A plate with $1 \times 1\ m^2$ is used, being the sandwich structure composed of a core with thickness $t_c = 16\ mm$ and two face sheets which are composed of a stacking of 4 steered or unsteered fiber-reinforced laminas (variable stiffness and constant stiffness, respectively), in a total of 8 design variables. Each face sheet has a total thickness of $t_f = 2\ mm$.

The optimization problem is formulated in the following way:

$$\begin{aligned} &\text{maximize} \quad f(\boldsymbol{x}) \\ &\text{with} \quad \boldsymbol{x} \in \mathbb{Z} \\ &\text{subjected to} \quad g_i(\boldsymbol{x}) \geq 0, \quad i = 1, ..., N_L \end{aligned} \tag{4.4}$$

where $\boldsymbol{x}$ is the vector containing the decision variables $[<T_0, T_1>]_i$ for each lamina i, in the case of

curvilinear fibers, and $[T_0]_i$, in the case of straight fibers, $f(\boldsymbol{x})$ is the objective function (fundamental frequency in vibration and critical buckling load in buckling) and $g_i(\boldsymbol{x})$ are the nonlinear constraints, being N_L the number of laminas.

For curvilinear fibers, since the fiber orientation law chosen is defined with a linear function, there are two decision variables per lamina. In this work, the sandwich structure is symmetric, that is, the composite laminates (top face sheet and bottom face sheet) are symmetric to one another about the midplane of the sandwich core but the face sheets themselves are not necessarily symmetric. Thus, the total amount of decision variables is eight. Moreover, it is assumed that the decision variables can only take integer values and not the general case of being a real number. That is due to the fact that the variation of the decision variables (T_0 and T_1 for each lamina) in the decimal places would not differ significantly from their nearest integer counterpart. Furthermore, the inclusion of the possibility of x taking on real values would cause a slower convergence. In addition, the manufacturing of these types of sandwich structures, in this scenario, would be harder to obtain since the processes used typically do not have precision of many decimal places. The decision variables have a lower and upper bound of -90° and 90° , respectively.

The non linear constraints, $g_i(\boldsymbol{x})$, concern, in this case, the curvature constraint given by equation 2.8. This constraint is explicitly expressed, in the case of curvilinear fibers, in the genetic algorithm so that the steered cases are, in fact, respecting such constraint. In case of straight fibers, by default the curvature is zero and does not vary, so the constraint is implicitly employed due to the intrinsic nature of constant stiffness laminates.

The properties of the materials used in the optimization processes of both core and face sheets are summarized in tables 4.1 and 4.2. For the cores, two types of aluminium honeycomb material are used: one of lower density and stiffness denoted aluminium honeycomb of low stiffness (AH-L) and one of higher density and stiffness denoted aluminium honeycomb of high stiffness (AH-H). According to Vescovini and Dozio [32], the mechanical properties of these cores are obtained through the approach employed by [54], where typical aluminium foil properties are used with $E = 72$ GPa and $\nu = 0.3$. It is also stated that the upper bound of the prediction of [54] is used as the value for the transverse shear stiffness G_{13}. A carbon fiber reinforced polymer (CFRP) is used for the face sheets and, in terms of boundary conditions, simply supported in all side faces and edges (SSSS) as well as clamped boundary conditions (CCCC), are applied.

Table 4.1: Properties of the cores used in the optimization processes [32].

	E_{11} (MPa)	E_{22} (MPa)	E_{33} (MPa)	ν_{12}	ν_{13}	ν_{23}	G_{12} (MPa)	G_{13} (MPa)	G_{23} (MPa)	ρ (kg/mˆ3)
AH-H	12	12	4608	0.99	7.74e-4	7.76e-4	7	1108	664	192
AH-L	0.44	0.44	1536	0.99	8.64e-5	8.64e-5	0.27	369	222	72

Table 4.2: Properties of the face sheet material used in the optimization processes [32].

	E_{11} (MPa)	E_{22} (MPa)	E_{33} (MPa)	ν_{12}	ν_{13}	ν_{23}	G_{12} (MPa)	G_{13} (MPa)	G_{23} (MPa)	ρ (kg/mˆ3)
CFRP	173000	7200	7200	0.29	0.29	0.29	3760	3760	3760	1540

4.3 Constraint handling methodology

The presence of non linear constraints in the optimization process causes the need for the genetic algorithm to resort to a secondary algorithm for dealing with this kind of constraints. To this extent, *Matlab* genetic algorithm has two options available: the augmented lagrangian genetic algorithm (ALGA) and the penalty algorithm. Since the ALGA is typically used for problems without integer constraints, this work opts for the usage of the penalty algorithm.

4.3.1 Penalty Algorithm

Penalty algorithms are frequently used in cases of generic search methods, such as the genetic algorithm used here. However, most of these penalty algorithms rely on a penalty function consisted of multiple parameters that are manually configured and that must be set to proper and adequate values, based on the problem in hands, in order to obtain reliable solutions from the genetic algorithm. Thus, there is a dependency, in various penalty algorithms, of the performance of the genetic algorithm on the penalty parameters chosen, which in turn led to the more in-depth research of news ways to adapt the penalty algorithm. The objective is that these new penalty algorithm variants do not influence as much the performance of the genetic algorithm, while, at the same time, maintaining its main advantage of providing a good way of dealing with non linear constraints.

The available penalty algorithm in the *Matlab* genetic algorithm is one of the proposed solutions to overcome the dependency verified in other algorithms. This proposed method, formulated by Deb [55], makes use of the characteristics of the pair-wise comparison in tournament selection (included as option in the genetic algorithm) to develop a new algorithm that executes one of the following steps, depending on the scenario: in the comparison of two feasible solutions, the one who possesses the better objective function value is chosen; in the comparison of one feasible and one infeasible solution, the feasible solution is chosen; in the comparison of two infeasible solutions, the one who possesses the smaller value of constraint violation is chosen.

The main difference between this method and other penalty algorithms is that, in the discussed algorithm, the solutions are never compared, simultaneously, in what concerns its objective function and constraint violation. This way, the need for penalty parameters becomes dispensable. In any of the possible scenarios when it comes to pair-wise comparison of solutions (the three presented above are the only ones possible in a pair-wise comparison), the best is always the preferred and chosen one in any of those scenarios. Moreover, the fact that infeasible solutions are compared, between each other, based only on the constraint violation value makes unnecessary the computation of the objective function of infeasible solutions, in which, being infeasible, there is no interest of computing, by the designer, the respective objective function values, allowing for a better computational efficiency.

The mathematical formulation for the implementation of the fitness function of this algorithm is given

by equation 4.5 as follows:

$$F(\boldsymbol{x}) = \begin{cases} f(\boldsymbol{x}) & \text{if} \quad \langle g_j(\boldsymbol{x}) \rangle \geq 0 \quad \forall j = 1, 2, ..., m, \\ f_{max} + \sum_{j=1}^{m} \langle g_j(\boldsymbol{x}) \rangle & \text{otherwise} \end{cases} \tag{4.5}$$

where f_{max} is the value of the feasible solution, in the current population, with the worst objective function value.

With this expression, a feasible solution is always preferred to an infeasible solution and, if compared with another feasible solution, the one with the highest fitness function value (that, in case of feasible solutions, is equal to the objective function value) is chosen. In the case of infeasible solutions, the fitness function depends, besides the constraint violation, also in the population evaluated through f_{max}. Since all fitness function values for infeasible solutions are given by summing to the fitness function value of worst feasible solution the corresponding constraint violation of that infeasible solution, the penalty method encourages the genetic algorithm to generate infeasible solutions that, at subsequent populations, come closer to the feasible space. Thus, the intent is that, at each generation, the genetic algorithm generates more feasible solutions and the infeasible solutions generated, besides being progressively smaller in number, have a lower constraint violation than previous populations. To better visualize the algorithm described, figure 4.3 is presented, where the six solid dots on the x axis represent solutions of the GA population, with its corresponding fitness function value, constraint violation and objective function value.

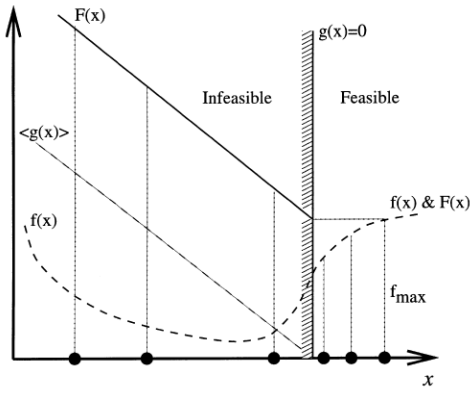

Figure 4.3: Constraint handling methodology proposed by Deb [55].

4.4 Framework Execution

This section presents the methodology followed in the optimization process. Both *Python* script, responsible for the model creation and structural analysis in *Abaqus*, and *Matlab* script, responsible for the optimization process, play a key role and the interactions between them are essential for the optimization execution.

As previously mentioned in chapter 3, *Python* scripts are used to create the finite element model

of the structure. Furthermore, these scripts also receive the values for T_0 and T_1 for the four laminas generated from the *Matlab* scripts and then use them in the model in analysis. Afterwards, when the structural analysis is completed, it sends to the *Matlab* script, where the optimization algorithm is being processed, the results: fundamental frequency, in case of vibration, and critical buckling factor, in case of buckling.

Regarding the *Matlab* software component, multiple scripts are created to ensure a correct and successful optimization process execution. There are five scripts in total. The main script is used to establish values for the optimization parameters as well as to execute the *Matlab* genetic algorithm function. Another script is used to formulate the objective function of the problem, where the *Python* script is called and executed and, therefore, the analysis is made. The objective function script also verifies if a determined individual was already analysed. This is done resorting to two new scripts, one which saves each individual properties (T_0 and T_1 for each of the four lamina) and respective analysis result in a history matrix and another which verifies if a combination of the 8 design variables generated by the genetic algorithm was already analysed (it is verified if this individual is already in the matrix of individuals analysed). Finally, the fifth script is related to the curvature constraint implemented in the model, ensuring that the right member of equation 2.8 does not surpass the maximum allowed curvature value in the optimization process (3.28 m^{-1}).

In a more detailed description, the optimization framework execution is governed by the following steps: initially, the genetic algorithm (in *Matlab*) generates 8 design variables and verifies if this individual has been already analysed. This is relevant since it allows for a better efficiency of the algorithm with a lower computational cost, avoiding redundant analysis of the same individual. In case of a repeated individual, then the *Python* script is not executed (i.e., structural analysis is not made). Otherwise, the design variables are passed to the *Python* script in order to execute the analysis on the individual in study.

The next step concerns the structural analysis itself, where the *Python* script creates the geometry, mesh, properties, type of analysis, loads, boundary conditions and other constraints (*Tie constraint*, for example) necessary for the pre-determined analysis to be made. In order to generate the model, the script reads a file containing the values of the design variables generated by the genetic algorithm to then accordingly specify the orientation in each element local coordinate system. When the analysis is completed, the script saves the relevant result information (fundamental frequency or critical buckling factor) in a text file. Afterwards, the *Matlab* genetic algorithm reads this file and saves the individual properties (design variables and result value) in the history matrix. This process is done for all individuals in a given generation. At the end of each generation the algorithm checks, according to the stopping criteria established, if convergence is reached, in which case the algorithm halts and the optimization process is completed. If the stopping criteria has not yet been met, then a new generation is created resorting to the use of the genetic algorithm fundamental operators: selection, crossover and mutation.

Figure B.1, in annex, presents a flowchart which summarizes and visually represents the steps that are described in this chapter.

Chapter 5

Optimization Results

5.1 Sensitivity Analysis: Orthogonal Arrays

The definition of the values to use for the genetic algorithm optimization parameters can be a truly difficult task since the most adequate values to use vary from problem to problem. Thus, there are no objective and universal values for these parameters. The only solution is to do a sensitivity analysis in the parameters that seem the most important for the convergence and obtainment of good results.

It is of great importance to choose not only which and how many parameters to test but also the range of values tested for each of the parameters. All of these definitions must be carefully thought of due to their impact on the computational cost of the sensitivity analysis and the optimization process overall. A higher number of parameters and higher range of values for each parameter translates into a high computational time turning the analysis cumbersome and unfeasible. However, testing only few parameters or in a small range of values results in a poor and incomplete sensitivity analysis.

Due to the high number of parameters available in the *Matlab* genetic algorithm used, a decision had to be made concerning which parameters to choose based on their importance. Therefore, the following parameters are the ones evaluated in the sensitivity analysis [50]:

- **Crossover fraction** - this parameter defines the percentage of children, present in the next generation, that is derived from the crossover of two parents from the previous generation. This parameter can take values from 0 to 1. The crossover fraction value also has an indirect impact on the percentage of children derived from mutation. A high crossover fraction (above 0.9, for example) results in a very low mutation rate which encourages the algorithm to search for solutions in a certain limited region of the solution space (high exploitation, low exploration). On the other hand, a smaller value of crossover (such as 0.5 or 0.6 or lower) translates into a higher value of mutation children in the next generation, which encourages the algorithm to search for outside of the box solutions, looking for solutions in a bigger area of the feasible space (low exploitation, high exploration).
- **Population size** - number of individuals that are created at each generation. This parameter is extremely important in the convergence of the algorithm since the creation of generations with

a high number of individuals will result in a high exploration of possibilities in terms of the design variables values in each generation but, on the other hand, the time to analyse an entire generation is also increased. A low number of individuals per generation will result in a more rapid analysis of generations, though in each generation the design variables are poorly explored.

- **Function and constraint tolerance** - one of the stopping criteria available in the algorithm. It defines the tolerance in terms of best fitness value achieved in a pre-setted number of generations. When the variation is smaller than this threshold, then the algorithm stops. More concretely, in case the average relative change in the best fitness function value, over a number of generations specified by the parameter *MaxStallGenerations*, is less or equal to the value defined for *FunctionTolerance*, the algorithm halts. *ConstraintTolerance* determines the feasibility of solutions with respect to nonlinear constraints (curvature constraint, in this case).

- **Maximum stall generations** - another stopping criteria that works together with *FunctionTolerance*. As previously mentioned, it defines the number of generations to evaluate the average relative change in the best fitness function value. If this change is less or equal to *FunctionTolerance*, then the algorithm stops.

In addition to these parameters, there are other parameters such as the definition of the crossover or mutation function as well as other stopping criteria including maximum number of generations or maximum time of the algorithm execution. These and other parameters that are not mentioned are not taken into account in the sensitivity analysis due to the unfeasibly high computational cost that the analysis would have if all of the parameters were to be studied.

The sensitivity analysis includes, therefore, the four parameters described in detail previously with three possible values for each one. The possible values that each of the parameters can take on are summarized in the table 5.1.

Table 5.1: Values tested in the sensitivity analysis for each of the parameters.

Parameters	Possible values		
Crossover fraction	0.7	0.8	0.9
Population size	75	95	115
Function/Constraint tolerance	1×10^{-3}	1×10^{-4}	1×10^{-5}
Maximum stall generations	5	15	20

Usually, a sensitivity analysis with four parameters, each with three possible values, would result in 81 (3^4) different cases to test every possible combination of the parameters available, which is a very high number that would cause the analysis to be very time consuming. The sensitivity analysis made in this work with the structure of parameters and respective values displayed in the table above is only possible, in a acceptable amount of analysis execution time, due to the use of orthogonal arrays.

An orthogonal array (Taguchi's orthogonal arrays) of s elements is an $N \times m$ matrix with the particular characteristic that, in any pair of columns selected, each of the possible ordered pairs of elements appear the same number of times. For a better understanding of this definition, table 5.2 is presented [56].

Table 5.2: Example of an orthogonal array with $N = 4$ test runs (4 rows), $m = 3$ factors (3 columns) and $s = 2$ elements (2 possible values for each factor, 0 or 1). Adapted from Kacker et al. [56]

Row	Column		
	a	b	c
a	0	0	0
b	0	1	1
c	1	0	1
d	1	1	0

From the table, which represents a 4×3 matrix, it is possible to see that, selecting any pair of columns, each of the possible 4 ordered pairs (0,0), (0,1), (1,0) and (1,1) appear exactly once [56]. This is the main property of any orthogonal array.

With the main property illustrated in the previous paragraph, the N rows of an orthogonal array are, in its essence, a subset of the possible s^m test runs, with m factors (parameters), each with s possible values. Thus, orthogonal arrays allow for a robust sensitivity analysis with a much smaller number of test runs, more precisely, with only a N/s^m fraction of the complete factorial test plan s^m. In this work this translates into running only 9 tests instead of 81, that is, 9 times less test runs.

The definition of an orthogonal array also includes the fact that, if an orthogonal array is changed in such a way that its columns are permuted or its row are permuted or the elements within a column are permuted, then the new changed array still remains as an orthogonal array. These three properties derived directly from the definition can be easily explained: the permutation of columns consists in the relabeling of factors; the permutation of elements within a column consist in the relabeling of the values that each factor can take on; the permutation of rows just changes the order of test runs. Thus, this allows for a multitude of different orthogonal arrays that have the same number of rows, columns and elements, being the order of the rows, columns and elements inside each column arbitrary. Although arbitrary, if one orthogonal array can be obtained from an initial orthogonal array through row permutation, column permutation, permutation of elements within a column or a combination of these, then these arrays are defined as equivalent [56].

The orthogonal array created for this work is derived from the design principles available in [57] for the Taguchi design with $N = 9$ and $m = 4$ (in the reference, m appears as k). Table 5.3 presents the orthogonal array used in this work.

Table 5.3: Orthogonal array used for the sensitivity analysis.

Test runs	Population size	Function/Constraint Tolerance	Max Stall Generations	Crossover fraction
T-A	75	1×10^{-5}	5	0.7
T-B	75	1×10^{-3}	15	0.8
T-C	75	1×10^{-4}	20	0.9
T-D	95	1×10^{-5}	15	0.9
T-E	95	1×10^{-3}	20	0.7
T-F	95	1×10^{-4}	5	0.8
T-G	115	1×10^{-5}	20	0.8
T-H	115	1×10^{-3}	5	0.9
T-I	115	1×10^{-4}	15	0.7

The orthogonal array created is slightly different from the design table of [57] in order to incorporate a test (Test G) which has the most restrictive values for population size, function/constraint tolerance and maximum stall generations. Nonetheless, this altered array is still an orthogonal array and it is equivalent to the one displayed in the reference.

The results obtained for the sensitivity analysis in vibration are expressed in figure 5.1.

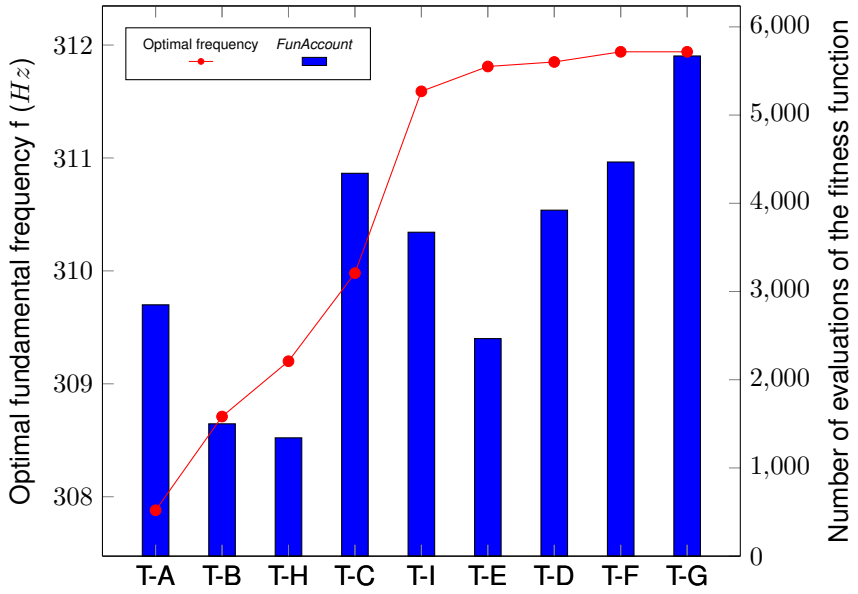

Figure 5.1: Fundamental frequency values (red curve) and computational cost in the form of number of fitness function evaluations (blue bars) for each of the test cases of the sensitivity analysis.

It is possible to conclude that the optimal frequency value varies significantly from tests A, B, H, C and I. Between tests E, D, F and G this difference is minimal. However, the number of times that the algorithm evaluates the fitness functions of individuals (*FunAccount*), that translates into how much computational effort is needed for the whole optimization process, is very different in these tests, ranging from 2466, in test E, to 5670, in test G. Thus, due to the fact that the value for the optimal fundamental frequency stabilizes at test E and being test E the one who leads to a lower computational time (lower *FunAccount*), from the set of tests whose optimal value are close to each other, the parameters used in test E are the ones chosen for the optimization process. In terms of buckling, the parameters used are similar.

5.2 Aluminium Honeycomb Core of High Stiffness Results

The first set of optimization results concerns, as previously mentioned, a sandwich structure whose core is of high stiffness. The terms ”high” and ”low” for the stiffness of the cores tested are used to distinguish these same cores, being the one currently in analysis of higher stiffness than the subsequent one. However, the present core is still, nonetheless, an aluminium honeycomb whose stiffness is, in general and comparing with other types of materials, low.

The sandwich structures are subjected to four independent uni-objective optimization processes in four different structural analysis: free vibration, x buckling, y buckling and shear buckling. The design

variables of each lamina in what concerns the optimal solution are presented in 4 different columns (corresponding to the 4 laminas) in the form $< T_0, T_1 >_i$ for the i lamina.

In annex, table C.1 presents the values for maximum curvature values for each of the optimal VSS configurations obtained (for the boundary conditions and cores tested). The conclusion is that all configurations respect the previously mentioned curvature constraint, as expected.

5.2.1 Constant Stiffness Face Sheets

In addition to the optimization of VSS, CSS optimization is also done to constitute a set of results for comparison. Table 5.4 presents the optimal face sheet configurations and corresponding results and number of generations for vibration, buckling in x direction, buckling in y direction and shear buckling, for CCCC boundary conditions.

The first conclusion is rather interesting, concerning the vibration results. In this case, the optimal solution is characterized by three laminas with x direction orientation ($0°$) and one lamina (the outer one) aligned with the y direction, achieving a fundamental frequency value of $277.804\ Hz$. To understand the effect of the lamina whose direction is perpendicular to the remain three, a vibration analysis to a configuration with all 4 lamina aligned with the x direction is made. In this analysis, the fundamental frequency reached $273.490\ Hz$ and the mode shape is virtually identical to the optimal VSS configuration. Comparing these results, it can be concluded that the introduction of the y oriented lamina results in a more robust and stiffer structure as whole.

Regarding the x buckling results, a similar trend is verified. The optimal face sheet configurations presents three (out of the four) laminas with an orientation close to the x direction ($11°$, $10°$ and $6°$), with an optimal critical buckling load factor of 22.129. This is expected since the direction of highest stiffness of the laminas, which resists the majority of the stresses in the structure, is the fiber direction. Thus, considering that, in this case, there is a load applied in the x direction, the optimal solution is the one with face sheets whose lamina majority is x oriented. Nonetheless, similarly to the vibration result, there is one lamina that does not follow the pattern, albeit, in this case, the lamina in consideration is oriented at $-58°$ instead of $90°$.

The results concerning buckling in the y direction demonstrate an analogous situation to that verified in the previous buckling result. In this case, three lamina are also aligned with the direction of the load applied (y direction) so that, in this way, the fibers stiffer direction (its axial direction, in this case oriented at close to $90°$) is colinear with the load direction, resulting in a better handling of stresses for the whole structure.

The shear buckling results shows an optimal CSS configuration composed of two laminas oriented with the x direction (laminas 1 and 3), one almost aligned with the y direction (lamina 4) and one closely aligned with $45°$ orientation (lamina 2). An interesting fact is that this optimal CSS configuration leads to, as seen in figure 5.2, local instabilities in the corners of the structure $(x, y) = (0, 0)$ and $(x, y) = (1, 1)$. A further investigation on this optimal CSS configuration was made and a conclusion was reach that, in fact, these instabilities decrease significantly the performance of CSS, since the global typical mode

only begins to appear more evidently at bigger buckling load factors (around 50). Therefore, this is the first time, including the studies made in chapter 3, that local instabilities emerge in the presence of CSS. It appears that sandwich structures with low density cores are more susceptible to the onset of local instabilities in shear buckling.

Mode shapes results for optimal CSS configurations with AH-H core, in CCCC conditions, are presented in figure 5.2.

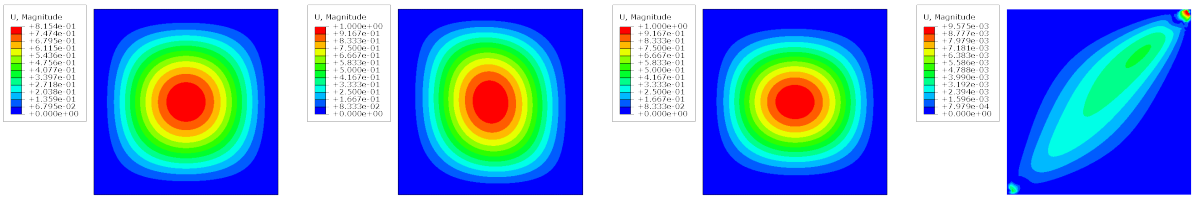

(a) Vibration. (b) Buckling in x. (c) Buckling in y. (d) Shear buckling.

Figure 5.2: Optimal CSS face sheet configurations (with AH-H core) mode shape results in vibration, buckling in x direction, buckling in y direction and shear buckling, subjected to CCCC boundary conditions.

Table 5.4: Optimization results for vibration, buckling x, buckling y and shear buckling for CCCC boundary conditions with AH-H material as core and constant stiffness composite face sheets.

Aluminium honeycomb core of high stiffness (AH-H)						
Structural Analysis	Boundary conditions					
	CCCC					
	Optimal face sheet configuration				Optimal result	Generations
	$< T_0, T_1 >_1$	$< T_0, T_1 >_2$	$< T_0, T_1 >_3$	$< T_0, T_1 >_4$		
Vibration (f in Hz)	$< 0, 0 >$	$< 0, 0 >$	$< 0, 0 >$	$< -90, -90 >$	277.804	24
Buckling x (λ_{crit})	$< -58, -58 >$	$< 11, 11 >$	$< 10, 10 >$	$< 6, 6 >$	22.129	28
Buckling y (λ_{crit})	$< 89, 89 >$	$< 89, 89 >$	$< -2, -2 >$	$< 88, 88 >$	21.394	18
Shear buckling (λ_{crit})	$< 0, 0 >$	$< 36, 36 >$	$< 0, 0 >$	$< 88, 88 >$	39.587	19

Table 5.5 presents the optimal face sheet configurations, corresponding optimal results and number of generations in the optimization algorithm for vibration, buckling in x direction and buckling in y direction, for SSSS boundary conditions. Vibration, buckling in x direction and buckling in y direction have as optimal face sheet configuration a set of 4 lamina at around positive or negative $45°$. Besides this major difference to the CCCC boundary conditions results, in SSSS the optimal face sheet configurations tends to adopt either a symmetric or antisymmetric face sheet configuration while in previous CCCC results it does not happen. While, in SSSS conditions, optimal face sheet configuration is antisymmetric for vibration and buckling in x direction, for buckling in y direction the optimal configuration is symmetric. Optimal results of 165.282, 9.947 and 10.094 are achieved in vibration, buckling in x direction and buckling in y direction, respectively.

5.2.2 Variable Stiffness Face Sheets

Following the optimization of CSS structures, an optimization to evaluate whether VSS can, in fact, possess improved structural performance over CSS, for the geometry, number of laminas and remaining

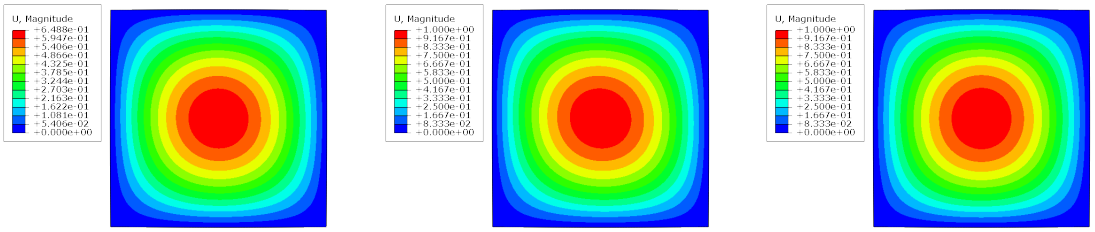

(a) Vibration. (b) Buckling in x. (c) Buckling in y.

Figure 5.3: Optimal CSS face sheet configurations (with AH-H core) mode shape results in vibration, buckling in x direction and buckling in y direction, subjected to SSSS boundary conditions.

Table 5.5: Optimization results for vibration, buckling x and buckling y for SSSS boundary conditions with AH-H material as core and constant stiffness composite face sheets.

Aluminium honeycomb core of high stiffness (AH-H)						
Structural Analysis	Boundary conditions					
	SSSS					
	Optimal face sheet configuration				Optimal result	Generations
	$< T_0, T_1 >_1$	$< T_0, T_1 >_2$	$< T_0, T_1 >_3$	$< T_0, T_1 >_4$		
Vibration (f in Hz)	$< 44, 44 >$	$< -44, -44 >$	$< 47, 47 >$	$< -43, -43 >$	165.282	18
Buckling x (λ_{crit})	$< 44, 44 >$	$< 44, 44 >$	$< -44, -44 >$	$< -43, -43 >$	9.947	19
Buckling y (λ_{crit})	$< -41, -41 >$	$< 46, 46 >$	$< 45, 45 >$	$< -46, -46 >$	10.094	17

conditions tested, is made. Optimal VSS face sheet configuration, with a sandwich core made of AH-H material, and respective optimal result as well as the number of generations needed to achieved them, for the four types of structural analysis made, subjected to CCCC boundary conditions, are presented in table 5.6.

Regarding the vibration result, the only similarity to the optimal CSS result is that the optimal VSS result has a face sheet configuration that includes an almost constant stiffness lamina aligned closely with the x direction (lamina 2 with $T_0 = -9$, $T_1 = -4$), as it occurred in the CSS (3 laminas aligned with the x direction, $T_0 = T_1 = 0°$). The remaining laminas of the optimal VSS reveal the higher design flexibility of this type of sandwich structure over CSS, with all three laminas being aligned, at the half-length of the structure ($x = a/2 = 0.5m$), with the y direction ($T_0 = 90°$ or $T_0 = -90°$) and, at $x = 0m$ and $x = a = 1m$, closely aligned with the x direction ($(T_1)_1 = 0$, $(T_1)_3 = 2°$ and $(T_1)_4 = -3°$). Furthermore, another observation that can be made is that lamina 3 and 4 are antisymmetric.

Looking at the mode shape of both CSS and VSS optimal configurations for vibration (figures 5.2 and 5.9), the introduction of steered fibers flattens the mode shape behaviour in y direction, in comparison with the CSS mode shape, which is more circular all around. This can be explained by analysing the optimal VSS fiber paths, present in figure 5.4. Laminas 1, 3 and 4 have a fiber concentrated region aligned with the y direction at $x = a/2$, which magnifies the y stiffness effect and, consequently, the robustness of the structure, in that region, to free vibration stresses. On the other hand, the x direction optimal VSS robustness is not as high at $x = a/2$ (due, precisely, to the fiber orientation at this region), especially when compared to the CSS optimal face sheet configuration, which has three x oriented laminas, leading to a higher x stiffness in that region. All of the before mentioned aspects contribute to a

non-circular mode shape in optimal VSS, with a flattening effect present in y direction (derived from lower stiffness in that region in x direction, compared to the y direction, and the bigger difference between x and y stiffness at $x = a/2$, in comparison to CSS). This optimal VSS fiber path distribution in the face sheets reaches a significant 11.083% higher fundamental frequency performance, in CCCC boundary conditions, than the optimal CSS configuration.

One extra study that is made concerning this vibration optimization result involves the study of the influence of the relative position between laminas. In this test sample, lamina 2 changes position with lamina 3. This change leads to a VSS structure with a fundamental frequency of $298.50\ Hz$, around 4% smaller than the optimal VSS result. Therefore, it is possible to conclude that the relative position between laminas impacts the results, in vibration, albeit in a moderate manner.

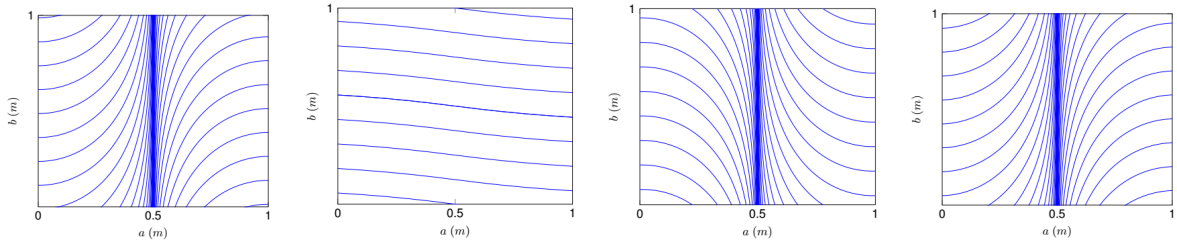

(a) 1^{st} lamina. (b) 2^{nd} lamina. (c) 3^{rd} lamina. (d) 4^{th} lamina.

Figure 5.4: Fiber paths for optimal VSS face sheet configuration in vibration with AH-H core and CCCC boundary conditions.

The tendency for antisymmetric or close to antisymmetric laminas, in results of buckling in the x direction, is even more visible, being lamina 1 almost antisymmetric of lamina 2 and lamina 3 almost antisymmetric of lamina 4. However, the two first laminas have a completely different fiber path orientation evolution than the latter two. Lamina's 1 and 2 fiber path begins with a 14° (or -14°) orientation at $x = 0$, therefore close to being aligned with the x direction. Afterwards, it progressively evolves to an orientation almost aligned with the y direction (-79° or 81°) at $x = a/2$, returning to the initial orientation value at $x = a$. On the other hand, lamina's 3 and 4 fiber path initiates with an orientation close to a 45° (or -45°) angle, more noticeable in lamina 3 ($(T_1)_3 = 41^\circ$ while $(T_1)_4 = -33^\circ$), and then evolves to an orientation, at $x = a/2$, practically aligned with the x direction ($(T_0)_3 = -2^\circ$ and $(T_0)_4 = 1^\circ$). This VSS configuration provides a critical buckling load factor, λ_{crit}, 27.073% higher than the optimal CSS configuration.

The observation of the differences between the two mode shapes (optimal CSS and VSS) allows for a better comprehension of the significant difference in performance. The introduction of antisymmetric laminas in the optimal VSS configuration leads to a more uniform well distributed stiffness across the entire structure: lamina 1 and 2 provide the extra stiffness in y direction (closely y fiber orientation in that region) and laminas 3 and 4 provide more stiffness in x direction (closely x fiber orientation in that region), at $x = a/2$; at $x = 0$ and $x = a$, the inverse occurs, that is, the more x oriented fibers in laminas 1 and 2 now provided more x stiffness while the more y oriented fibers in laminas 3 and 4 provide more y stiffness. Although, the optimal VSS mode shape in buckling in x direction may appear, at first sight, as a standard mode shape that could be achieved with any CSS configuration, the underlying factors (i.e., the

face sheet fibers paths) that cause this mode shape are radically different from the ones that could be achieved with a CSS. Furthermore, it leads, as described before, to an impressive buckling performance, therefore to the conclusion that the capability of VSS fibers paths to have variable stiffness across its path, in the same lamina, (and, consequently, providing different degrees of stiffness in different regions of the structure) has a tremendous impact in performance. This constitutes a major advantage for VSS since this property is impossible to have in CSS, which leads to worse results than those verified with optimal VSS.

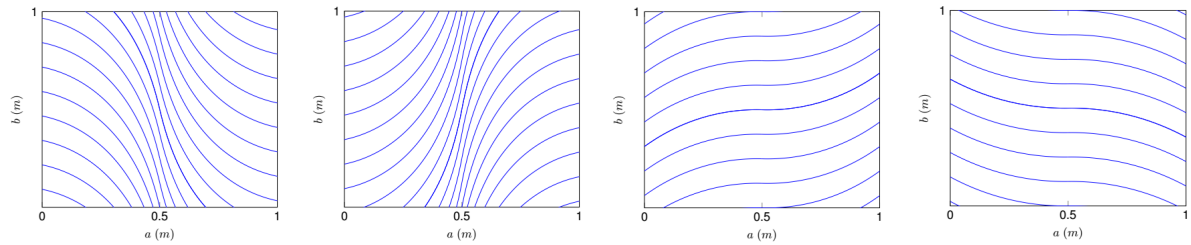

(a) 1^{st} lamina. (b) 2^{nd} lamina. (c) 3^{rd} lamina. (d) 4^{th} lamina.

Figure 5.5: Fiber paths for optimal VSS face sheet configuration in buckling in x direction with AH-H core and CCCC boundary conditions.

A relative lamina position study is also made concerning buckling in x direction. A new configuration, with positions of laminas 1 and 4 changed, leads to, not only a smaller value for critical buckling load factor (26.741, a decrease of around 5% in comparison with optimal VSS), but also in the mode shape as seen in figure 5.6. Therefore, the laminas position is relevant not only in vibration, but also in buckling. This decrease in performance can be explained by the fact that the original lamina 4, which has a greater region (in comparison with original lamina 1) in which fiber orientation is closely aligned with the x direction, is now closer to the core. It is known that the stiffness (the stiffness matrices) of standard unsteered composite laminates depends heavily on the relative position of the laminas. Therefore, it is possible to conclude that VSS have some similarities, in that regard, with the previously mentioned composite laminates: the stiffness of the structure increases with the distance between a lamina with high stiffness, in a certain direction, to the midplane of the structure. In the case of buckling in x direction, the original lamina 4 is the one with the highest stiffness in that direction. Thus, lamina 4 being closer to the core causes a decrease in performance.

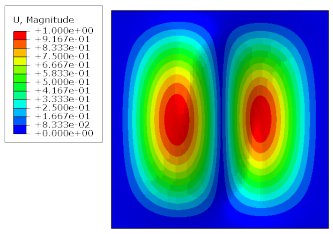

Figure 5.6: Mode shape of lamina relative position study in buckling in x direction.

In relation to the buckling in the y direction result, the use of VSS reveals to be even more beneficial, in a performance point of view, than in buckling in the x direction, since the optimal VSS configuration achieves a 67.304% critical buckling load factor improvement in comparison to the optimal result obtained

with CSS. The optimal VSS result is achieved with a face sheet configuration composed of two (out of four) virtually equal laminas (laminas 1 and 4), with an orientation, at $x = 0$ and $x = a$, closely aligned with the y direction ($(T_1)_1 = -84°$ and $(T_1)_4 = -83°$), then developing towards to an orientation direction closer to the x direction than the y direction ($(T_0)_1 = -30°$ and $(T_0)_4 = -32°$), at $x = a/2$. Lamina 2 is practically an antisymmetric configuration of the two previous mentioned laminas, being only lamina 3 the "outsider" with $T_0 = -57°$ and $T_1 = -6°$ values significantly different from the remaining laminas. Although lamina 2 is antisymmetric of lamina 1 and 4, these three laminas all have in common a starting orientation very close to the y direction and a half-length ($x = a/2$) orientation than tends towards the x direction, being only the fiber path orientation evolution the significant difference. Therefore, to a certain degree, there is one possible similarity than can be establish between optimal configurations CSS and VSS results, since, in the former, there is, as well, an outsider lamina (lamina 3) with an orientation completely different than the remaining three.

An interesting observation is that optimal CSS critical buckling load factor values for buckling in x and y direction does not vary much: 22.129 in buckling in x direction and 21.394 in buckling in y direction (a difference of only 3.436% taking the smaller value as reference). On the other hand, the same conclusion does not apply to VSS results, with the critical buckling load factor in y direction being significantly higher than the one verified in the x direction (35.793 and 28.120, respectively, a difference of 27.289% taking the smaller value as reference). This difference as well as the higher performance difference between optimal VSS and CSS configuration verified in buckling in y direction can be explained by the fiber orientation law used. Indeed, as demonstrated by the fiber paths of the optimal configurations represented in figure 5.7, in the buckling in y direction there is a concentration, namely in laminas 1,2 and 4, of load direction oriented fibers (that is, fibers oriented in the load direction, which is, in this case, the y direction) in small regions in the extremities of the sandwich structure (near $x = 0$ and $x = a$). This leads to a higher structural stiffness since multiple fibers are accumulated in that concentrated region, oriented in the load direction, magnifying the stiffness effect and, therefore, increasing quite significantly the critical buckling load factor. In fact, for the fiber orientation law used, is not possible to have, for buckling in x direction, two regions of concentrated load oriented fibers with the same length or effectiveness as in the case of buckling in y direction. Therefore, the performance improvement verified in the latter is higher.

The mode shape of the optimal VSS configuration in buckling in y direction is presented in figure 5.9. In comparison with the mode shape obtained for optimal CSS, the flattening effect of the mode shape present in the x direction is more pronounced in the VSS case. Furthermore, contrasting with the CSS result, the VSS mode shape has a slight tilt, in relation to the x direction, due to the fibers paths exhibited by the different laminas. The buckling performance improvement is explained by the y stiffness magnification effect provided by the two concentrated y oriented fibers regions (at $x = 0$ and $x = a$), resulting in an overall better structural capability of the sandwich, in comparison with CSS.

In shear buckling, optimal VSS can, as well, improve the structural performance, in this case up to 47.192% higher critical shear buckling load factor than optimal CSS, in CCCC boundary conditions and with AH-H core. This performance improvement is achieved with a VSS configuration composed of one

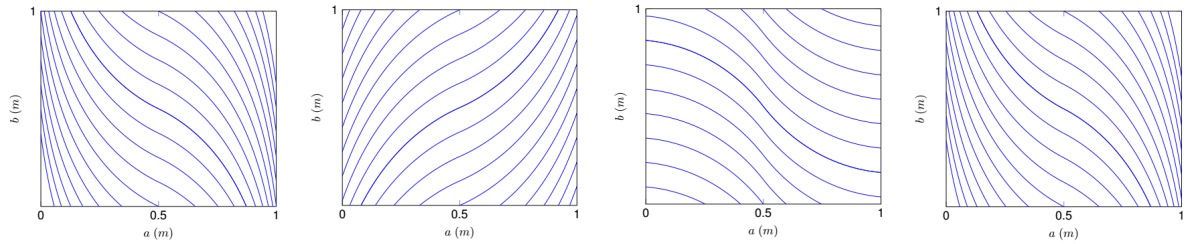

(a) 1^{st} lamina. (b) 2^{nd} lamina. (c) 3^{rd} lamina. (d) 4^{th} lamina.

Figure 5.7: Fiber paths for optimal VSS face sheet configuration in buckling in y direction with AH-H core and CCCC boundary conditions.

almost straight lamina (lamina 1) combined with two antisymmetric laminas (laminas 2 and 3) and a final lamina that, although being almost straight, it has a small steering effect that allows for some fiber concentration at $x = 0$ and $x = a$, as seen in figure 5.8. The optimal VSS configuration in shear buckling is characterized, namely, by a less pronounced curvature in all laminas, contrasting with some optimal configurations in other structural analysis. This leads to a mode shape as the one presented in figure 5.9. In fact, just as it occurred in the optimal CSS configuration, local instabilities emerge at the same corners but, in this case, the critical buckling mode shape is, in its majority, a global mode, which allows to conclude that these instabilities, opposed to the ones verified in optimal CSS, do not have a major impact in buckling performance. Moreover, this mode shape is particularly different from the remaining optimal VSS mode shapes of other analysis, since it has two noticeable separated regions in which the highest displacement is observed.

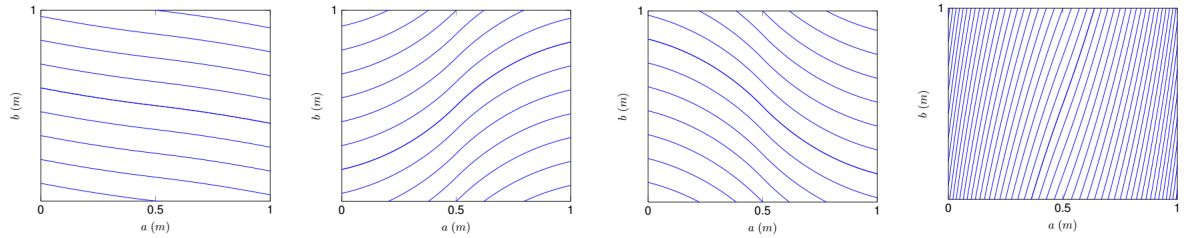

(a) 1^{st} lamina. (b) 2^{nd} lamina. (c) 3^{rd} lamina. (d) 4^{th} lamina.

Figure 5.8: Fiber paths for optimal VSS face sheet configuration in shear buckling with AH-H core and CCCC boundary conditions.

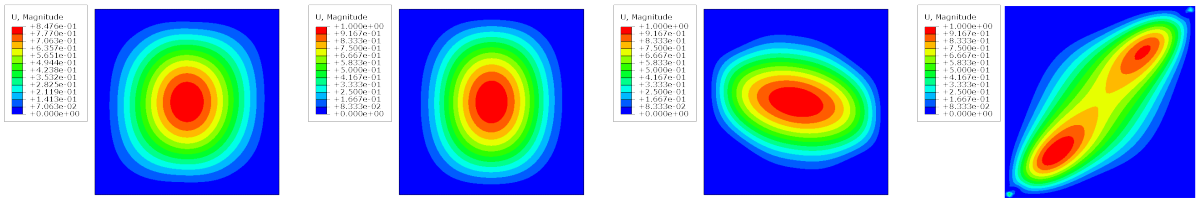

(a) Vibration. (b) Buckling in x. (c) Buckling in y. (d) Shear buckling.

Figure 5.9: Optimal VSS face sheet configurations (with AH-H core) mode shape results in vibration, buckling in x direction, buckling in y direction and shear buckling, subjected to CCCC boundary conditions.

Regarding VSS optimization with SSSS boundary conditions, in a sandwich structure with AH-H as

Table 5.6: Optimization results for vibration, buckling x, buckling y and shear buckling for CCCC boundary conditions with AH-H material as core and variable stiffness composite face sheets.

Aluminium honeycomb core of high stiffness (AH-H)						
Structural Analysis	Boundary conditions					
	CCCC					
	Optimal face sheet configuration				Optimal result	Generations
	$< T_0, T_1 >_1$	$< T_0, T_1 >_2$	$< T_0, T_1 >_3$	$< T_0, T_1 >_4$		
Vibration (f in Hz)	$< 90, 0 >$	$< -9, -4 >$	$< -90, 2 >$	$< 90, -3 >$	308.592	28
Buckling x (λ_{crit})	$< -79, -14 >$	$< 81, 14 >$	$< -2, 41 >$	$< 1, -33 >$	28.120	29
Buckling y (λ_{crit})	$< -30, -84 >$	$< 28, 74 >$	$< -57, -6 >$	$< -32, -83 >$	35.793	36
Shear buckling (λ_{crit})	$< -8, -13 >$	$< 50, 15 >$	$< -51, -17 >$	$< 73, 84 >$	58.269	31

core, table 5.7 presents the results for vibration, buckling in x direction and buckling in y direction, as well as the number of generations for each type of structural analysis that is needed in order to achieve the optimal structural results. Under SSSS boundary conditions, the sandwich structures become more flexible, and therefore, less stiffer, leading to lower optimal values of critical buckling load factors and fundamental frequency in comparison to CCCC boundary conditions results.

Vibration results lead to the conclusion that, unlike the CCCC boundary condition case, the difference in fundamental frequency performance between optimal VSS and CSS configurations is virtually negligible. Indeed the difference is only of 0.01% which allows to infere that, realistically, the introduction of steered fibers in sandwich structure's face sheets does not improve the verified performance in CSS. The observation of the fiber paths, present in figure 5.10, of the optimal VSS leads to the conclusion that these are practically identical to a CSS configuration. This scenario, however, does not repeat neither in buckling in x direction or buckling in y direction.

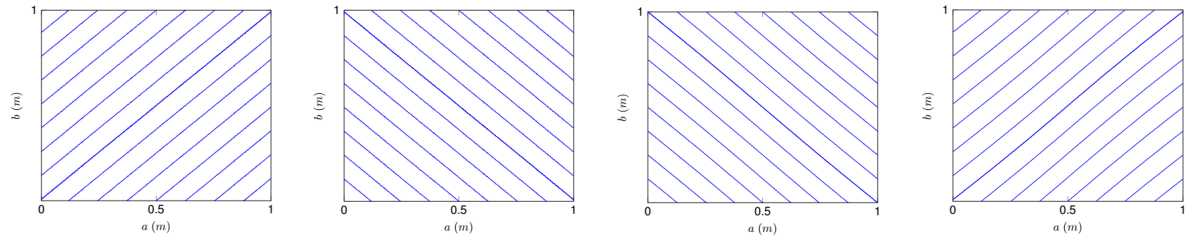

(a) 1^{st} lamina. (b) 2^{nd} lamina. (c) 3^{rd} lamina. (d) 4^{th} lamina.

Figure 5.10: Fiber paths for optimal VSS face sheet configuration in vibration with AH-H core and SSSS boundary conditions.

Concerning the buckling in x direction result, the performance improvement of the optimal VSS over CSS, albeit not being equally as high as occurred under CCCC boundary conditions, ascends to 20% in terms of critical buckling load factor. To achieve such performance, optimal VSS configuration includes, in its composition, two antisymmetric laminas (lamina 1 and 2) and two symmetric laminas (lamina 3 and 4), a peculiarity first seen in all of the optimal face sheet configurations until here analysed. The two antisymmetric laminas are characterized by a smooth fiber path orientation, with a less pronounced curvature than in, for example, the analogous result in CCCC conditions. In fact, the SSSS optimal face sheet configuration has a maximum difference between T_0 and T_1 of 57° while the CCCC optimal face

sheet configuration has a maximum of $67°$, leading to the conclusion that, under SSSS conditions, a better structural performance is achieved with more moderate values of fiber steering curvature.

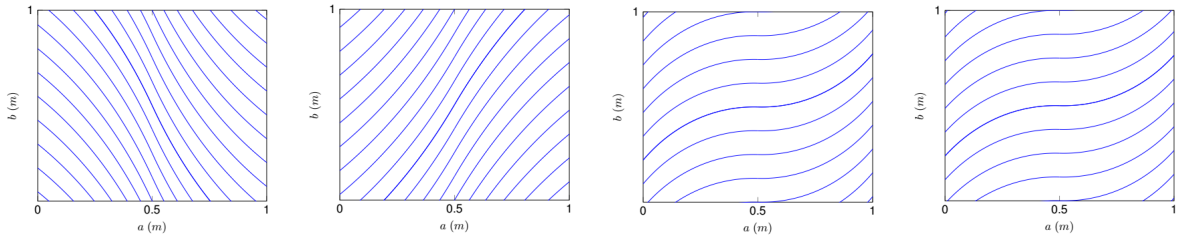

(a) 1^{st} lamina. (b) 2^{nd} lamina. (c) 3^{rd} lamina. (d) 4^{th} lamina.

Figure 5.11: Fiber paths for optimal VSS face sheet configuration in buckling in x direction with AH-H core and SSSS boundary conditions.

In relation to the buckling in y direction result, the performance improvement of VSS is, once again, smaller than in CCCC conditions, being, nonetheless, significant. The difference between VSS and CSS ascends to 24.5% in terms of critical buckling load factor. Although the performance improvement in buckling in y direction is still higher than the one verified in buckling in x direction, due to the reasons already mentioned in the CCCC boundary conditions results analysis, it appears that the change from CCCC to SSSS conditions leads to a mitigation of the magnification verified in the previous boundary condition scenario. Opposite to the optimal CCCC configuration, the optimal SSSS face sheet configuration is composed of two pairs of (almost) antisymmetric laminas: lamina 1 with lamina 2 and lamina 3 with lamina 4. The fiber paths for optimal VSS configuration in buckling in y direction are presented in figure 5.12.

The mode shapes of optimal CSS and VSS configurations are shown in figures 5.3 and 5.13, respectively. While optimal CSS configuration mode shapes have a traditional centered mode shape, the same does not happen in the optimal VSS case, namely in buckling in x and y directions. In these scenarios, there is a tendency for an offset mode shape, in the load direction, towards the extremities of the structure. This may be due to the impact that SSSS boundary conditions have in the case of an optimal VSS, which does not happen (i.e., the offsetted mode shape) in the optimal CSS. Nevertheless, in case of the optimal VSS configuration in buckling in x direction, a similar pattern regarding the fiber paths disposition (figure 5.11) is verified: two laminas (lamina 1 and 2) tend to provide more y stiffness at $x = a/2$ (with more y oriented fibers) and also contribute in terms of x stiffness at $x = 0$ and $x = a/2$ (with fibers progressively changing orientation towards the x direction); the other two laminas (3 and 4) provided more x stiffness at the center region and y stiffness at the extremities. The ability of steered fibers to provide completely different stiffness characteristics allows optimal VSS structure to have better performance than CSS.

5.3 Aluminium Honeycomb Core of Low Stiffness Results

In order to study and analyse possible differences in optimal results derived from the use of different sandwich core materials, an optimization process identical to the previous one is made with a sandwich

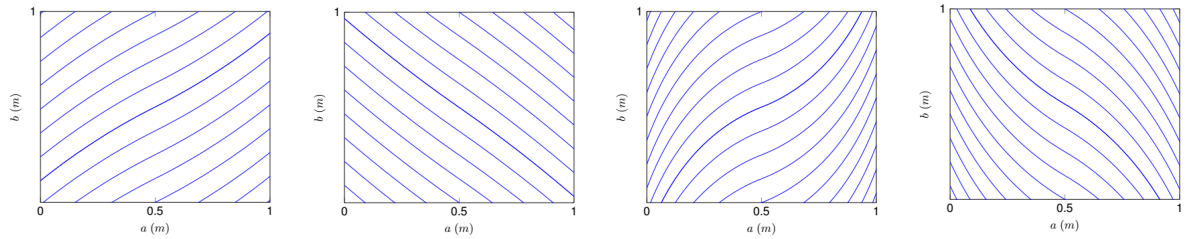

(a) 1^{st} lamina. (b) 2^{nd} lamina. (c) 3^{rd} lamina. (d) 4^{th} lamina.

Figure 5.12: Fiber paths for optimal VSS face sheet configuration in buckling in y direction with AH-H core and SSSS boundary conditions.

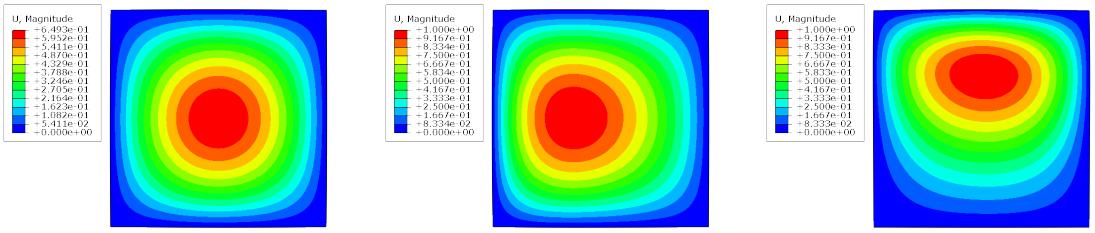

(a) Vibration. (b) Buckling in x. (c) Buckling in y.

Figure 5.13: Optimal VSS face sheet configurations (with AH-H core) mode shape results in vibration, buckling in x direction and buckling in y direction, subjected to SSSS boundary conditions.

Table 5.7: Optimization results for vibration, buckling x and buckling y for SSSS boundary conditions with AH-H material as core and variable stiffness composite face sheets.

Aluminium honeycomb core of high stiffness (AH-H)						
Structural Analysis	Boundary conditions					
	SSSS					
	Optimal face sheet configuration				Optimal result	Generations
	$< T_0, T_1 >_1$	$< T_0, T_1 >_2$	$< T_0, T_1 >_3$	$< T_0, T_1 >_4$		
Vibration (f in Hz)	$< 44, 45 >$	$< -44, -45 >$	$< -46, -44 >$	$< 46, 43 >$	165.499	24
Buckling x (λ_{crit})	$< -69, -44 >$	$< 64, 45 >$	$< -2, 55 >$	$< -2, -53 >$	11.937	32
Buckling y (λ_{crit})	$< 31, 44 >$	$< -40, -46 >$	$< 25, 73 >$	$< -35, -69 >$	12.568	38

structure whose core is an aluminium honeycomb core of lower stiffness (AH-L) than the previous one. The structures are subjected to the same types of analysis (vibration, buckling in x direction, buckling in y direction and shear buckling).

5.3.1 Constant Stiffness Face Sheets

Optimization results of CSS with AH-L as core and subjected to CCCC boundary conditions are presented in table 5.8. The values achieved for optimal results in the different structural analysis show that, in comparison to CSS with AH-H as core subjected to the same CCCC boundary conditions, optimal fundamental frequency result with AH-L is higher while optimal critical buckling load factor in both buckling in x and buckling in y directions are lower. Indeed, the use of AH-L as core, in comparison to AH-H, leads to a decrease in both stiffness and density (ρ). The decrease in stiffness inevitably leads to the decrease observed in critical buckling load factors since the structure is less robust to cope with

the buckling forces. The change in density is, probably, the main driver of the increase of performance verified in vibration, since lower density structures, typically, have higher fundamental frequencies, while higher density structures (as in the sandwich cases with AH-H), due to inertia reasons, tend to vibrate at lower frequencies.

A more in-depth analysis of the vibration result reveals that the optimal CSS face sheet configuration does not change with the change of core from AH-H to AH-L, being the optimal CSS face sheets composed of three laminas aligned with the x direction and one lamina (lamina 4) aligned with the y direction. The only difference verified is the one already mentioned: the increase in the optimal fundamental frequency value due to, especially, the decrease in density of the core used.

Regarding the buckling in x direction result, the optimal face sheet configuration is practically identical to the one achieved in vibration analysis, with only relative position of the laminas being different. Furthermore, in comparison with CSS optimal result with AH-H as core, it is possible to observe that, in general, the optimal face sheet configurations obtained are similar, with three laminas virtually aligned with the x direction in both cases. The more noticeable difference resides in the inclusion of a y aligned lamina in the AH-L result, while in AH-H optimal configuration there is a $-60°$ oriented lamina.

In terms of buckling in y direction, the optimal face sheet configurations is composed of two y oriented laminas, instead of three as in the analogous CCCC result. The remaining two laminas of this optimal configurations have an orientation that tends to be aligned to the x direction, although not as pronounced as the more x oriented lamina seen in thee CCCC result ($-2°$).

Shear buckling optimal CSS configuration, under CCCC boundary conditions, has three laminas tending towards $45°$ (or $-45°$) orientation, in accordance with one of the studies of chapter 3, in which it is explained that fibers at this orientation are more capable of supporting shear state stresses. This leads to the mode shape presented in figure 5.14, characterized by a continuous band of highest displacement oriented at near $45°$.

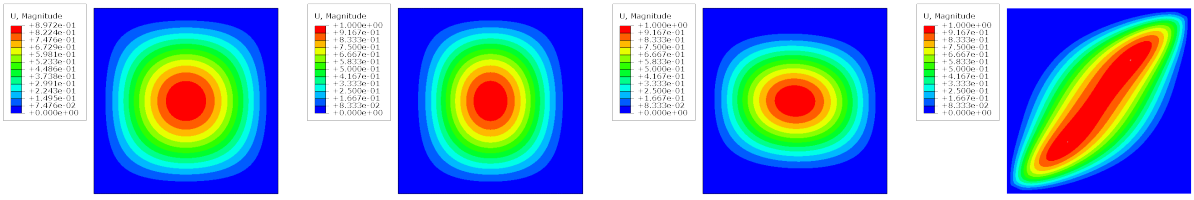

(a) Vibration. (b) Buckling in x. (c) Buckling in y. (d) Shear buckling.

Figure 5.14: Optimal CSS face sheet configurations (with AH-L core) mode shape results in vibration, buckling in x direction and buckling in y direction, subjected to CCCC boundary conditions.

Table 5.9 presents the results for optimal CSS configurations subjected to SSSS boundary conditions.

In regard to vibration, there is, once again, a noticeable decrease in performance due to the decrease in stiffness caused by the change from CCCC to SSSS boundary conditions, for CSS configurations. Furthermore, a similar trend to that verified in SSSS boundary conditions when using the AH-H sandwich core is observed when using AH-L: although not as pronounced as the former, there is a general tendency for the optimal CSS face sheet configuration to be composed of laminas with orientation near

Table 5.8: Optimization results for vibration, buckling x, buckling y and shear buckling for CCCC boundary conditions with AH-L material as core and constant stiffness composite face sheets.

Aluminium honeycomb core of low stiffness (AH-L)						
Structural Analysis	Boundary conditions					
	CCCC					
	Optimal face sheet configuration				Optimal result	Generations
	$< T_0, T_1 >_1$	$< T_0, T_1 >_2$	$< T_0, T_1 >_3$	$< T_0, T_1 >_4$		
Vibration (f in Hz)	$< 0, 0 >$	$< 0, 0 >$	$< 0, 0 >$	$< -90, -90 >$	289.259	21
Buckling x (λ_{crit})	$< 0, 0 >$	$< -90, -90 >$	$< 0, 0 >$	$< 0, 0 >$	19.198	21
Buckling y (λ_{crit})	$< 18, 18 >$	$< -24, -24 >$	$< 89, 89 >$	$< 89, 89 >$	17.864	18
Shear buckling (λ_{crit})	$< -15, -15 >$	$< 39, 39 >$	$< 42, 42 >$	$< -40, -40 >$	31.982	22

$45°$ (or $-45°$).

Optimal CSS configuration for buckling in x direction, in SSSS boundary conditions, consists of a set of $45°$ (or $-45°$) oriented fibers, once again showing that optimal CSS configurations tend towards $45°$ oriented fibers in SSSS conditions (thus, having the imposed boundary condition a great impact in the result).

The tendency for $45°$ (or $-45°$) oriented fibers is also visible in the optimal CSS face sheet configurations for buckling in y direction, under SSSS boundary conditions. One particular aspect regarding this result is that the change in core does not reflect into a major difference in the optimal face sheet configuration obtained for SSSS boundary conditions. However, the change in the characteristics of the core is still noticeable in the present optimal result, which is almost 15% lower than the one obtained with AH-H core.

Mode shapes of these results are presented in annex.

Table 5.9: Optimization results for vibration, buckling x and buckling y for SSSS boundary conditions with AH-L material as core and constant stiffness composite face sheets.

Aluminium honeycomb core of low stiffness (AH-L)						
Structural Analysis	Boundary conditions					
	SSSS					
	Optimal face sheet configuration				Optimal result	Generations
	$< T_0, T_1 >_1$	$< T_0, T_1 >_2$	$< T_0, T_1 >_3$	$< T_0, T_1 >_4$		
Vibration (f in Hz)	$< -37, -37 >$	$< 56, 56 >$	$< 47, 47 >$	$< -44, -44 >$	172.620	21
Buckling x (λ_{crit})	$< 43, 43 >$	$< 44, 44 >$	$< -44, -44 >$	$< -43, -43 >$	8.723	18
Buckling y (λ_{crit})	$< 50, 50 >$	$< -42, -42 >$	$< -44, -44 >$	$< 44, 44 >$	8.800	19

5.3.2 Variable Stiffness Face Sheets

Table 5.10 presents the results of optimal VSS face sheet configurations and its results for CCCC boundary conditions and AH-L core.

Optimal VSS face sheet configuration, in vibration, for an AH-L sandwich core, is very similar to that obtained when using AH-H sandwich core. In fact, both optimal configurations try to take maximum advantage of the curvature constraint, leading to configurations with highly steered fibers. This does

not constitute a problem, since as seen in previous studies in chapter 3, local instabilities that could cause performance issues are very rare or inexistent in vibration analysis. The main difference that arises between using AH-H or AH-L as sandwich core resides in the optimal result obtained: for AH-L, due to primarily its lower density, the optimal VSS face sheet configuration achieves a slightly higher optimal fundamental frequency value than in the case of AH-H. This optimal VSS configuration achieves a fundamental frequency improvement of 7.795% over the optimal CSS configuration, in CCCC boundary conditions.

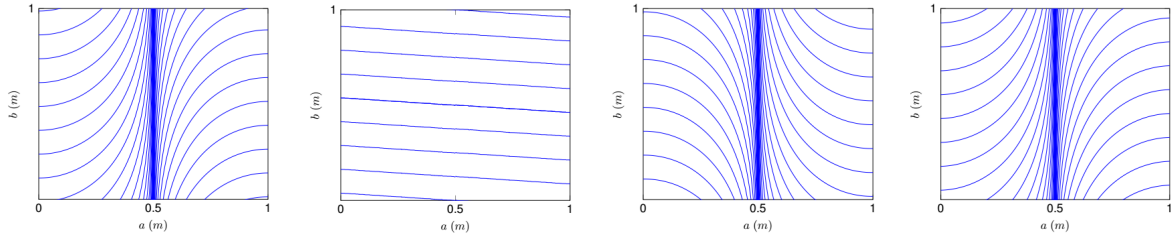

(a) 1^{st} lamina. (b) 2^{nd} lamina. (c) 3^{rd} lamina. (d) 4^{th} lamina.

Figure 5.15: Fiber paths for optimal VSS face sheet configuration in vibration with AH-L core and CCCC boundary conditions.

Regarding optimal results obtained in buckling in x direction, optimal VSS critical buckling load factor achieved with AH-L sandwich core is lower (19.218%) than the AH-H VSS case, due to its lower stiffness. The optimal VSS face sheet configuration has, in its composition, three virtually identical laminas (laminas 1,2 and 4), which start with a orientation value near the -45° mark, at $x = 0$, then progressively evolves to higher orientation values, reaching, at $x = a/2$, a orientation closely aligned with the x direction ($(T_0)_1 = 16^{\circ}$, $(T_0)_2 = 15^{\circ}$, $(T_0)_4 = 12^{\circ}$). The remaining lamina (lamina 3) has a completely different path evolution: starts with an orientation close to 45° , eventually evolving towards a completely y direction orientation (90°). This optimal VSS configuration achieves an buckling performance improvement of 22.862% over optimal CSS configuration. This value is smaller than the one verified in optimal configurations with AH-H core. Therefore, this proves that extremely low stiffness cores penalize the performance improvement provided by optimal VSS configurations over CSS. This may be due to the fact that, in the presence of softer cores, there is a higher probability of local instabilities that decrease significantly VSS performance, as seen in studies made in chapter 3, while also narrowing the range of possible VSS that can outperform CSS.

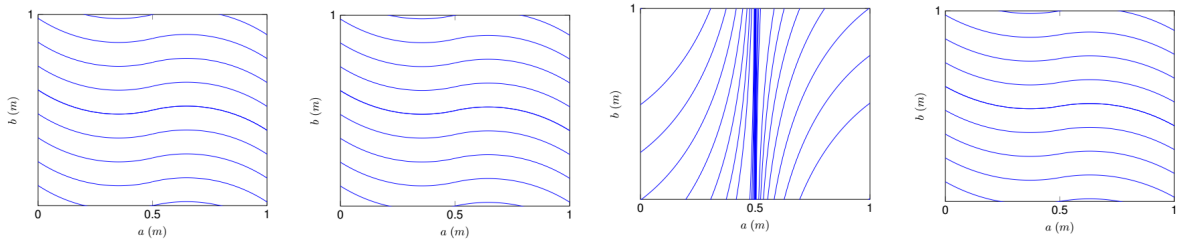

(a) 1^{st} lamina. (b) 2^{nd} lamina. (c) 3^{rd} lamina. (d) 4^{th} lamina.

Figure 5.16: Fiber paths for optimal VSS face sheet configuration in buckling in x direction with AH-L core and CCCC boundary conditions.

Taking into consideration the buckling in y results, the use of steered fibers in the face sheets of the sandwich structure, subjected to CCCC boundary conditions, leads to a 55.301% critical buckling load factor improvement over CSS. This improvement is, however, smaller than the one verified with AH-H, which allows to conclude that the core structural characteristics has a major impact on the buckling in y direction performance improvement provided by VSS over CSS, since the corresponding optimal VSS configurations, in CCCC conditions, with AH-H and with AH-L, are similar.

Still remaining on the topic of the buckling in y, the lower stiffness of the AH-L core leads to, as it occurred in the buckling in x direction, a significantly lower optimal value for critical buckling load factor (27.743, which is 29.016% lower than the value obtained with optimal configuration with AH-H core). There is, nonetheless, more similarities, in what concerns the optimal face sheet configurations composition in each of the cores, than in the buckling in x direction. In both core cases, the optimal face sheet configuration has two almost equal laminas (laminas 1 and 4 in both cases) with lamina 2 being an almost antisymmetric counterpart of the previous two. Lamina 3 is where the biggest difference resides, with lamina 3 of the present optimal configuration having a more pronounced curvature ($(T_0)_3 = -71^\circ$, therefore, closer to y direction orientation than $(T_0)_3 = -57^\circ$ verified in AH-H optimal configuration).

The difference between optimal VSS configuration critical buckling load factors, with AH-L core, in buckling in x and y direction is of the order of 17.620%, smaller than the difference verified, in the same CCCC boundary conditions, for optimal VSS configuration with AH-H core. Therefore, it is possible to conclude that, not only the less stiff core leads to a narrower window of improvement provided by VSS over CSS, but also causes optimal critical buckling load factors in buckling in x and y direction to be closer to each other. This can be explained, once again, by the fact that the concentration, in small areas of the structure near its extremities, of multiple load oriented fibers, which magnify the stiffness effect, culminates into a higher probability of local instabilities that decrease structural performance. Therefore, it mitigates the particular advantage that the present fiber orientation law used provides to VSS structures in buckling in y direction over buckling in x direction.

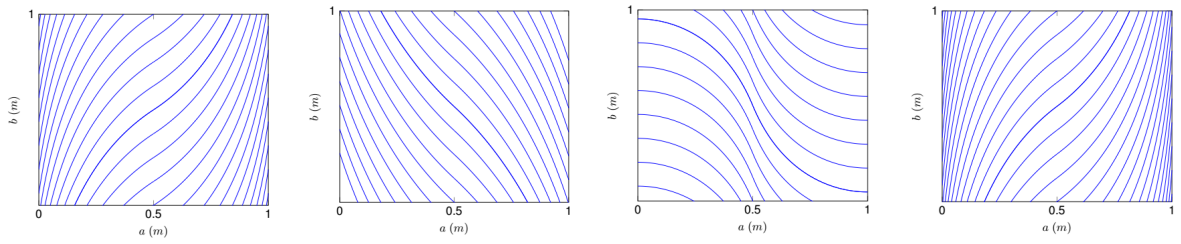

(a) 1^{st} lamina. (b) 2^{nd} lamina. (c) 3^{rd} lamina. (d) 4^{th} lamina.

Figure 5.17: Fiber paths for optimal VSS face sheet configuration in buckling in y direction with AH-L core and CCCC boundary conditions.

The impact of the change from AH-H to AH-L and consequent decrease of stiffness is also noticeable in shear buckling result, with optimal VSS achieving a critical buckling load factor, in shear buckling, of 33.394, which represents a 41.763% decrease to the value obtained by optimal VSS with AH-H core. Furthermore, the core change also has a major impact in the performance improvement provided by optimal VSS. The performance achieved by optimal VSS is 6.103% higher than the one verified with

optimal CSS. This improvement is drastically smaller than the one verified with optimal VSS over optimal CSS in the presence of an AH-H core. This can be explained by the fact that local instabilities that occur for some VSS configurations with this core drastically decrease the corresponding critical buckling load. Therefore, it decreases the possibilities of VSS configurations that could improve over CSS. Once again, optimal VSS configuration is characterized by laminas with moderate values of curvature. The mode shape obtained with this configuration, present in figure 5.19, is very similar to the one obtained with optimal CSS.

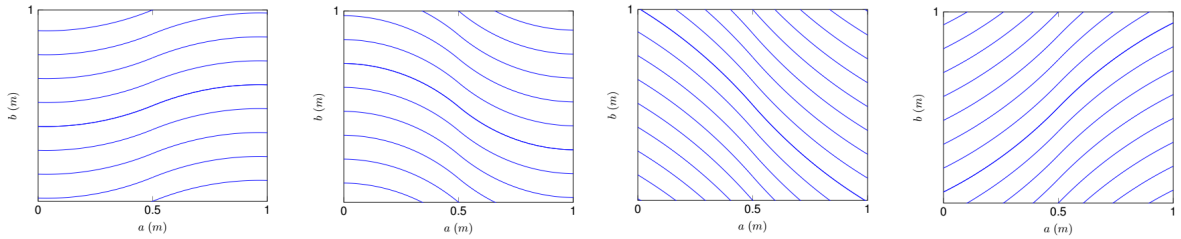

(a) 1^{st} lamina. (b) 2^{nd} lamina. (c) 3^{rd} lamina. (d) 4^{th} lamina.

Figure 5.18: Fiber paths for optimal VSS face sheet configuration in shear buckling with AH-L core and CCCC boundary conditions.

The mode shapes obtained for optimal VSS configurations in vibration, buckling in x direction and buckling in y direction and shear buckling are presented in figure 5.19. Once again, as seen in previous cases, the mode shape regarding buckling in x direction has a slightly tilt derived from the curvature exhibited by the fiber paths in the various laminas. Furthermore, the underlying reason for performance improvement obtained in buckling in x direction is the same as other previous optimal VSS cases: the capability of steered fibers to provide different stiffness characteristics in different reasons, whose combined effect (of all steered laminas) results into an overall more robust structure (in this case, more robust to buckling in x direction). A particular mode shape is obtained in buckling in y direction. The use of a very low stiffness core (AH-L) combined with three (out of four) laminas with very pronounced curvature (with orientation at $x = 0$ and $x = a$ very close to $90°$) results in some local instabilities near the four corners of the structures. These local instabilities are, however, small, being the overall global buckling (quite visible) the dominant mode. This explains the fact that the performance improvement obtained using optimal VSS in AH-L is considerably lower than in AH-H: in the former, although VSS still have better performance than CSS, the presence of local instabilities (albeit small) leads to a decrease in the potential of such structure, while in the latter these instabilities do not occur due to, predominantly, the use of higher stiffness core (AH-H).

Results for optimal VSS configurations with AH-L core in SSSS boundary conditions are presented in table 5.11. Due to the same reasoning followed in the analysis made in sandwich structures with AH-H as core, the adoption of SSSS boundary conditions leads to lower values of optimal results.

More concretely, in terms of vibration, the performance improvement provided by VSS is virtually negligible, just as it happened in AH-H cases, with VSS optimal result being only 0.7% higher than those verified with CSS configurations. In this regard, it can be concluded that SSSS boundary conditions have a bigger impact in vibration results than in other structural analysis since all optimal configurations, either

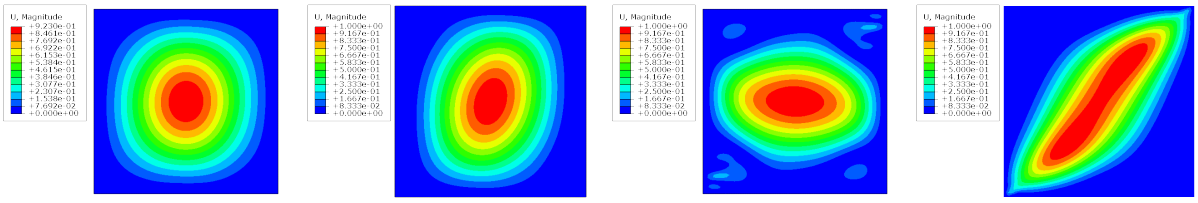

(a) Vibration. (b) Buckling in x. (c) Buckling in y. (d) Shear buckling.

Figure 5.19: Optimal VSS face sheet configurations (with AH-L core) mode shape results in vibration, buckling in x direction, buckling in y direction and shear buckling, subjected to CCCC boundary conditions.

Table 5.10: Optimization results for vibration, buckling x, buckling y and shear buckling for CCCC boundary conditions with AH-L material as core and variable stiffness composite face sheets.

Aluminium honeycomb core of low stiffness (AH-L)						
Structural Analysis	Boundary conditions					
	CCCC					
	Optimal face sheet configuration				Optimal result	Generations
	$< T_0, T_1 >_1$	$< T_0, T_1 >_2$	$< T_0, T_1 >_3$	$< T_0, T_1 >_4$		
Vibration (f in Hz)	$< 90, 0 >$	$< -5, -4 >$	$< -90, 1 >$	$< 90, 2 >$	311.808	26
Buckling x (λ_{crit})	$< 16, -38 >$	$< 15, -37 >$	$< 90, 42 >$	$< 12, -34 >$	23.587	33
Buckling y (λ_{crit})	$< 38, 83 >$	$< -48, -75 >$	$< -71, 0 >$	$< 42, 86 >$	27.743	37
Shear buckling (λ_{crit})	$< 26, -2 >$	$< -45, -1 >$	$< -54, -36 >$	$< 51, 31 >$	33.934	32

with AH-H or AH-L, CSS or VSS, have orientations always close to $45°$ or $-45°$. The small oscillations around this constant value of orientation are only seen, to this extent, under SSSS boundary conditions for vibration analysis.

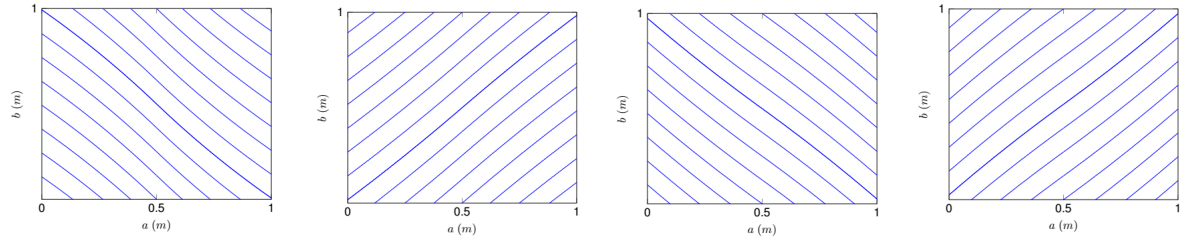

(a) 1^{st} lamina. (b) 2^{nd} lamina. (c) 3^{rd} lamina. (d) 4^{th} lamina.

Figure 5.20: Fiber paths for optimal VSS face sheet configuration in vibration with AH-L core and SSSS boundary conditions.

Buckling in x direction optimal face sheet configuration, under SSSS boundary conditions, is composed of, as it occurred many times in other optimal configurations, two antisymmetric laminas (lamina 2 and 4), that, as seen in figure 5.21, stregthen the center region of the structure in the load (x) direction (both have an orientation at $x = a/2$ closely aligned with the x direction). The improvement provided by VSS over CSS, in SSSS boundary conditions, is of the order of 18.331%. Mode shapes regarding these results are presented in annex.

In relation to buckling in y direction, the performance improvement achieved by the optimal VSS configuration over the optimal CSS configuration ascends to 23.477%. While optimal CSS adopts similar orientation parameters in all laminas (all laminas have an orientation around $45°$ or $-45°$), optimal

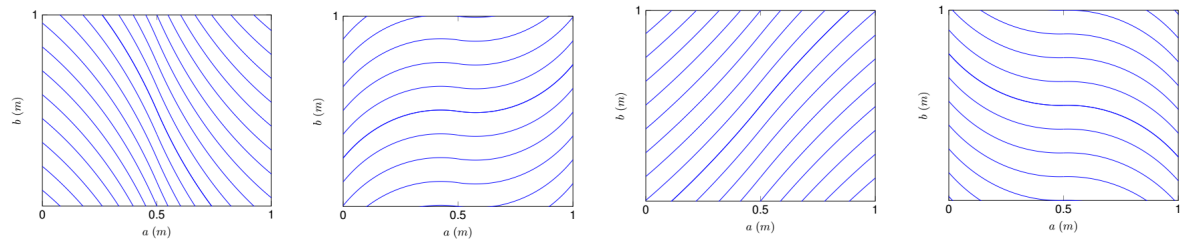

(a) 1^{st} lamina. (b) 2^{nd} lamina. (c) 3^{rd} lamina. (d) 4^{th} lamina.

Figure 5.21: Fiber paths for optimal VSS face sheet configuration in buckling in x direction with AH-L core and SSSS boundary conditions.

VSS, benefiting from its capability fiber steering, is composed of one lamina (lamina 2) which has load oriented fiber concentration in the extremities, just as in other reported cases, which inevitably increases its buckling robustness. Lamina 3, although less pronounced than lamina 2, also contributes to the fiber concentration in the structures extremities, with a $T_1 = 59°$ as seen in figure 5.22. Nevertheless, laminas 1 and 4 also contribute to the increase in stiffness in the center region of the plate (although in a lesser impact), being fiber orientations of these laminas, at $x = a/2$, closer to the y direction, in contrast with the orientation verified in laminas 2 and 3 (which are almost x direction oriented at the $x = a/2$).

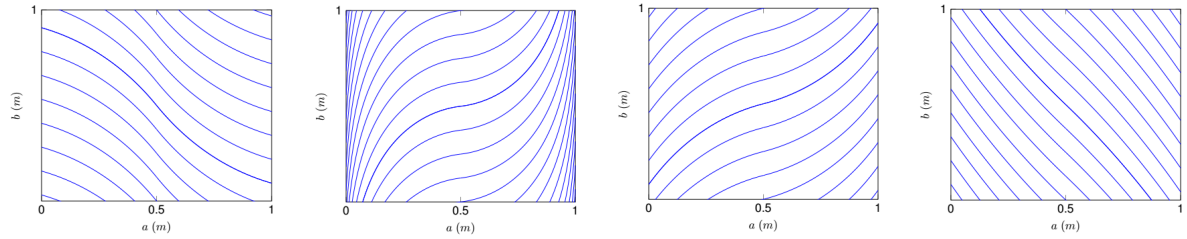

(a) 1^{st} lamina. (b) 2^{nd} lamina. (c) 3^{rd} lamina. (d) 4^{th} lamina.

Figure 5.22: Fiber paths for optimal VSS face sheet configuration in buckling in y direction with AH-L core and SSSS boundary conditions.

Table 5.11: Optimization results for vibration, buckling x and buckling y for SSSS boundary conditions with AH-L material as core and variable stiffness composite face sheets.

Aluminium honeycomb core of low stiffness (AH-L)						
Structural Analysis	Boundary conditions					
	SSSS					
	Optimal face sheet configuration				Optimal result	Generations
	$< T_0, T_1 >_1$	$< T_0, T_1 >_2$	$< T_0, T_1 >_3$	$< T_0, T_1 >_4$		
Vibration (f in Hz)	$< -49, 40 >$	$< 46, 42 >$	$< -41, -46 >$	$< 41, 46 >$	173.829	25
Buckling x (λ_{crit})	$< -70, -45 >$	$< -10, 56 >$	$< 56, 46 >$	$< 2, -54 >$	10.322	33
Buckling y (λ_{crit})	$< -56, -19 >$	$< 8, 87 >$	$< 17, 59 >$	$< -49, -60 >$	10.866	34

Chapter 6

Conclusions

The present chapter presents the main conclusions, results and corresponding achievements of this work. Ideas for future studies to be performed following this work are also addressed.

6.1 Achievements

The work done herein constitutes an elaborated foundation for the study and optimization of VSS. An in-depth study of the structural behaviour of VSS, in comparison with CSS, prior to the optimization process, is done. The set of studies had, as objective, the comprehension, from an holistic point of view, of the structural performance of VSS, ranging from the impact of the sandwich core stiffness on performance results, to a comparison, in multiple boundary conditions, of structural performance between CSS and VSS, to a multitude of structural analysis (comprising statics, vibration and various types of buckling) of VSS with low density and stiffness sandwich core. From these studies it was concluded that VSS do not have a major impact in the structural performance of sandwich structures with a high stiffness core. In fact, in a substantial portion of the cases, CSS reveals to be the better option when a considerable high stiffness core is used. However, in the presence of low density and stiffness sandwich cores, which constitute the majority of types of core used in aerospace, it was possible to identify some trends and performance evolution with parameter variation (T_0 and T_1) of VSS. The results obtained pointed in the direction that VSS were structurally superior to CSS configurations in multiple cases. This was the basis that justified the posterior optimization process done in this work. Although some VSS configurations showed better structural performance than CSS, for the set of configurations tested in the studies, from the core influence study it was concluded that, in some buckling in y direction cases, namely in the presence of low density and stiffness core, certain variable stiffness laminas, specifically those with high curvature, can exhibit some local instabilities in their mode shapes. It was concluded that these instabilities can, in fact, in some of the configurations, decrease drastically the structural performance of VSS.

After concluding that VSS can have the potential to surpass CSS in terms of structural performance, an optimization process, resorting to a genetic algorithm, was done. The framework behind this process

consisted in two major phases: the optimization algorithm itself, that was executed via *Matlab* scripts and the structural analysis phase, executed through *Python* scripts. The set of optimization processes completed comprised of vibration, buckling in x direction, buckling in y direction and shear buckling (the latter only in CCCC), with the objective of maximizing the fundamental frequency and the critical buckling load factor. Furthermore, two different aluminium honeycombs were tested: one with substantially low stiffness (designated aluminium honeycomb of low stiffness, AH-L) and one with higher stiffness than the previous one (designated aluminium honeycomb of high stiffness, AH-H). In addition, CCCC and SSSS boundary conditions were also part of the optimization study.

It was concluded that, in the vast majority of the optimization cases tested, VSS have a better or a much better structural performance than CSS. For example, the performance improvement achieved by VSS over CSS, in buckling in y direction, for CCCC boundary conditions, ascended to 67%. Furthermore, it was also concluded that the fiber orientation law used in this work benefits buckling in y direction more than buckling in x direction, with performance improvements provided by VSS over CSS being higher in the former than in the latter. The capability of steered fibers to provide for different stiffness characteristics in different regions of the structure reveals to be essential for the improvements verified. This is due to the fact that the same fiber can improve stiffness in different directions in different regions of the same lamina, unlike unsteered fibers which can only provide stiffness uniformly in one direction, across the entire length of the lamina.

6.2 Future Work

This work shows that, indeed, VSS couples low density characteristics with extraordinary structural capabilities, namely in terms of vibration and buckling. However, there is a lot of room for further exploration in this topic. For example, the use of other fiber orientation laws which can be more accurate in certain scenarios. VSS are not only obtained through fiber orientation variation, as mentioned in this work. New studies concerning VSS with variable layer thickness or functionally graded materials can be accomplished and a comparative study can be done to assess the advantages and disadvantages of each type of VSS. The use of other types of geometry is also a study possibility, namely to comprehend how does the structural behaviour of VSS change in the presence of curved surfaces in its geometry, for example. Different low density core configurations can also be tested such as geometric corrugated core configurations and an evaluation can be done concerning their impact on the structural performance of the whole structure, in combination with variable stiffness face sheets.

Regarding the optimization topic, genetic algorithms have been proven countless times as an effective tool in composite structure optimization. Nevertheless, the use of other algorithms can be a possible study. In the meta-heuristic area, for example, recent algorithms can be tested, such as the ant colony optimization algorithm. Gradient-based methods can also be subjected to a performance study, both in results and computational time, regarding VSS. Multi objective optimization processes comprising various types of structural analysis (vibration, various types of buckling and even statics) can be performed to assess, in an holistic way, the structural improvement provided by optimal VSS configurations.

Bibliography

[1] T. Devezas. Trends in aviation: rebound effect and the struggle composites x aluminum. *Technological Forecasting and Social Change*, 160:120241, 2020. doi: https://doi.org/10.1016/j.techfore.2020.120241.

[2] P. Vieira. Current airframe manufacturing technologies in the aeronautical industry and trends for future developments. 2013. MSc Thesis.

[3] N. Hoff and S. Mautner. The buckling of sandwich-type panels. *Journal of the Aeronautical Sciences*, 12(3), 1945. doi: https://doi.org/10.2514/8.11246.

[4] B. Castanie, C. Bouvet, and M. Ginot. Review of composite sandwich structure in aeronautic applications. *Composites Part C: Open Access*, 1:100004, 2020. doi: https://doi.org/10.1016/j.jcomc.2020.100004.

[5] W. Becker, K. Worden, M. Battipede, and C. Surace. Uncertainty analysis of a dynamic model of a novel remotely piloted airship. *Journal of Aircraft*, 48:1028–1035, 2011. doi: 10.2514/1.C031207.

[6] D. Punera and P. Mukherjee. Recent developments in manufacturing, mechanics, and design optimization of variable stiffness composites. *Journal of Reinforced Plastics and Composites*, 2022. doi: 10.1177/07316844221082999.

[7] Y. Xu, J. Zhu, Z. Wu, Y. Cao, Y. Zhao, and W. Zhang. A review on the design of laminated composite structures: constant and variable stiffness design and topology optimization. *Advanced Composites and Hybrid Materials*, 1(3):460–477, 2018. doi: https://doi.org/10.1007/s42114-018-0032-7.

[8] M. R. Islam and M. E. Hossain. Chapter 7 - monitoring and global optimization. In *Drilling Engineering*, Sustainable Oil and Gas Development Series, pages 529–618. Gulf Professional Publishing, 2021. doi: https://doi.org/10.1016/B978-0-12-820193-0.00007-1.

[9] MATLAB. *R2021b*. The MathWorks Inc., Natick, Massachusetts, 2021.

[10] M. Smith. *ABAQUS/Standard User's Manual, Version 6.22*. Dassault Systèmes Simulia Corporation, United States, 2021.

[11] G. Huang, H. Wang, and G. Li. An efficient reanalysis assisted optimization for variable-stiffness composite design by using path functions. *Composite Structures*, 153:409–420, 2016. doi: https://doi.org/10.1016/j.compstruct.2016.06.043.

[12] Z. Wu, G. Raju, and P. Weaver. *Buckling of VAT Plates Using Energy Methods*. 2012. doi: 10.2514/6.2012-1463.

[13] O. Falcó, J. Mayugo, C. Lopes, N. Gascons, A. Turon, and J. Costa. Variable-stiffness composite panels: As-manufactured modeling and its influence on the failure behavior. *Composites Part B: Engineering*, 56:660–669, 2014. doi: https://doi.org/10.1016/j.compositesb.2013.09.003.

[14] Z. Gürdal, B. Tatting, and C. Wu. Variable stiffness composite panels: Effects of stiffness variation on the in-plane and buckling response. *Composites Part A: Applied Science and Manufacturing*, 39(5):911–922, 2008. doi: https://doi.org/10.1016/j.compositesa.2007.11.015.

[15] M. M. M. Fernandes. Path planning and fiber angle optimization of continuous fiber composites for additive manufacturing. 2019. MSc Thesis.

[16] P. T. Langley. Finite element modeling of tow-placed variable-stiffness composite laminates. Master's thesis, Faculty of the Virginia Polythecnic Institute and State University, 1999.

[17] A. Crosky, C. Grant, D. Kelly, X. Legrand, and G. Pearce. 4 - fibre placement processes for composites manufacture. In *Advances in Composites Manufacturing and Process Design*. Woodhead Publishing, 2015.

[18] D. Evans. Fiber placement. In *ASM Handbook: Composites*, volume 21, pages 476–487. ASM International, 2001.

[19] J. F. Carvalho. Fundamental frequency optimization of variable-angle tow laminates. Master's thesis, Instituto Superior Técnico - Universidade de Lisboa, 2021.

[20] B. C. Kim, K. Potter, and P. M. Weaver. Continuous tow shearing for manufacturing variable angle tow composites. *Composites Part A: Applied Science and Manufacturing*, 43(8):1347–1356, 2012. doi: https://doi.org/10.1016/j.compositesa.2012.02.024.

[21] K. Uhlig, L. Bittrich, A. Spickenheuer, and J. H. S. Almeida. Waviness and fiber volume content analysis in continuous carbon fiber reinforced plastics made by tailored fiber placement. *Composite Structures*, 222:110910, 2019. doi: https://doi.org/10.1016/j.compstruct.2019.110910.

[22] B. C. Kim, K. Hazra, P. Weaver, and K. Potter. Limitations of fibre placement techniques for variable angle tow composites and their process-induced defects. In *18th International Conference on Composite Materials*, 2011.

[23] O. Thomsen. Sandwich materials for wind turbine blades - present and future. *Journal of Sandwich Structures & Materials*, 11(1):7–26, 2009. doi: 10.1177/1099636208099710.

[24] K. F. Karlsson and B. T. Åström. Manufacturing and applications of structural sandwich components. *Composites Part A: Applied Science and Manufacturing*, 28(2):97–111, 1997. doi: https://doi.org/10.1016/S1359-835X(96)00098-X.

[25] H. Akhavan and P. Ribeiro. Natural modes of vibration of variable stiffness composite laminates with curvilinear fibers. *Composite Structures*, 93(11):3040–3047, 2011. doi: https://doi.org/10.1016/j.compstruct.2011.04.027.

[26] C. Waldhart. Analysis of tow-placed, variable-stiffness laminates. Master's thesis, Faculty of the Virginia Polytechnic Institute and State University, 1996.

[27] A. W. Blom. *Structural Performance of Fiber-Placed, Variable-Stiffness Composite Conical and Cylindrical Shells*. PhD thesis, Technische Universiteit Delft, 2010. PhD Thesis.

[28] B. C. Kim, P. M. Weaver, and K. Potter. Manufacturing characteristics of the continuous tow shearing method for manufacturing of variable angle tow composites. *Composites Part A: Applied Science and Manufacturing*, 61:141–151, 2014. doi: https://doi.org/10.1016/j.compositesa.2014.02.019.

[29] A. Soriano and J. Díaz. Failure analysis of variable stiffness composite plates using continuum damage mechanics models. *Composite Structures*, 184:1071–1080, 2018. doi: https://doi.org/10.1016/j.compstruct.2017.10.065.

[30] O. T. Thomsen and W. M. Banks. An improved model for the prediction of intra-cell buckling in cfrp sandwich panels under in-plane compressive loading. *Composite Structures*, 65(3):259–268, 2004. doi: https://doi.org/10.1016/j.compstruct.2003.11.002.

[31] M. Kaminski, J. Amdahl, E. Fasano, P. Frieze, M. Grundy, M. Hess, P. Kawamoto, J. Kujala, U. Paik, B. Röhr, Simonsen, and J. Gordo. Ultimate strength. In *4th International Ship and Offshore Structures Congress*, volume 1, 2000.

[32] R. Vescovini and L. Dozio. A variable-kinematic model for variable stiffness plates: Vibration and buckling analysis. *Composite Structures*, 142:15–26, 2016. doi: https://doi.org/10.1016/j.compstruct.2016.01.068.

[33] B. H. Coburn and P. M. Weaver. Buckling analysis, design and optimisation of variable-stiffness sandwich panels. *International Journal of Solids and Structures*, 96:217–228, 2016. doi: https://doi.org/10.1016/j.ijsolstr.2016.06.007.

[34] J. N. Reddy. *Mechanics of Laminated Composites Plates and Shells. Theory and Analysis.* CRC Press, 2003.

[35] R. L. Pastel, J. E. Caruthers, and W. Frost. Airplane wing vibrations due to atmospheric turbulence, 1981. Document Type: Contractor Report.

[36] F. Tornabene, N. Fantuzzi, and M. Bacciocchi. Foam core composite sandwich plates and shells with variable stiffness: Effect of the curvilinear fiber path on the modal response. *Journal of Sandwich Structures & Materials*, 21(1):320–365, 2019. doi: 10.1177/1099636217693623.

[37] M. Loja, F. Marques, and A. Mota. Variable stiffness composites: Optimal design studies. *Journal of Composites Science*, 4:80, 2020. doi: 10.3390/jcs4020080.

[38] S. Honda and Y. Narita. Natural frequencies and vibration modes of laminated composite plates reinforced with arbitrary curvilinear fiber shape paths. *Journal of Sound and Vibration*, 331(1): 180–191, 2012. doi: https://doi.org/10.1016/j.jsv.2011.08.019.

[39] A. Houmat. Nonlinear free vibration of laminated composite rectangular plates with curvilinear fibers. *Composite Structures*, 106:211–224, 2013. doi: https://doi.org/10.1016/j.compstruct.2013.05.058.

[40] X. Chen, G. Nie, and Z. Wu. Global buckling and wrinkling of variable angle tow composite sandwich plates by a modified extended high-order sandwich plate theory. *Composite Structures*, 292: 115639, 2022. doi: https://doi.org/10.1016/j.compstruct.2022.115639.

[41] R. Vescovini, M. D'Ottavio, L. Dozio, and O. Polit. Buckling and wrinkling of anisotropic sandwich plates. *International Journal of Engineering Science*, 130:136–156, 2018. doi: https://doi.org/10.1016/j.ijengsci.2018.05.010.

[42] A. Hassan and N. Kurgan. Modeling and buckling analysis of rectangular plates in ansys. *International Journal Of Engineering and Applied Sciences*, 11:310–329, 2019. doi: 10.24107/ijeas.531011.

[43] T. Ye, G. Jin, and Z. Su. Three-dimensional vibration analysis of sandwich and multilayered plates with general ply stacking sequences by a spectral-sampling surface method. *Composite Structures*, 176:1124–1142, 2017. doi: https://doi.org/10.1016/j.compstruct.2017.06.008.

[44] M. Kheirikhah, S. Khalili, and K. Malekzadeh. Buckling analysis of soft-core composite sandwich plates using 3d finite element method. *Applied Mechanics and Materials*, 105-107, 2011. doi: 10.4028/www.scientific.net/AMM.105-107.1768.

[45] K. Foo, L. Seah, and G. Chai. Low-velocity impact failure of aluminium honeycomb sandwich panels. *Composite Structures*, 85(1):20–28, 2008. doi: 10.1016/j.compstruct.2007.10.016.

[46] N. El-Omari. Sea lion optimization algorithm for solving the maximum flow problem. *IJCSNS International Journal of Computer Science and Network Security*, 20(8):30–68, 2021.

[47] Y. Xu and T. You. Minimizing thermal residual stresses in ceramic matrix composites by using iterative mapreduce guided particle swarm optimization algorithm. *Composite Structures*, 99:388–396, 2013. doi: https://doi.org/10.1016/j.compstruct.2012.11.027.

[48] W. Wang, S. Guo, N. Chang, and W. Yang. Optimum buckling design of composite stiffened panels using ant colony algorithm. *Composite Structures*, 92(3):712–719, 2010. doi: https://doi.org/10.1016/j.compstruct.2009.09.018.

[49] D. Goldberg. *Genetic Algorithms in Search, Optimization and Machine Learning*. Addison-Wesley Longman Publishing Co., Inc., USA, 1989.

[50] *Matlab* genetic algorithm documentation. `https://www.mathworks.com/help/gads/genetic-algorithm.html`. Accessed: 13th August, 2022.

[51] V. Chahar, S. Katoch, and S. Chauhan. A review on genetic algorithm: Past, present, and future. *Multimedia Tools and Applications*, 80(5):8091–8126, 2021. doi: 10.1007/s11042-020-10139-6.

[52] G. Soon, T. Guan, C. On, R. Alfred, and P. Anthony. A comparison on the performance of crossover techniques in video game. In *Proceedings - 2013 IEEE International Conference on Control System, Computing and Engineering, ICCSCE 2013*, pages 493–498, 2013.

[53] K. Deep, K. Singh, M. Kansal, and C. Mohan. A real coded genetic algorithm for solving integer and mixed integer optimization problems. *Applied Mathematics and Computation*, 212(2):505–518, 2009. doi: 10.1016/j.amc.2009.02.044.

[54] W. Burton and A. Noor. Assessment of continuum models for sandwich panel honeycomb cores. *Computer Methods in Applied Mechanics and Engineering*, 145(3):341–360, 1997. doi: https://doi.org/10.1016/S0045-7825(96)01196-6.

[55] K. Deb. An efficient constraint handling method for genetic algorithms. *Computer Methods in Applied Mechanics and Engineering*, 186(2):311–338, 2000. doi: https://doi.org/10.1016/S0045-7825(99)00389-8.

[56] R. Kacker, E. Lagergren, and J. Filliben. Taguchi's orthogonal arrays are classical designs of experiments. *Journal of Research of the National Institute of Standards and Technology*, 96(5):577–591, 1991. doi: 10.6028/jres.096.034.

[57] Table of taguchi designs (orthogonal arrays). `https://www.mathworks.com/help/gads/genetic-algorithm.html`. Accessed: 20th August, 2022.

Appendix A

Structural Behaviour of Variable Stiffness Sandwich

A.1 Model Implementation and Validation

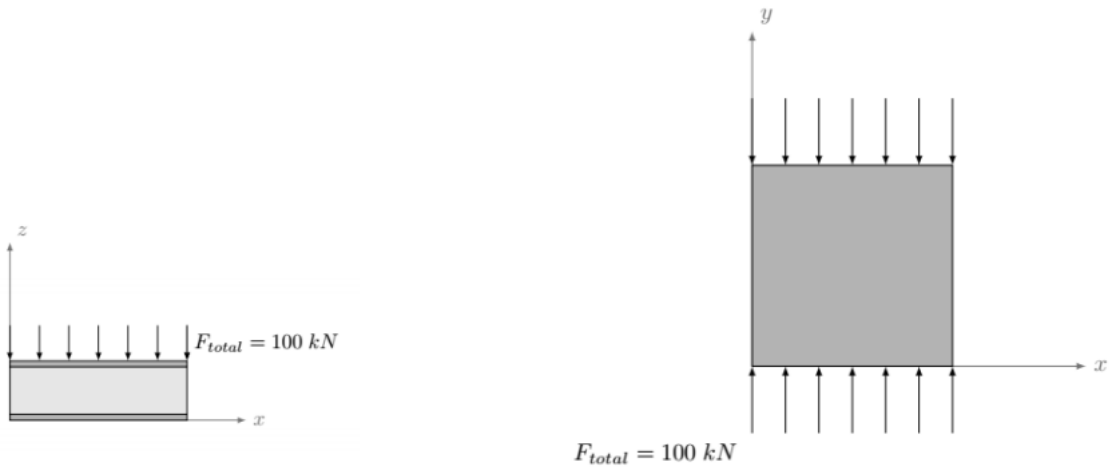

Figure A.1: Visual load representation in structural statics and buckling in y direction analysis.

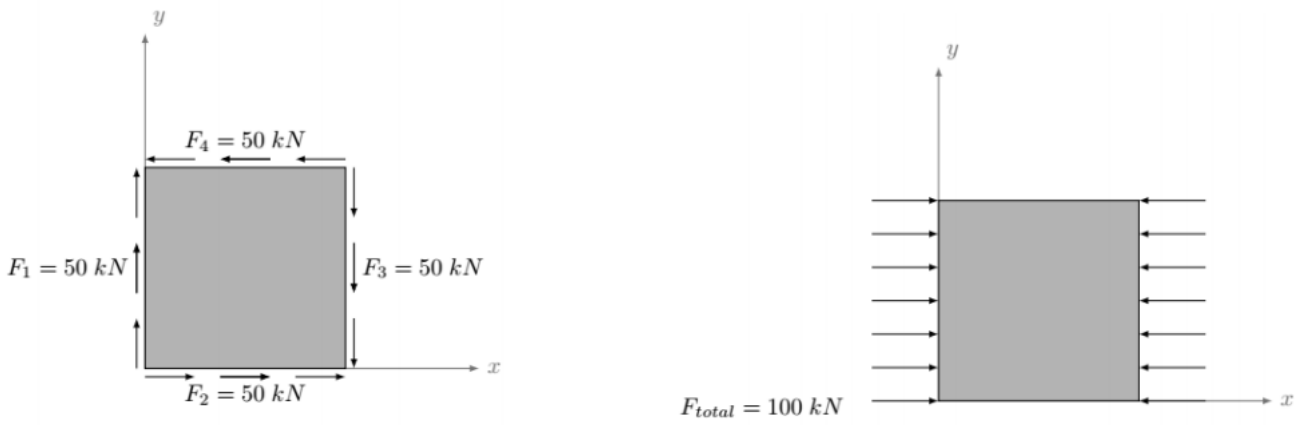

Figure A.2: Visual load representation in shear buckling and buckling in x direction analysis.

A.2 Low Stiffness Core Variable Stiffness Sandwich Study

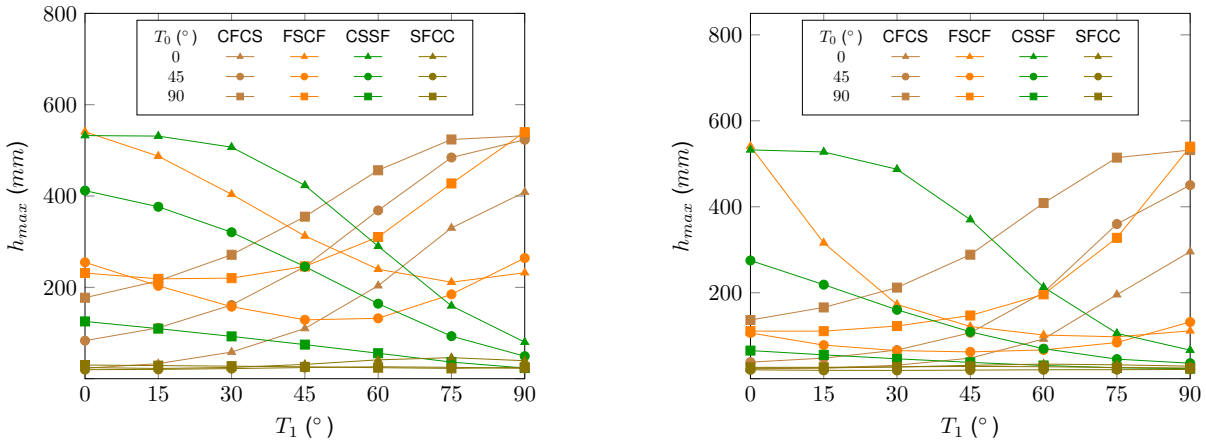

Figure A.3: Maximum static deflection h_{max} (mm) evolution with T_0 and T_1 for symmetric (left plot) and antisymmetric (right plot) face sheet configurations in multiple boundary conditions.

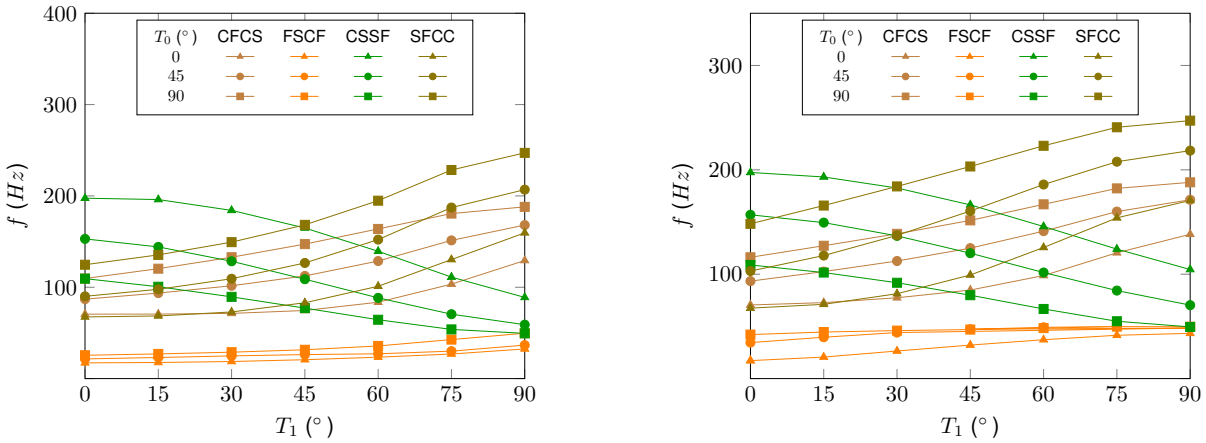

Figure A.4: Fundamental frequency f (Hz) evolution with T_0 and T_1 for symmetric (left plot) and antisymmetric (right plot) face sheet configurations in multiple boundary conditions.

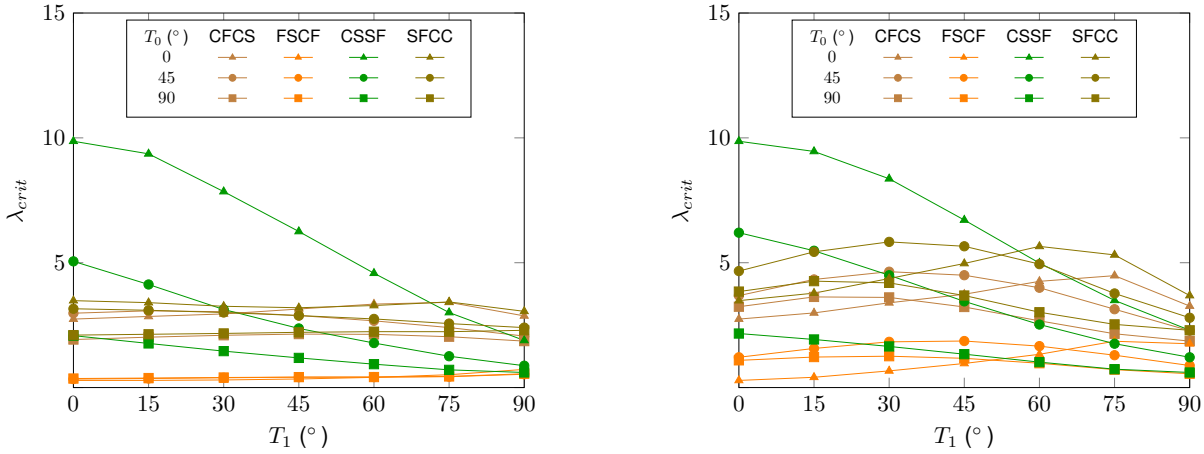

Figure A.5: Uniaxial x buckling critical load factor (λ_{crit}) evolution with T_0 and T_1 for symmetric (left plot) and antisymmetric (right plot) face sheet configurations in multiple boundary conditions.

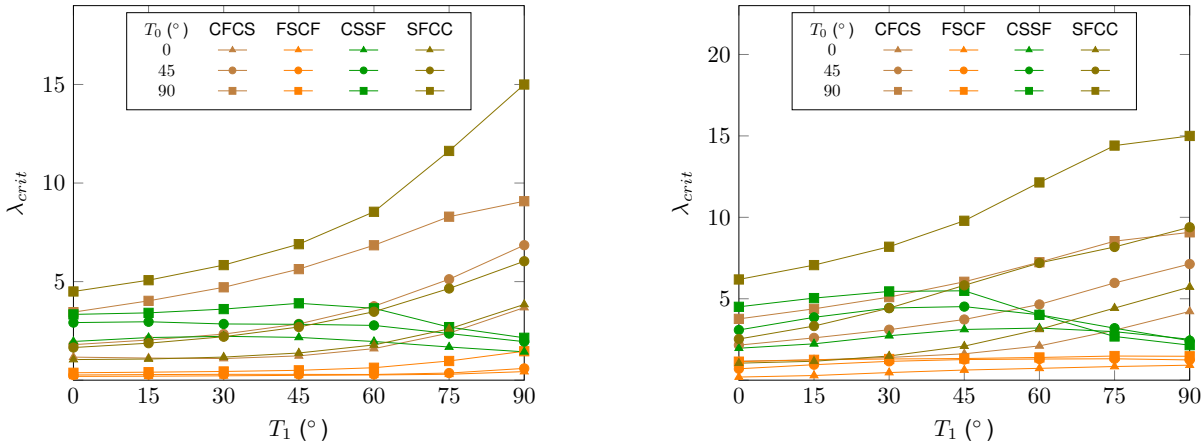

Figure A.6: Uniaxial y buckling critical load factor (λ_{crit}) evolution with T_0 and T_1 for symmetric (left plot) and antisymmetric (right plot) face sheet configurations in multiple boundary conditions.

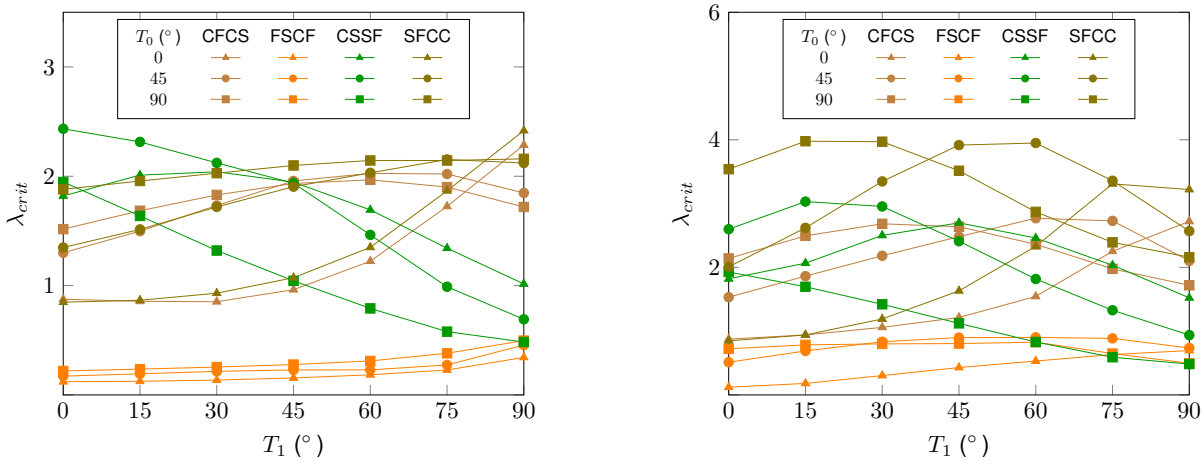

Figure A.7: Biaxial buckling critical load factor (λ_{crit}) evolution with T_0 and T_1 for symmetric (left plot) and antisymmetric (right plot) face sheet configurations in multiple boundary conditions.

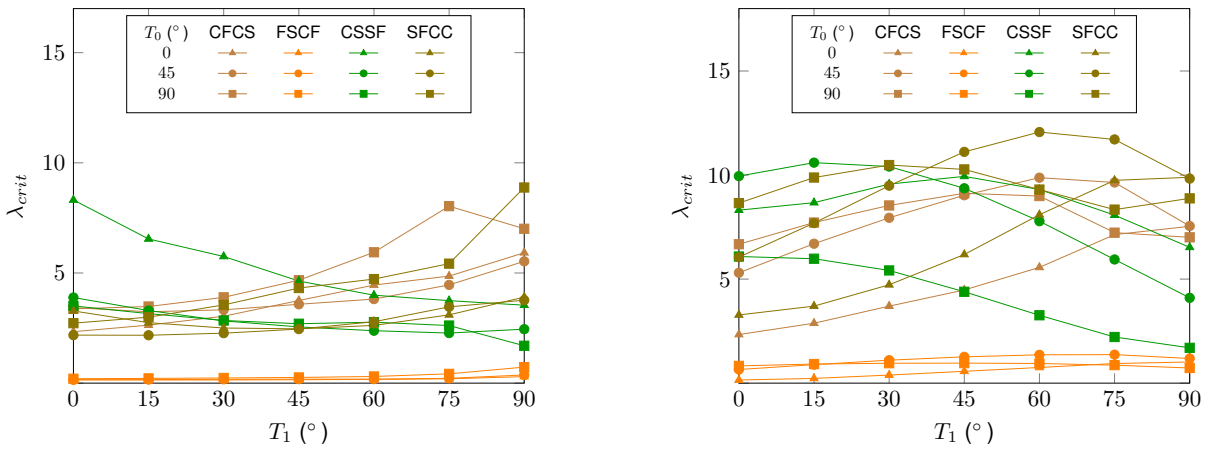

Figure A.8: Shear buckling critical load factor (λ_{crit}) evolution with T_0 and T_1 for symmetric (left plot) and antisymmetric (right plot) face sheet configurations in multiple boundary conditions.

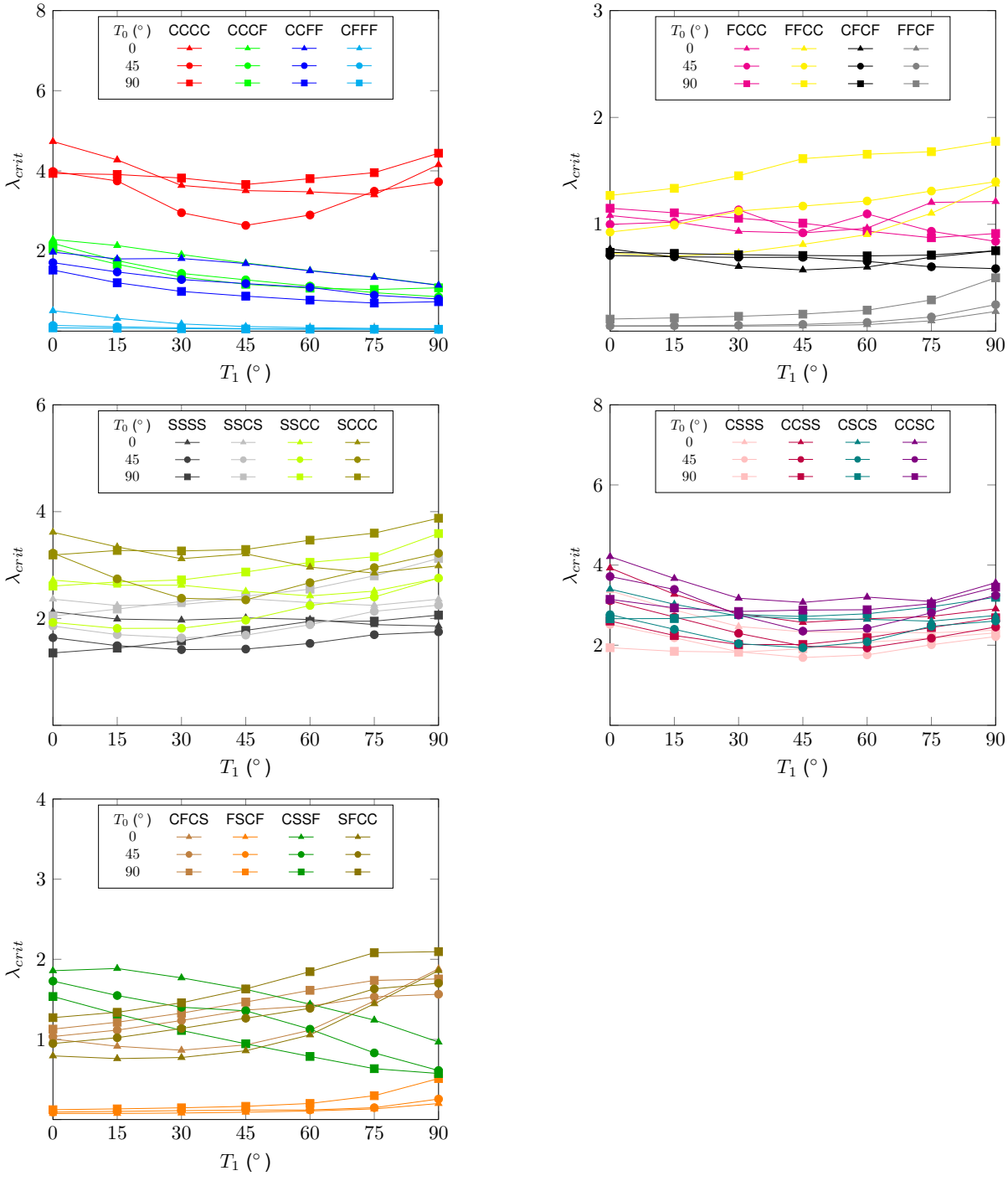

Figure A.9: Multi-load buckling critical load factor (λ_{crit}) evolution with T_0 and T_1 in multiple boundary conditions.

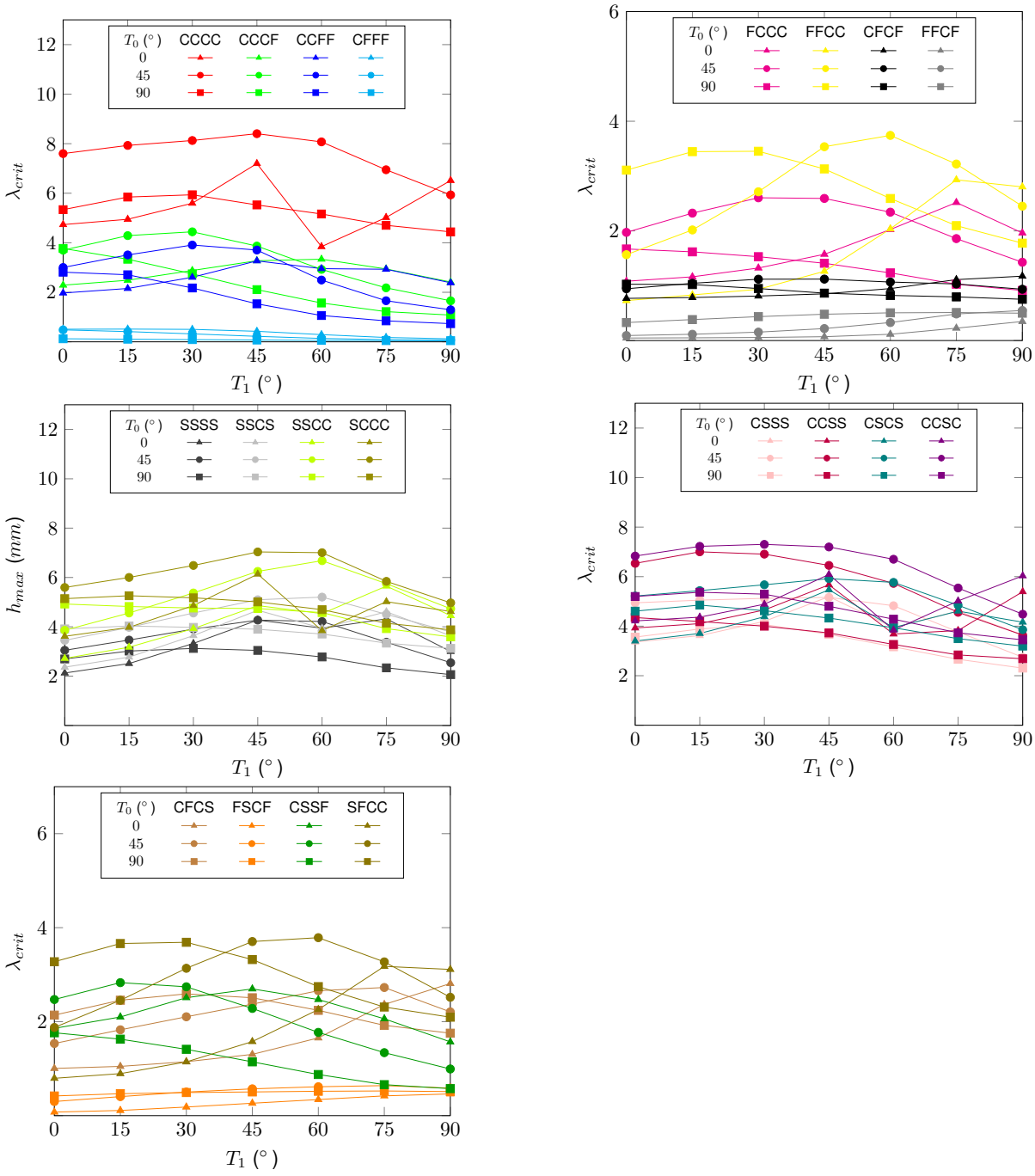

Figure A.10: Multi-load buckling critical load factor (λ_{crit}) evolution (antisymmetric facesheet configuration) with T_0 and T_1 in multiple boundary conditions.

Appendix B

Optimization Methods and Framework Execution

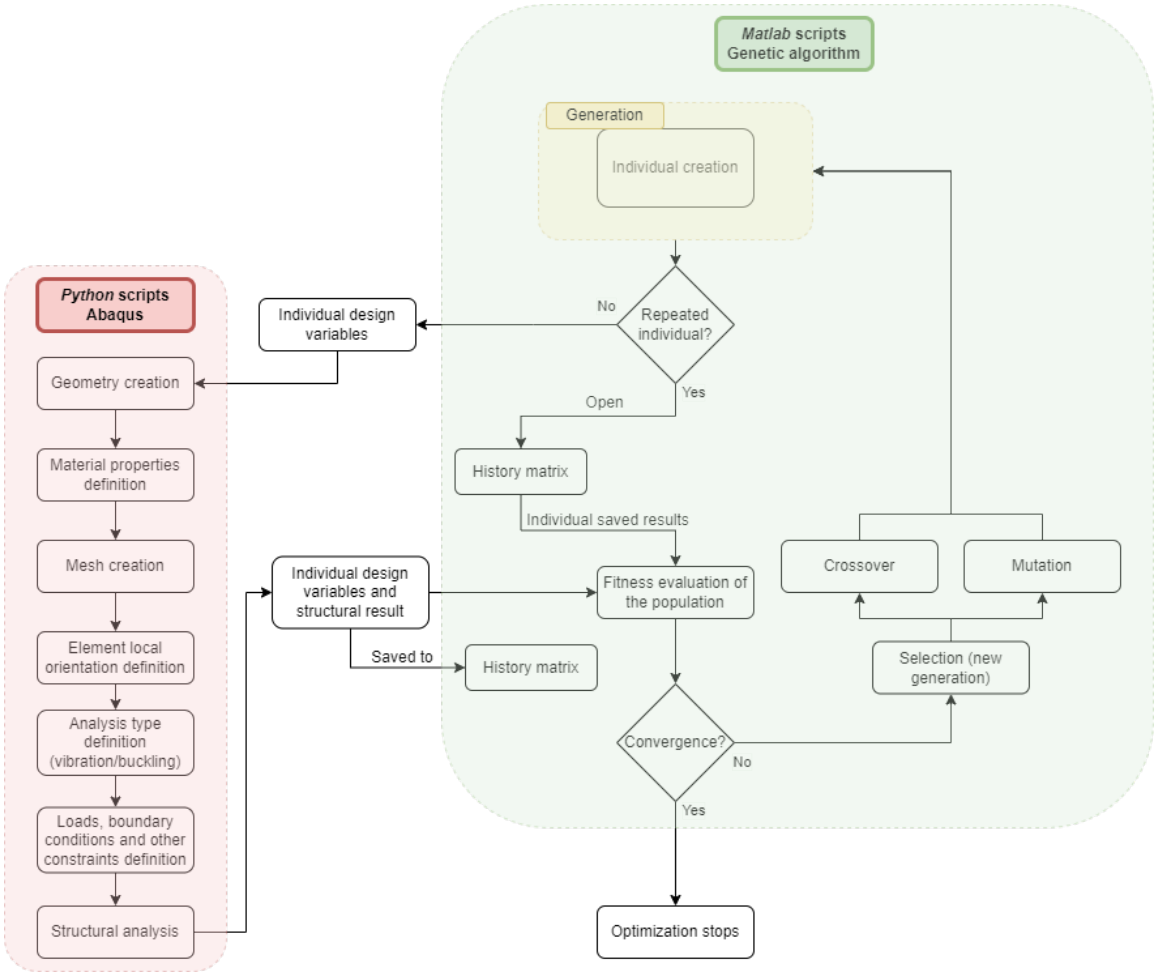

Figure B.1: Flowchart of the optimization framework execution.

Appendix C

Optimization Results

Table C.1: Maximum curvature values for optimal VSS configurations.

Core	Structural analysis	Boundary conditions	Maximum curvature value (m^{-1})
AH-H	Vibration	CCCC	3.246
		SSSS	0.077
	Buckling x	CCCC	2.252
		SSSS	1.990
	Buckling y	CCCC	1.766
		SSSS	1.503
	Shear buckling	CCCC	1.175
AH-L	Vibration	CCCC	3.176
		SSSS	0.240
	Buckling x	CCCC	1.885
		SSSS	2.303
	Buckling y	CCCC	2.477
		SSSS	2.716
	Shear buckling	CCCC	1.535

C.1 Aluminium Honeycomb Core of Low Stiffness Results

C.1.1 Constant Stiffness Face Sheets

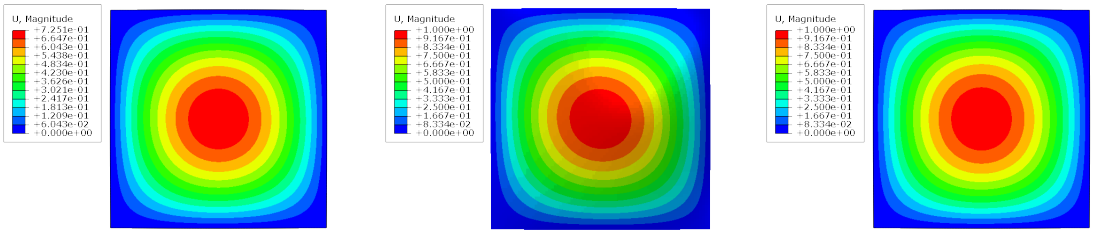

(a) Vibration. (b) Buckling in x direction. (c) Buckling in y direction.

Figure C.1: Optimal CSS face sheet configurations (with AH-L core) mode shape results in vibration, buckling in x direction and buckling in y direction, subjected to SSSS boundary conditions.

C.1.2 Variable Stiffness Face Sheets

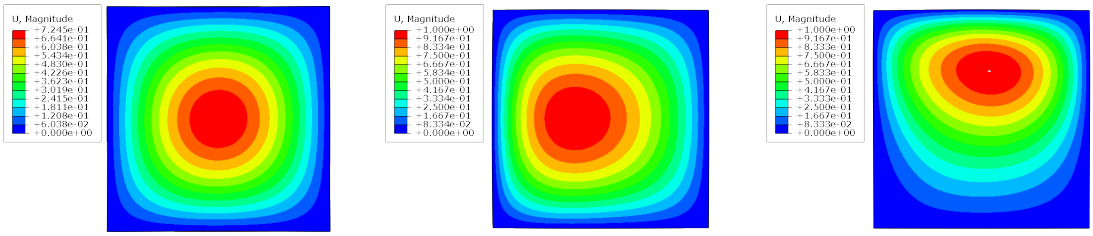

(a) Vibration. (b) Buckling in x direction. (c) Buckling in y direction.

Figure C.2: Optimal VSS face sheet configurations (with AH-L core) mode shape results in vibration, buckling in x direction and buckling in y direction, subjected to SSSS boundary conditions.